Studies on the protein translocation in *Escherichia coli*: analysis of the integral membrane proteins SecYEG and YidC employing biochemical and crystallographic methods

Dissertation

zur Erlangung des Doktorgrades

der Naturwissenschaften

vorgelegt beim Fachbereich für Biochemie, Chemie und

Pharmazie der Johann Wolfgang Goethe Universität

in Frankfurt am Main

von Mirko Lotz

aus Schlüchtern

Frankfurt am Main 2007

(D F 1)

vom Fachbereich für Biochemie, Chemie und Pharmazie der Johann Wolfgang Goethe Universität als Dissertation angenommen.

Dekan: Prof. Dr. Harald Schwalbe

Gutachter: Prof. Dr. Robert Tampé
                      Prof. Dr. Werner Kühlbrandt

Datum der Disputation:

Summary

Transport of proteins into or across cellular membranes is mediated by the conserved and ubiquitous Sec-machinery. The Sec-homologue in the inner membrane of *Escherichia coli* is SecYEG. Sec-mediated insertion of numerous membrane proteins is aided by YidC, another protein integral to the inner membrane of *Escherichia coli*. YidC fulfils in addition the integration of a variety of membrane proteins Sec-independently. It belongs to a conserved but structurally uncharacterised family of proteins important for membrane protein biogenesis and comprises homologues in mitochondria and chloroplasts.

By modification of a former crystallisation protocol two-dimensional crystals of SecYEG were grown in presence of the signal sequence peptide of LamB. Recording of structural data by electron cryo-microscopy and calculation of a difference structure comparing a former SecYEG projection structure with the one of SecYEG crystallised in presence of the substrate revealed several new and vacant densities. These hint to signal peptide binding close to the translocation pore and to significant rearrangements in proximity to the lateral exit site for transmembrane domains in SecYEG. The difference structure suggests that dimeric SecYEG is an asymmetric molecule consisting of one active and one inactive SecYEG monomer.

Detergent removal from a mixture of purified YidC and lipids produced two-dimensional crystals that were highly dependent on the ionic strength and lipid composition for their growth. Electron cryo-microscopy on the frozen-hydrated crystals and image processing visualised structural details at about 10 Å resolution. Averaging two alternative projection structures in p2 and p121_a symmetry, respectively, yielded essentially the same features. Four YidC monomers form one unit cell (dimensions 82 x 71 Å, included angle 85 ° and 90 °, respectively) and seem to be arranged as two sets of dimers integrated in an anti-parallel fashion into the membrane. An area of low density in the centre of each YidC monomer resembles possibly a constriction of the membrane, which could have particular relevance for the integration of substrate proteins into the lipid bilayer.

Introduction

1   Membrane proteins

'Soluble proteins' reside in the aqueous compartments of the cell. In contrast, 'membrane proteins' are embedded or anchored within cellular membranes. Proteins of the latter variety reviewed by von Heijne (von Heijne 1996) are embedded into membranes with either hydrophobic α-helices (transmembrane helices) or segments formed from β-strands with hydrophobic outer surfaces, called 'β-barrels'. Due to their hydrophobic transmembrane regions, membrane proteins are usually poorly water soluble, if at all. Membrane proteins spanning the membrane several times are called 'polytopic'. According to several genome projects, 25 to 30 % of all encoded proteins are membrane proteins, which suggests their biological importance, reviewed by Byrne and Iwata (Byrne and Iwata 2002). They fulfil important functions in the exchange of ions, water and macromolecules and confer furthermore signal transduction, cell-cell contact, respiration, energy conversion, nervous potential transduction and metabolic processes.

2   General definition of protein translocation

All proteins, which have to leave the compartment of their synthesis, have to cross membrane barriers in the cell. The transport of proteins across or their integration into membranes is called 'protein translocation' and is essential for life.

3   Signal sequences

Günter Blobel and Bernhard Dobberstein formulated the "hypothesis for the transfer of proteins across membranes" (Blobel and Sabatini 1971; Blobel and Dobberstein 1975a). Proteins that have to be transferred across membranes have amino-terminal amino acid stretches, called 'signal sequences' that trigger the attachment of the translating ribosomes to protein-conducting channels in the ER membrane (Blobel and Dobberstein 1975a). The ribosomes do not attach to the membrane if the mRNAs do not code for signal sequences (Blobel and Dobberstein 1975a). The targeting information for a protein is encoded in its mRNA, not in the protein synthesis apparatus (Blobel and Dobberstein 1975b). Signal sequences of membrane proteins

that have the amino-terminus on the non-cytoplasmic side in their mature form and signal sequences of secretory proteins are cleaved off by 'leader peptidases' (Blobel and Dobberstein 1975a; Blobel and Dobberstein 1975b; Dalbey and Wickner 1985; Holland and Drickamer 1986). The translation of every mRNA starts on free ribosomes and is initiated by the same mechanism (Blobel and Dobberstein 1975a). The existence of protein-conducting channels in the ER membrane was demonstrated by electrophysiological studies (Simon and Blobel 1991; Simon and Blobel 1992; Crowley et al. 1994).

4   Sec-mediated translocation in *Escherichia coli*

4.1   The Sec-translocon

The key components of the protein secretion apparatus were identified by genetic studies in *Escherichia coli* and yeast (Oliver and Beckwith 1981; Shultz et al. 1982; Ito et al. 1983; Deshaies and Schekman 1987; Rothblatt et al. 1989; Schatz et al. 1989; Stirling et al. 1992). The Sec-translocon of *Escherichia coli* is a heterotrimeric complex of the proteins SecY, SecE and SecG (SecYEG) that span the cytoplasmic membrane 10, 3 and 2 times, respectively (Akiyama and Ito 1987; Schatz et al. 1989; Brundage et al. 1992; Douville et al. 1994; Nishiyama et al. 1994; Nishiyama et al. 1996). SecY and SecE resemble the components, which are minimally required for a functional Sec-translocon in all organisms (Brundage et al. 1990; Hartmann et al. 1994). SecG is not essential for translocation, but stabilises the complex and enhances the activity of SecYE (Hanada et al. 1994; Nishiyama et al. 1995).

Later, the mammalian homologue Sec61, called 'Sec61p' in yeast, was found tightly associated with membrane bound ribosomes (Görlich et al. 1992b; Görlich and Rapoport 1993) and forms the protein-conducting channels proposed earlier (Blobel and Dobberstein 1975a; Müsch et al. 1992; Görlich et al. 1992b; Görlich and Rapoport 1993; Hanein et al. 1996). These are employed for the integration of membrane proteins into the ER membrane as well as for the transfer of proteins across (High et al. 1993a; Oliver et al. 1995). Sec61 and its homologues are referred to as the Sec-translocon, Sec-complex or the Sec-machinery. 'Sec-mediated translocation' including most involved components is ubiquitous, ancient and conserved (Bernstein et al. 1989; Görlich et al. 1992b; Görlich and Rapoport 1993; Hartmann et al. 1994; Prinz et al. 2000). The Sec61-complex may function also as a proteasome receptor

and mediate the back-transport of improperly folded proteins into the ER (Kalies et al. 2005). Thereby, ribosomes may compete with proteasomes for binding to the Sec-translocon (Kalies et al. 2005).

4.2   Post-translational translocation

Escherichia coli are capable of post-translational protein translocation decoupled from the ribosomal polypeptide synthesis, driven by the dimeric cytoplasmic ATP synthase SecA (Oliver and Beckwith 1982; Cabelli et al. 1988; Cunningham et al. 1989; Kawasaki et al. 1989; Akita et al. 1991; Driessen 1993). SecA recognises hydrophobic signal sequences with amino-terminal positive charges (Cunningham and Wickner 1989; Akita et al. 1990) as also shown by NMR studies (Chou and Gierasch 2005). During translocation, SecA associates with the lipid bilayer and employs SecYEG as translocation channel (Bacallao et al. 1986; Cabelli et al. 1988; Cunningham et al. 1989; Lill et al. 1989; Brundage et al. 1990; Driessen and Wickner 1990; Tokuda et al. 1990; Akimaru et al. 1991; Douville et al. 1995). In bacteria, the tetrameric chaperone SecB forms complexes with substrate proteins of SecA and stabilises them in an unfolded translocation competent conformation (Collier et al. 1988; Weiss et al. 1988; Kumamoto 1989; Kusters et al. 1989; Lecker et al. 1989; Watanabe and Blobel 1989; Lecker et al. 1990; Breukink et al. 1992). Thereby, SecB recognises a motif of mostly basic or aromatic amino acids which statistically occurs every 20 to 30 residues (Knoblauch et al. 1999) as also supported by X-ray crystallographic studies (Xu et al. 2000; Dekker et al. 2003).

SecB binds to the carboxy-terminus of SecA and passes the preproteins to SecA (Hartl et al. 1990; Hoffschulte et al. 1994; Breukink et al. 1995). During the initial phase of translocation, SecB is released from SecA (Fekkes et al. 1997). In accordance to a recent model, nucleotide binding and hydrolysis induces conformational changes within SecA that lead to a cyclic association and dissociation to SecYEG and insertion of the substrate protein into the translocon (Hunt et al. 2002). However, the mechanism of processive polypeptide transport through SecYEG remains unclear (Hunt et al. 2002). The hydrolysis of ATP therefore may have further effects when SecA is associated with SecYEG (Hunt et al. 2002). ATP dependent post-translational translocation was demonstrated in yeast as well (Hansen et al. 1986; Rothblatt and Meyer 1986a), for which the Sec translocon in yeast, the Sec61p complex, associates with the integral membrane proteins Sec62p and Sec63p

(Rothblatt et al. 1989; Deshaies et al. 1991; Panzner et al. 1995). So far, there is little evidence suggesting post-translational translocation across the mammalian ER (Klappa et al. 1994).

4.3   Co-translational translocation

The signal recognition particle (SRP), a multimeric cytoplasmic protein complex, which is associated with a RNA component, binds to hydrophobic signal sequences when they protrude out of the large ribosomal subunit. This was first demonstrated for eukaryotes (Walter et al. 1981; Walter and Blobel 1981a; Walter and Blobel 1981b; Walter and Blobel 1982). Later, a functional and structural homologous SRP was also found in *Escherichia coli* (Bernstein et al. 1989; Römisch et al. 1989; Luirink et al. 1992; Phillips and Silhavy 1992; Bernstein et al. 1993). The membrane anchored protein FtsY resembles the mammalian signal recognition particle receptor (SR) in *Escherichia coli*, but in contrast to the dimeric eukaryotic SR it is monomeric (Bernstein et al. 1989; Römisch et al. 1989; Poritz et al. 1990; Ribes et al. 1990). SRP and FtsY confer in *Escherichia coli* co-translational translocation in a manner similar to the eukaryotic pathway (Muller et al. 1982; Luirink et al. 1994; Miller et al. 1994; Powers and Walter 1997). SRP and FtsY comprise GTP-binding domains (Bernstein et al. 1989; Römisch et al. 1989). Simultaneous binding of GTP by SRP and FtsY establishes a SRP/FtsY-complex (Miller et al. 1994; Kusters et al. 1995), whereas signal sequence binding by SRP does not require GTP as shown for the eukaryotic SRP (Zopf et al. 1993; Rapiejko and Gilmore 1994). Binding of the SRP to FtsY targets the ribosome-nascent chain complex to the Sec-translocon (Powers and Walter 1997). Upon GTP hydrolysis, the SRP dissociates from its receptor (Miller et al. 1994).

The complex between SRP and FtsY is established by a co-operative binding of GTP in form of a substrate-twinning motif, as shown by two independent X-ray crystallographic studies (Egea et al. 2004; Focia et al. 2004). This motif is to date unprecedented in literature (Egea et al. 2004; Focia et al. 2004). FtsY binds furthermore to SecY (Angelini et al. 2005). This might serve to modulate the signal sequence release from the SRP/FtsY-complex by SecY (Angelini et al. 2005). The SRP-mediated translocation in *Escherichia coli* is mainly engaged for the integration of membrane proteins (Macfarlane and Müller 1995; de Gier et al. 1996; Seluanov and Bibi 1997; Ulbrandt et al. 1997; Scotti et al. 1999), although some secretory

proteins are translocated in a co-translational manner as well (Qi and Bernstein 1999; Kim et al. 2001). Several membrane proteins are integrated by a sequential interaction of SRP and SecA which serves obviously for the translocation of substantial periplasmic domains (Neumann-Haefelin et al. 2000; Koch et al. 2002; Urbanus et al. 2002; van der Laan et al. 2004a; Deitermann et al. 2005).

4.4   Pathway discrimination

Post-translational and co-translational translocation converge in *Escherichia coli* and yeast at the Sec-translocon (Hansen et al. 1986; Rothblatt and Meyer 1986a; Görlich et al. 1992b; Valent et al. 1998; Koch et al. 1999). In both organisms, the SRP recognises proteins destined for co-translational translocation and therefore discriminates between the two routes (Ng et al. 1996; Lee and Bernstein 2001). Furthermore, SecB targets proteins towards post-translational translocation in *Escherichia coli* (Ernst et al. 1994). For this, the cytoplasmic protein 'trigger factor' (TF) might already sort the nascent peptide chain to the SecB/SecA-mediated pathway (Beck et al. 2000). SRP as well as TF docks to the ribosomal subunit L23, which lines the ribosomal exit channel (Gu et al. 2003; Ullers et al. 2003). Binding of SRP to L23 or the emerging signal sequence could hence be in competition with TF (Eisner et al. 2003; Ullers et al. 2003; Eisner et al. 2006), or SRP and TF could bind simultaneously and examine the nascent peptide in parallel (Raine et al. 2004; Schlunzen et al. 2005). In an alternative model, SRP, SecA and TF associate and dissociate from the emerging polypeptide on the ribosome until one of the factors binds with high affinity (Karamyshev and Johnson 2005). In consequence, the nascent is sorted either by SecA towards post-translational translocation, by SRP towards co-translational translocation or by TF towards secretion into the cytoplasm (Karamyshev and Johnson 2005) (Fig. 1).
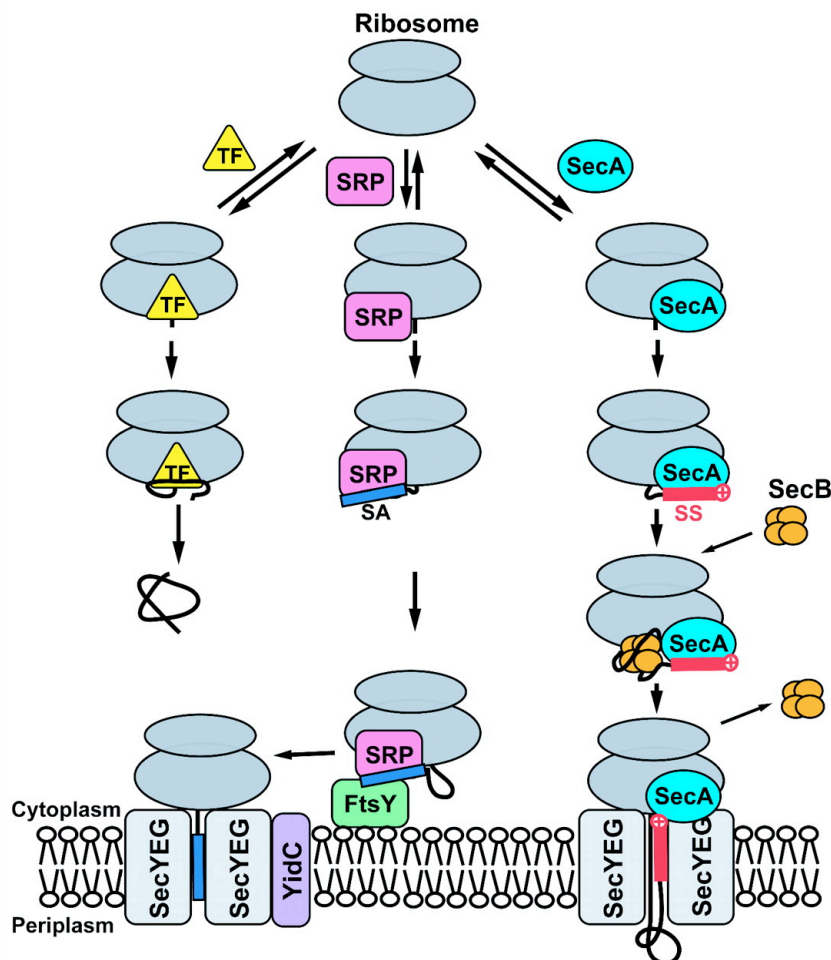
Fig. 1   Mechanism for sorting proteins emerging from the bacterial ribosome. SS: Signal sequence, which is recognised by SecA. SA: Signal anchor sequence, which is recognised by SRP and integrated into the lipid bilayer. Modified from (Karamyshev and Johnson 2005). See text.

4.5   Molecular mechanisms of protein translocation

Signal sequences form α-helical structures and insert as loops into the Sec-translocon, which is a conserved process (Emr and Silhavy 1983; Shaw et al. 1988; Plath et al. 1998). Each transmembrane helix of the growing peptide is fully synthesised before it is released into the lipid bilayer from the Sec-translocon (Görlich et al. 1992b; Mothes et al. 1994; Do et al. 1996; Mothes et al. 1998; McCormick et al. 2003). The integration of signal sequences and transmembrane helices into the Sec-translocon does not require lipids, although lipids are stimulating the process (Mothes et al. 1998). The Sec-complex seems to help transmembrane domains to bypass the barrier posed by the polar head groups of the lipids and to equilibrate in the membrane and is a determinant for proper folding of the integrated membrane proteins (Heinrich et al. 2000; Hessa et al. 2005; Shimohata et al. 2007). The ability of a transmembrane

segment to integrate into the lipid bilayer is determined by its hydrophobicity and the intrinsic location of polar amino acid residues (Hessa et al. 2005). The gradient of positive charges across the plasma membrane, called 'membrane potential', repels positive charges towards the cytoplasm and thus provides orientation to integration of transmembrane domains (positive inside rule) (Whitley et al. 1995; Wallin and von Heijne 1998; Schuenemann et al. 1999a). It furthermore aids the Sec-complex to initiate translocation and stimulates the translocation of several proteins (Tani et al. 1989; Driessen and Wickner 1990; Tokuda et al. 1990; Schiebel et al. 1991; Mori and Ito 2003).

In order to investigate the mechanism of co-translational translocation, several involved components were reconstructed based on the electron cryo-microscopic investigation of single molecules (single particle reconstruction). The mammalian SRP and the protein 'elongation factor' (EF) compete to a large extend for the same binding site on the ribosome (Halic et al. 2004). As EF is needed by the ribosome for chain elongation, this possibly explains an early observed elongation arrest upon SRP binding in eukaryotes (Walter and Blobel 1981b; Halic et al. 2004). The ribosome undergoes a conformational change when the translocon binds, which could influence the interaction with cytoplasmic factors like SRP or might influence directly the interaction between ribosome and nascent chain (Beckmann et al. 1997; Beckmann et al. 2001). Two alternating modes of co-translational translocation are suggested (Beckmann et al. 2001). If a helical transmembrane domain inserts as a loop into the Sec-translocon, the growing peptide is translocated across the membrane (first mode) (Beckmann et al. 2001). In the second mode, the transmembrane domain inserts in a non-loop conformation, which results in the release of the nascent chain into the cytoplasm (Beckmann et al. 2001). Alternation of both modes leads to the generation of a polytopic membrane protein (Beckmann et al. 2001). Based on earlier studies, the ribosome, and not the Sec-complex, recognises features of the growing polypeptide and induces the switch between the two modes (Liao et al. 1997).

The Sec-complex was investigated by crystallographic techniques. Crystallisation of SecYEG in a lipid bilayer (two-dimensional crystallisation) and investigation by electron cryo-microscopy yielded for the first time a picture of a Sec-complex at 8 Å resolution (Collinson et al. 2001; Breyton et al. 2002). All 15 predicted transmembrane helices were visible, but the helices could not be assigned. Later, an X-ray crystallographic study of the archaeal SecYEG homologue from *Methanococcus jannaschii*, SecYEβ, yielded high-resolution data of the detergent-

solubilised complex (van den Berg et al. 2004). Each SecYEβ monomer had a translocation pore, which disproved the previous idea that the protein-conducting channel is formed in the interface between two monomers (Breyton et al. 2002; van den Berg et al. 2004). On its narrowest point, the channel is lined by six hydrophobic residues that likely form a seal to prevent a flux of ions through the channel (van den Berg et al. 2004). This agrees with earlier data obtained from single particle reconstructions and argues against a sealing by lumenal factors like the eukaryotic BiP or Kar2p (Hamman et al. 1998; Menetret et al. 2000; Beckmann et al. 2001).

The signal sequence intercalation site is located between transmembrane helices 2 and 7, which was also supported by cross-linking studies (van den Berg et al. 2004; Wang et al. 2004). Transmembrane segments can only be released from one side of the translocon into the lipid bilayer, referred to as the 'front' of the monomer; accordingly, the opposite site is referred to as the 'back' (van den Berg et al. 2004). The front side exhibits a lateral exit site for transmembrane domains of substrate proteins, posed by transmembrane helices 2b, 3, 7 and 8 of SecY (Fig. 2). A putative plug domain closes the translocation pore like a lid on the periplasmic side (van den Berg et al. 2004) (Fig. 2). Binding of the signal sequence probably induces a relocation of the plug domain, which opens the channel (van den Berg et al. 2004; Bostina et al. 2005; Tam et al. 2005). During translocation, the plug and the pore might be kept in an open state by the substrate polypeptide (van den Berg et al. 2004). After the polypeptide chain left the channel, the plug flips back and seals the translocation pore (van den Berg et al. 2004). In this model, only one SecYEβ monomer is active during translocation, but resides as dimer in the membrane (van den Berg et al. 2004). The data obtained from electron-crystallography has been combined with that yielded by X-ray crystallography (Breyton et al. 2002; van den Berg et al. 2004; Bostina et al. 2005): the dimer formation of SecYEG is suggested to induce a slight reposition of the plug domain from the inner pore towards the periplasm and to slightly 'open' the Sec-complex, which primes the Sec-complex for translocation (Bostina et al. 2005). This is also supported by biochemical experiments (Tam et al. 2005). Probably, the plug domain only switches to its fully open state for the translocation of secreted domains whereas it stays partially closed while the lateral release of transmembrane segments and avoids then the diffusion of small molecules through the pore (Bostina et al. 2005). According to the newer data, the second SecY molecule could also serve to maintain the interaction with SecA during post-translational translocation (Osborne and Rapoport 2007).
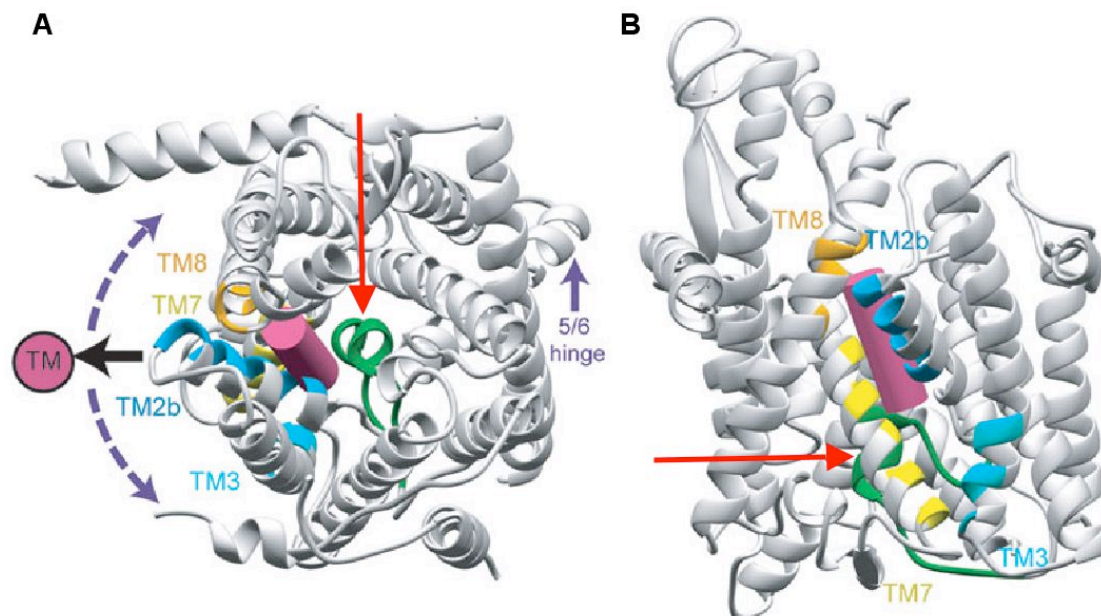
Fig. 2   Signal sequence (represented by violet cylinder) binding and lateral exit site in SecYEβ. **A**: Top view from the cytoplasm. TM: Transmembrane domain, released on the front side of the monomer through the lateral exit site into the lipid bilayer. **B**: Side view. The proposed plug domain is indicated by red arrows. Modified from (van den Berg et al. 2004).

The data obtained by X-ray crystallography was imposed into a single particle reconstruction of the bacterial ribosome exposing a nascent chain bound to SecYEG (Mitra et al. 2005). The study proposes a 'front-to-front arrangement' of two SecYEG monomers (Mitra et al. 2005), instead of the 'back-to-back' arrangement observed earlier (Breyton et al. 2002). It is suggested, that the transmembrane segments are released laterally from an exit site between the two monomers, thus engaging the whole dimer in translocation (Mitra et al. 2005). The proposed plug domain then seals the monomer, which is not active (Mitra et al. 2005).

5   Oxa1 family of membrane proteins

5.1   Oxa1

A protein termed according to its function in oxidase assembly 'Oxa1' (formerly known as 'Pet1420') is essential for the integration of proteins into the inner mitochondrial membrane (Hell et al. 1998). Oxa1 integrates nuclear encoded proteins in a post-translational fashion from the mitochondrial matrix (Hell et al. 1998). The import of nuclear encoded proteins into the mitochondrial matrix prior to integration

is reviewed by Endo and co-workers (Endo et al. 2003). The α-helical carboxy-terminus of Oxa1 protrudes into the mitochondrial matrix and associates with mitochondrial ribosomes, which could serve a co-translational integration of substrate proteins that are encoded in mitochondria (Hell et al. 2001; Jia et al. 2003; Szyrach et al. 2003). Oxa1 substrates include subunits Cox1, Cox2 and Cox3 of the cytochrome oxidase complex, cytochrome b, subunits Su8 and Atp9 of the F_1F_0-ATP synthase and Oxa1 itself (Bauer et al. 1994; Bonnefoy et al. 1994a; Altamura et al. 1996; He and Fox 1997; Hell et al. 1997; Meyer et al. 1997; Hell et al. 1998; Hell et al. 2001; Ii and Mihara 2001; Jia et al. 2007). Atp9 thereby appears to be translocated in a post-translational fashion not involving interaction of the carboxy-terminus of Oxa1 with ribosomes, although Atp9 is mitochondria-encoded (Jia et al. 2007).

Some substrate proteins such as Su8 do not require any additional factors than Oxa1 for their membrane integration (Ii and Mihara 2001). The integration of others, like Cox2 or Oxa1, depends on the electrochemical potential across the inner mitochondrial membrane (Herrmann et al. 1995; He and Fox 1997; Herrmann et al. 1997; Rojo et al. 1999; Frazier et al. 2003). The mitochondrial matrix resembles the cytoplasm of prokaryotes, whereas the lumen resembles the prokaryotic periplasm. The membrane potential dependent integration by Oxa1 follows in principle the prokaryotic positive inside rule as positive net charges become oriented to the matrix side (Herrmann et al. 1995; Whitley et al. 1995; Wallin and von Heijne 1998; Rojo et al. 1999).

Oxa1 consists of four to five predicted hydrophobic transmembrane helices, embedded in the inner mitochondrial membrane, and its amino-terminus is located in the space between the outer and inner mitochondrial membrane (Bonnefoy et al. 1994a; Herrmann et al. 1997; Kermorgant et al. 1997; Meyer et al. 1997). Oxa1 is nuclear encoded and synthesised in the cytoplasm as a 42 kDa precursor protein carrying an amino-terminal targeting sequence for mitochondrial import (Bauer et al. 1994; Bonnefoy et al. 1994a; Herrmann et al. 1997; Meyer et al. 1997). This targeting sequence is cleaved off in the matrix by the mitochondrial processing peptidase, forming the mature Oxa1 with a molecular weight of 36 kDa (Herrmann et al. 1997; Meyer et al. 1997), which is suggested to form homotetramers in the membrane (Nargang et al. 2002).

The transmembrane segments of Oxa1 seem to be inserted pairwise into the inner mitochondrial membrane (Herrmann et al. 1997). Oxa1 seems to support particularly the equilibration of less hydrophobic transmembrane domains in the lipid

bilayer, probably by 'sandwiching' them between its own transmembrane domains (Saint-Georges et al. 2001). A similar mechanism is proposed for the eukaryotic translocating chain associating membrane protein (TRAM), which is closely associated with the Sec61-complex (Görlich et al. 1992a; Wang and Dobberstein 1999; Heinrich et al. 2000; Snapp et al. 2004). In general, the dependence on Oxa1 seems to be determined by the nature of the transmembrane domains and not by their position in the substrate protein (Herrmann and Bonnefoy 2004). Charged transmembrane domains appear to depend on Oxa1, whereas uncharged transmembrane domains are suggested to use an alternative, overlapping pathway (Preuss et al. 2001; Herrmann and Bonnefoy 2004). Oxa1 seems to interact with Tim23, the main protein import channel in the inner mitochondrial membrane (Reif et al. 2005).

Oxa1 homologues have been found in all organisms with fully sequenced genome and form an evolutionarily conserved family (Bonnefoy et al. 1994a; Bonnefoy et al. 1994b; Luirink et al. 2001; Yen et al. 2001). Most prokaryotes possess only one Oxa1 homologue, whereas many gram-positive bacteria and at least one archaeon have two (Yen et al. 2001). Eukaryotes may have up to six Oxa1 homologues in their organelles, but none could be found in the cytoplasmic membrane or the ER or the Golgi apparatus (Yen et al. 2001). All Oxa1 homologues exhibit a wide variation in protein size ranging from 225 to 795 amino acids (Yen et al. 2001). Although the sequence similarity is too low to declare a defined signature sequence, all Oxa1 homologues are predicted to share a core of four or five transmembrane segments, which harbours the 'membrane protein integrase' activity, and to exhibit three consensus sequences (Sääf et al. 1998; Yen et al. 2001). Oxa1 and its homologues are obviously of particular and conserved importance for the biogenesis of respiratory chain complexes (van der Laan et al. 2003).

5.2   Alb3

The Oxa1 homologue in chloroplasts, called 'Albino3' (Alb3), is essential for the post-translational integration of light harvesting chlorophyll-binding protein into thylakoid membranes, and explains why its depletion led to an *albino* phenotype in *Arabidopsis thaliana* (Long et al. 1993; Moore et al. 2000). Homologues of Alb3 are also required for the thylakoid biogenesis in cyanobacteria (Spence et al. 2004) and for the effective assembly of photosystems 1 and 2 in *Chlamydomonas reinhardtii*

(Bellafiore et al. 2002; Ossenbuhl et al. 2004). Chloroplast Alb3 is encoded in the nucleus and translated into a precursor protein with a molecular mass of approximately 60 kDa and an amino-terminal signal sequence for chloroplast import (Long et al. 1993). After import, Alb3 is processed to a mature protein with a molecular weight of approximately 48 kDa (Long et al. 1993). Five predicted hydrophobic transmembrane domains residing in the thylakoid membrane form the core of Alb3 (Long et al. 1993; Moore et al. 2000). Its amino-terminus protrudes into the lumen (Long et al. 1993; Moore et al. 2000). Alb3 seems to employ chloroplast SRP and FtsY and probably SecY for the integration of membrane proteins (Tu et al. 1999; Woolhead et al. 2001; Klostermann et al. 2002; Moore et al. 2003).

5.3   YidC

5.3.1   Sec-dependent function

The protein YidC is the Oxa1 homologue of *Escherichia coli* and is essential for the viability of the cells (Samuelson et al. 2000; Scotti et al. 2000). It was found associated with SecYEG by cross-linking studies (Scotti et al. 2000) and might be linked to SecYEG by SecDFyajC or SecDF complexes (Nouwen and Driessen 2002; Chen et al. 2005; Xie et al. 2006). Alb3 and Oxa1 can complement for YidC depletion in *Escherichia coli* and conversely YidC can complement for Oxa1 depletion in mitochondria, which shows their functional similarity (Jiang et al. 2002; Preuss et al. 2005; van Bloois et al. 2005). Like Oxa1 and TRAM, YidC seems to aid the lateral exit of transmembrane domains from the Sec-translocon and their equilibration in the lipid bilayer (Görlich et al. 1992a; Wang and Dobberstein 1999; Heinrich et al. 2000; Houben et al. 2000; Samuelson et al. 2000; Scotti et al. 2000; Saint-Georges et al. 2001; Samuelson et al. 2001; Urbanus et al. 2001; Snapp et al. 2004). For this, the substrate proteins are transferred to YidC from the Sec-complex (Beck et al. 2001; Urbanus et al. 2001; van der Laan et al. 2001; Houben et al. 2002; Houben et al. 2004). The transfer takes place when the nascent chain is elongated to approximately 50 amino acid residues (Houben et al. 2005). Two models for the Sec-dependent function of YidC are proposed. YidC could either support the formation of helix bundles and their integration into the membrane (Beck et al. 2001) or may aid membrane protein integration in a 'linear' manner, one by one for each transmembrane helix (Houben et al. 2004).

Identified substrates for the Sec-dependent pathway of YidC, also called 'SRP-dependent pathway of YidC', are SecE (Yi et al. 2003), leader peptidase (Houben et al. 2000; Samuelson et al. 2000; Houben et al. 2004), subunits a and b of the *Escherichia coli* F_1F_o-ATP synthase (Yi et al. 2003; Yi et al. 2004) and the bacterial secretory lipoproteins Mpp and Brp (Fröderberg et al. 2004). Also inserted by the Sec-dependent pathway of YidC are CyoA, the bacterial counterpart of Cox2 (van der Laan et al. 2003; van Bloois et al. 2006) as well as LacY, which folds in a wrong conformation into the cytoplasmic membrane if YidC is depleted (Nagamori et al. 2004). It has been shown that YidC also supports the SecA-dependent translocation of a hydrophilic protein across the membrane, which carries a hydrophobic signal sequence and is targeted by SRP to SecYEG (Pradel et al. 2005). Also CyoA is integrated in a mechanism employing concerted SRP, SecA and YidC (van Bloois et al. 2006). This suggests that the distinct translocation pathways are not mutually exclusive. Mitochondria lack a Sec-translocase (Glick and Von Heijne 1996). Therefore, Tim23 together with Oxa1 might play principally the same role as SecYEG and YidC in membrane protein insertion (Reif et al. 2005), and the same mechanism might be resembled in the interaction of SecY and Alb3 (Klostermann et al. 2002; Moore et al. 2003).

5.3.2 Sec-independent function

The phage coat proteins M13 procoat and Pf3 coat that require no Sec-translocon for their membrane integration and which were previously believed to insert spontaneously into the membrane of *Escherichia coli*, were demonstrated to require YidC (Ohno et al. 1983; Wolfe et al. 1985; Rohrer and Kuhn 1990; Cao and Dalbey 1994; Kiefer and Kuhn 1999; Samuelson et al. 2000; Samuelson et al. 2001; Chen et al. 2002a). The Sec-independent integration of Pf3 coat could also be reconstituted *in vitro* with purified YidC (Serek et al. 2004). Therefore, like Oxa1, YidC also has a dual function and mediates the integration of proteins Sec-dependently and Sec-independently (Chen et al. 2002a; Reif et al. 2005) (Fig. 3). An endogenous substrate for the Sec-independent pathway of YidC is subunit c of the *Escherichia coli* F_1F_o-ATP synthase (Yi et al. 2003; Yi et al. 2004; van der Laan et al. 2004a). Insertion by the Sec-independent pathway of YidC does not seem to require a membrane potential (Kuhn et al. 1990; Samuelson et al. 2001; Serek et al. 2004; Yi et al. 2004; van der Laan et al. 2004a). YidC does not affect the targeting and adhesion of Sec-

independent proteins to the membrane (Chen et al. 2002b). For translocation of some or all substrate proteins translocated via the Sec-independent route, translating ribosomes seem to be targeted by the SRP to YidC (Fröderberg et al. 2003; van Bloois et al. 2004; van Bloois et al. 2006; Facey et al. 2007). Mechanistic details of this targeting process however are unclear.
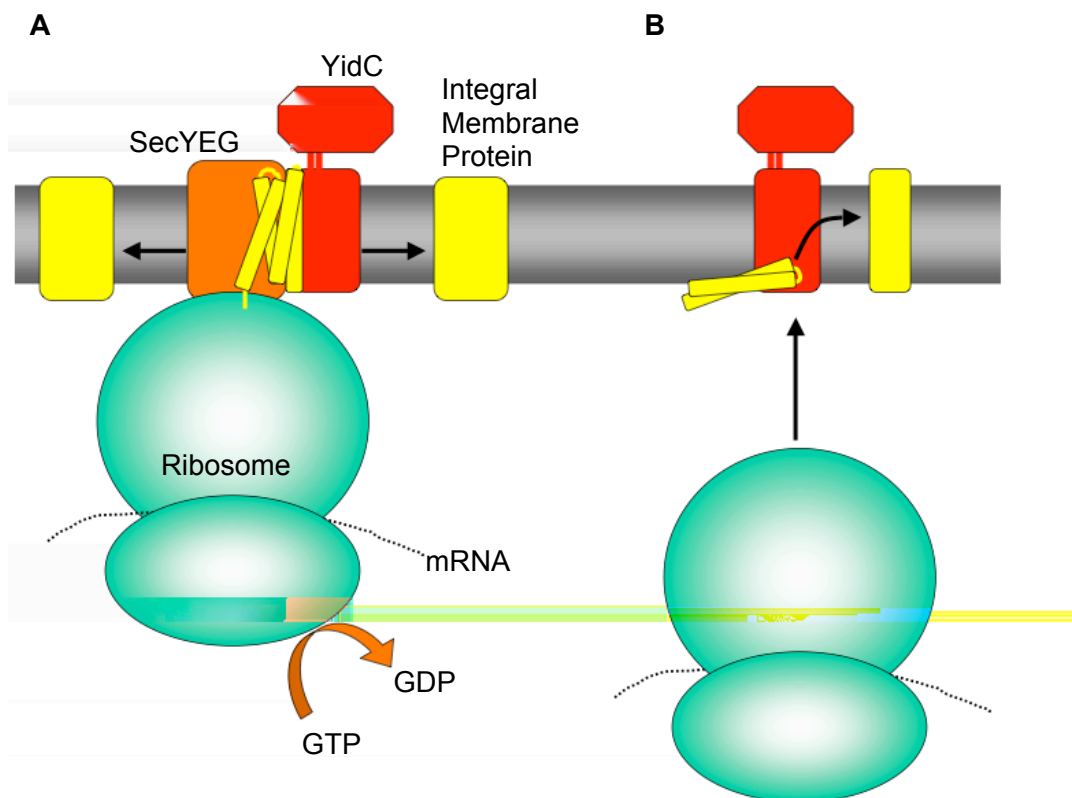
Fig. 3   Pathways of YidC-mediated membrane protein insertion. Sec-dependent (**A**) and Sec-independent (**B**) insertion. Not depicted is the putative junction between SecYEG and YidC, formed by SecDF or SecDFyajC complexes.

5.3.3   Biogenesis and topology of YidC

YidC is predominantly localised at the cell poles with an abundance of 2500 to 3000 copies per cell (Urbanus et al. 2002). Assuming 100 to 200 functional SecYEG complexes exist per cell, substantial amounts of YidC likely might stay unassociated which could include the fraction mediating Sec-independent membrane protein insertion (Urbanus et al. 2002). YidC has a size of 548 amino acids, a molecular weight of 60 kDa and spans the cytoplasmic membrane six times. Its amino- and carboxy-termini are on the cytoplasmic side (Sääf et al. 1998). The amino acid stretches similar amongst homologues of YidC are located in YidC within residues

355 to 371 in transmembrane helix 2, in residues 413 to 437 in helix 3 and in residue 497 to 524 in helix 5 and 6 (Yen et al. 2001).

The first amino-terminal transmembrane helix of YidC serves as an uncleaved signal sequence (Sääf et al. 1998). Transmembrane helices 1 and 2 are connected by a soluble periplasmic domain of 319 amino acids, which hence correlates with 58 % of the entire protein (Sääf et al. 1998). This loop is much smaller or even missing in many YidC homologues (Yen et al. 2001) and could be almost entirely depleted without visible phenotypes (Jiang et al. 2003). Probably, the soluble periplasmic domain of YidC serves to build-up a connection to SecF and SecDFyajC, respectively (Xie et al. 2006). YidC itself is assembled in the cytoplasmic membrane in a sequential action of SRP and SecA, whereas YidC does not support its own assembly (Koch et al. 2002; Urbanus et al. 2002). SecA is supposably required to translocate this large first periplasmic loop of YidC across the membrane (Deitermann et al. 2005).

The activity of YidC could not be knocked out completely by mutations of single residues (Jiang et al. 2003). Even tyrosine 516, which represents the only conserved amino acid throughout all Oxa1 homologues, could be changed to a serine without abolishing cell growth, although this impaired the proper translocation of the investigated substrates (Yen et al. 2001; Jiang et al. 2003). The same could be shown for five other residues, which are located in transmembrane helices 2 and 3 (Jiang et al. 2003). The activity of YidC depends obviously on the hydrophobicity of the conserved regions and not on particular amino acid side chains (Jiang et al. 2003). All deletions in the conserved core formed by the five carboxy-terminal helices of YidC lead to inactive protein (Jiang et al. 2003). In contrast, helices 4 and 5 could be completely exchanged by transmembrane segments of a non-related protein with no or only minor effects on the activity of YidC (Jiang et al. 2003). The last carboxy-terminal 13 amino acid residues of YidC could be removed completely without an effect on translocation or cell viability (Jiang et al. 2003).

6 Crystallographic studies of membrane proteins

6.1 Protein crystals

Crystals are a regular repetition of a smallest crystallographic unit, called the 'unit cell'. A repetition of the unit cell in two directions of space yields a two-dimensional,

in three directions a three-dimensional crystal. Proteins form crystals due to highly specific hydrogen or salt bridges or sometimes van-der-Waals interactions between the molecules (crystal contacts).

6.2 Purification

Often a particular membrane protein of interest is not well expressed in its natural environment. Therefore, the expression of these membrane proteins has to be artificially enhanced (over-expression) in order to facilitate the purification of the large amounts of protein required for crystallographic studies. Because of their hydrophobic nature, membrane proteins have to be solubilised with detergents to make the proteins accessible for analytical methods, performed in aqueous media. The hydrophobic chains of the detergents shield the hydrophobic parts of the membrane proteins. The polar head groups of the detergents protrude into the aqueous environment to form a hydrated shell to create a water-soluble protein-detergent complex. Specifically bound lipids may also be required for the stabilisation of the proteins. As detergents are artificial supplements required for membrane protein solubilisation, they also interfere with many analytical methods and particularly affect the formation of protein crystals. Therefore, the choice of detergent is a challenge in membrane protein purification, and is one of the major challenges in a structural analysis of these proteins.

6.3 Electron crystallography

The determination of (membrane) protein structures to high, occasionally to atomic resolution by electron microscopy of two-dimensional crystals is called 'electron crystallography'. Structure determination is usually achieved in two stages: first, by the determination of a two-dimensional projection structure, and second in the reconstruction of a three-dimensional structure. Examples are the projection structure of SecYEG (Collinson et al. 2001) and the high-resolution three-dimensional reconstructions of bacteriorhodopsin (Henderson et al. 1990) or LHC-II (Kühlbrandt et al. 1994).

6.3.1 Two-dimensional crystallisation of membrane proteins

Proteins, which are embedded in a lipid bilayer, can form crystal contacts between adjacent molecules. Two-dimensional membrane protein crystals form roundish 'vesicles', tubular proteoliposomes (tubes) or membrane layers (sheets). Two-dimensional crystals can also be formed by multiple membrane layers stacked on top of each other; for example two membrane layers of SecYEG form a single two-dimensional crystal (Collinson et al. 2001). For a crystallographic investigation, mono-layered two-dimensional crystals are preferred since the diffraction patterns of multiple crystal layers can often not be dissected, which then creates problems in the later data analysis or makes the analysis even impossible. Some membrane proteins form two-dimensional crystals naturally (Fig. 4). Two-dimensional crystals of membrane proteins can form *in vitro* by an enzymatic depletion of lipids from natural membranes (Mannella 1984; Misra and Malhotra 1985), an incubation of natural membranes with salts (Dux et al. 1985) or salt precipitation of solubilised membrane proteins (Kühlbrandt et al. 1983).
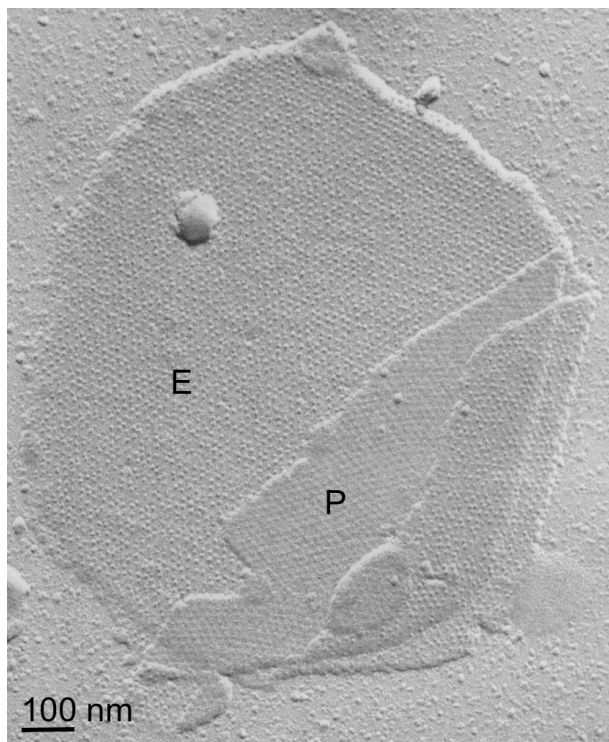
Fig. 4   Electron micrograph of a natural two-dimensional crystal. Photoreceptors in the thylakoid membrane of *Rhodopseudomonas viridis*. The membranes were shadowed with heavy metals for contrast enhancing. Double membrane. E: Exoplasmic surface. P: Plasmic surface, located in the interface between the two membranes. By courtesy of Prof. Dr. Werner Kühlbrandt.

In a different *in vitro* approach, the detergent can be removed from mixtures of purified detergent-solubilised membrane proteins and lipids. Thereby, the lipid to protein ratio (LPR) describes the ratio of lipid to protein in the crystallisation or

reconstitution sample - or of membrane proteins in lipid bilayers in general. During appropriate conditions, the membrane proteins then insert (reconstitute) densely into the resulting lipid membranes and form crystalline lattices. The detergent removal can be done by dialysis (Unwin and Henderson 1975; Dorset et al. 1983; Barnakov et al. 1990), by a detergent adsorption on hydrophobic material (Li and Hollingshead 1982; Rigaud et al. 1997) or by dilution (Jap et al. 1990; Walian and Jap 1990; Dolder et al. 1996).

6.3.2 Transmission electron microscopy

In 1931, Max Knoll and Ernst Ruska developed the first transmission electron microscope (TEM). Subsequently, the TEM has become a valuable tool for observing biological samples down to subcellular structures and macromolecules. Transmission electron microscopes contain principally the same arrangement of lenses as light microscopes. The smallest resolvable spatial distance between two objects that can be resolved by a microscope is related to the wavelength of the incident light or in this case electron wave. Since electrons have a much shorter wavelength than visible light waves, the resolution attainable by electron microscopes is much higher compared to light microscopes, by about 1,000 times; although the wavelength of electron waves is about 100,000 times shorter than that of light waves, electromagnetic lenses used to focus the electrons are more imperfect than the glass lenses used to focus light, which decreases the achievable resolution in electron microscopy.

Electrons interact strongly with atoms or any molecule in their path. Therefore, the whole electron microscope has to work under high vacuum. A technical hallmark of electron microscopes is the electron acceleration voltage. For the investigation of biological samples, acceleration voltages of 120 to 300 kV are state of the art (Frederik et al. 1991). For high-resolution data collection, field emission guns (FEGs) that produce an electron beam of high coherence are often used as electron source. A FEG consists basically of a tungsten crystal from which electrons are extracted by a strong electric field. In order to collect data of frozen-hydrated specimens, electron microscopes can be operated at liquid nitrogen (100 K) or even liquid helium (4 K) temperature (Fujiyoshi 1989; Fujiyoshi et al. 1991).

Sample preparation

The contrast of the specimens in the electron microscope can be increased by staining with heavy metal salts. The heavy metal salts attach to the protein surfaces and create a cast of the sample (negative stain) (Brenner and Horne 1959). Negative staining with uranyl acetate is fast, provides a high contrast and a long-term stability of the sample. However, the diameter of the uranyl grains reduces the theoretically possible resolution to about 15 Å and the ionic strength and pH of the reagent can produce staining artefacts and specimen deformation. Furthermore, only water-accessible parts of the specimen can be stained with uranyl acetate, which is a particular drawback for the investigation of membrane-embedded proteins.

For the acquisition of high-resolution data, the samples are usually investigated in the frozen-hydrated state (electron cryo-microscopy), which resembles the natural hydration state of the proteins. Furthermore, resolution is not limited by staining reagents and staining artefacts are avoided in electron cryo-microscopy. At low temperature the diffusion of fragments and radicals in the samples is slower and beam induced damage of organic samples is reduced (Knapek and Dubochet 1980). During the freezing procedure, the formation of damaging ice crystals must be prevented. This is achieved by freezing the specimens in liquid ethane or propane, which yields freezing rates that exceed the speed of the ice crystal formation (vitrification) (Dubochet et al. 1988). A complete vitrification thereby takes place at freezing rates of about 3×10^6 K/sec (Bald 1986). Alternatively, hydrophilic substances (cryo-protectants) such as glucose (Unwin and Henderson 1975), trehalose or tannin (Wang and Kühlbrandt 1991) can be used to preserve the hydrated state of proteins in the electron microscope. Contrast in electron microscopy is determined by the density difference of the analysed specimen and the surrounding medium (Dubochet et al. 1983). Therefore, higher amounts of sugars in the medium on the other hand can abolish contrast in the electron cryo-microscopic analysis of proteins (De Carlo et al. 1999). Parameters like the thickness of the ice layer and the type of the protecting substances influence the data collection tremendously and require a careful screening of freezing conditions.

Data collection

Images in the electron microscope can be recorded in digital format with a CCD camera. The latter is often useful in the immediate assessment of sample quality.

However, the collection of high-resolution data with CCD cameras is limited because of the large pixel size. Therefore, high-resolution data is nearly always collected on film. The films are then scanned for computational processing. Charging and heating of the specimen during data collection causes specimen drift, which impairs the data quality. This can be avoided by exposing the specimen to series of small spots (spot scan mode) instead of exposing it at once (Downing 1991).

Either images or electron diffraction patterns of the crystalline specimens can be recorded; electron diffraction does not suffer from specimen drift and lens imperfections, but is usually only suitable if the two-dimensional crystal lattices are very well-ordered and have diameters of approximately 1 μm or more. Furthermore, diffraction patterns contain no phase information, which is required for image reconstruction and therefore has to be obtained from other sources. The primary data from a single exposure of a two-dimensional crystal delivers only two-dimensional information. For the reconstruction of three-dimensional structures, data from tilted specimens are also required. Since the maximum tilt angle in an electron microscope is technically limited to about 60 °, the information in the third dimension is incomplete. This is a limitation in electron crystallography, known as the 'missing cone problem'.

6.3.3   Image processing

The signal to noise ratio of the primary data from two-dimensional crystals is initially low because of lattice imperfections, beam damage and the fact that images are usually taken close to focus in order to achieve a high-resolution of the structural details. For the purpose of increasing the signal to noise ratio, the data is usually filtered in digital format (filtering) and lattice imperfections are computationally corrected (unbending). For this, electron microscopic images are converted by Fourier transformation into 'reflections' in Fourier space, the latter also called 'reciprocal space'. The original image is thereby broken down into the amplitude and the phase of each reflection and by the pattern formed by the reflections in Fourier space (reciprocal lattice), respectively. The filtering and unbending, also called 'image processing', is described in more detail in Material and Methods, chapter 6. The computational procedures were originally developed from the programs used for the processing of X-ray crystallographic data (Henderson and Unwin 1975; Unwin and Henderson 1975).

6.4 X-ray crystallography

The determination of molecular structures by X-ray diffraction of three-dimensional crystals is called 'X-ray crystallography'. The first protein structure obtained by X-ray diffraction was reported about 50 years ago (Kendrew et al. 1958).

6.4.1 Three-dimensional crystallisation of membrane proteins

Three-dimensional membrane protein crystals can be thought of either stacked two-dimensional crystals (type 1), for example LHC-II (Standfuss et al. 2005), or created by crystal contacts between hydrophilic portions of proteins embedded in detergent micelles (type 2), for example NhaA (Screpanti et al. 2006). Type 2 membrane protein crystals therefore resemble the three-dimensional crystals of soluble proteins. In both membrane protein crystal types, the crystal contacts are mainly established between the membrane-exposed loops of the proteins. In order to achieve three-dimensional crystals, the membrane proteins are precipitated by agents that decrease their solubility (precipitants) and by increasing the protein concentration, respectively. Often vapour diffusion of water between a reservoir (mother liquor) and the protein/precipitant mixture (crystallisation drop) is used to increase the concentration of the protein and the precipitant. Like two-dimensional crystallisation, this usually requires an elaborate screening of all involved components.

The primary data obtained by X-ray crystallography consists of diffraction patterns, similar to the primary data obtained by electron diffraction. In this way, data can be collected from all orientations of the crystal in the X-ray beam; the missing cone problem therefore usually does not exist in X-ray crystallography. For data collection, the three-dimensional protein crystals are also usually cryo-preserved. Crucially, the primary data from X-ray crystallography lacks the phase information, which has to be determined indirectly experimentally (Taylor 2003). In some cases, electron crystallographic data can be used to provide the phase information for X-ray crystallographic data (Penczek et al. 1999; Standfuss et al. 2005) or vice versa (Gonen et al. 2004; Gonen et al. 2005).

7 Objectives

Structures have been determined of SecYEG, SecA and the ribosome - all components of the co- and post-translational translocation process. Only a low-resolution structure of the active complex has been determined (Mitra et al. 2005), and the conclusions they report are controversial. Therefore, the objective of the first project was to yield a projection structure of SecYEG with bound substrate and to compare it with a former one of SecYEG without substrate in order to yield information of SecYEG involved in translocation.

The second part of the work was directed to an analysis of YidC. Although all Oxa1 homologues fulfil important functions in the biogenesis of integral membrane proteins, no structural information is available for YidC or other members of the Oxa1 family of proteins. Therefore, the objective of the second project was to visualise YidC in the membrane. In order to achieve this goal, aim of the project was to grow two-dimensional crystals of YidC and to obtain a projection structure from the frozen-hydrated crystals.

Material and Methods

1   Standard laboratory chemicals and detergents

Standard laboratory chemicals were purchased from Sigma-Aldrich, Munich and Roth, Karlsruhe, respectively. $C_{12}E_9$ was purchased from Sigma-Aldrich. OG, DM and DDM were purchased from Glycon, Luckenwalde, Cymal 5, 6 and 7 from Anatrace, U.S.A.

2   Preparation of membrane proteins

2.1   Media

LB	10 g/l tryptone, 5 g/l yeast extract, 10 g/l NaCl
LB-agar plates	LB-medium supplemented with 15 g/l agar
2xYT	16 g/l tryptone, 10 g/l yeast extract, 5 g/l NaCl

Tryptone and yeast extract for bacterial growth media were purchased from BD Diagnostics, U.S.A. If required, the media were supplemented with ampicillin (0.2 μm filtered for sterilisation) after autoclaving and cooling down to approximately 55 °C.

2.2   Amplification and preparation of plasmid DNA

Escherichia coli XL1-Blue cells competent for the uptake of plasmid DNA (subcloning grade, Stratagene, U.S.A.) were transformed by heat-shock (45 secs at 42 °C) with plasmid DNA in accordance to the delivered protocol. Cells expressing the plasmid DNA were selected on LB-agar plates containing 100 μg/ml ampicillin. Selected colonies were amplified in LB-medium supplemented with 100 μg/ml ampicillin. Plasmid DNA was isolated from the cells using a QIAPrep Spin Miniprep Kit (Quiagen), following the delivered protocol (plasmid DNA eluted in buffer EB), employing a modified alkaline lysis (Birnboim and Doly 1979).

2.3 SecYEG

SecYEG was prepared as described (Collinson et al. 2001). In brief, *Escherichia coli* C43 cells (strain of *Escherichia coli* BL21 D3 (Miroux and Walker 1996)) were transformed with the operon coding for SecY, SecE and SecG, cloned into the tightly repressed arabinose-inducible pBAD/Myc-His expression vector (Invitrogen, Karlsruhe); by cloning of SecYEG into the pBAD/Myc-His expression vector, the open reading frame for SecE had been extended genetically by six amino-terminal His-residues (His-tag). The plasmid (pBAD/SecYEG/Myc-His) was a friendly gift from Dr. Ian Collinson. Cells were grown to an OD_{560} of 0.8, and over-expression of SecYEG was induced by addition of 0.2 % w/v arabinose. After 3 h, the cells were pelleted by centrifugation (4000 RPM, 10 °C, JS 4.2 rotor, Beckman Coulter, U.S.A.) and membranes were prepared from the cells.

Membrane proteins were solubilised with 1.5 % w/v OG in TSG (300 mM NaCl, 10 % v/v glycerol, 20 mM Tris-HCl, pH 8; 150 ml for membranes of 30 l cell culture). Membrane debris was removed by centrifugation (40000 RPM, 1 h, 4 °C, 45 Ti rotor, Beckman Coulter, U.S.A.) and SecYEG was purified by Nickel-chelating, size-exclusion (Superdex 200 26/60 prep grade gel filtration column, Amersham Pharmacia, U.S.A.) and anion-exchange chromatography. Final buffer of SecYEG was 120 mM NaCl, 0.2 % w/v $C_{12}E_9$, 20 mM Tris-HCl, pH 8.

2.4 YidC, $YidC_{\Delta278}$ and $YidC_{\Delta323}$

2.4.1 Plasmids

Over-expression of wild-type YidC

pBAD/YidC/Myc-His

Open reading frame coding for YidC, cloned into the tightly repressed arabinose-inducible pBAD/Myc-His expression vector (Invitrogen, Karlsruhe); by cloning into the pBAD/Myc-His expression vector, the open reading frame for YidC had been extended genetically by six carboxy-terminal His-residues (His-tag). The construct was a friendly gift from Dr. Ian Collinson.

Over-expression of truncated YidC

<u>pProEX/YidC$_{\Delta278}$/His and pProEX/YidC$_{\Delta323}$/His</u>

YidC truncated between amino acids 25 and 278 (YidC$_{\Delta278}$) and 25 and 323 (YidC$_{\Delta323}$), respectively, cloned into an IPTG-inducible expression vector (pProEX). In addition, YidC$_{\Delta278}$ and YidC$_{\Delta323}$ had been genetically extended by each time six carboxy-terminal His-residues (His-tags). The constructs were a friendly gift from Dr. Ross Dalbey and co-workers (Ohio State University, U.S.A.).

2.4.2   Over-expression and purification

Optimal detergents and gel filtration buffers are shown in chapter 8, Tab. 1 and Tab. 2, respectively.

Over-expression

Escherichia coli C43 cells (strain of *Escherichia coli* BL21 D3 (Miroux and Walker 1996), friendly gift from Sir John Walker) were prepared for uptake of plasmid DNA by treatment with ice cold CaCl$_2$-solution (0.1 M) and subsequently transformed by heat-shock (90 secs at 42 °C) with the respective genetic construct (2.4.1). Cells with plasmid DNA were selected on LB-agar plates containing 100 μg/ml ampicillin. From the selected colonies, pre-cultures (LB-medium, 100 μg/ml ampicillin) were prepared. 5 l Erlenmeyer flasks containing 2.5 l of 2xYT-medium supplemented with 100 μg/ml ampicillin were inoculated with each time 5 ml pre-culture. The cells were grown to an OD$_{560}$ of 0.8 (150 RPM, 37 °C, Multitron, Infors, Einsbach). Over-expression was induced by addition of 0.2 % w/v arabinose (YidC) or 0.5 mM IPTG (YidC$_{\Delta278}$, YidC$_{\Delta323}$). After 3.5 h cultivation, cells were pelleted by centrifugation (4000 RPM, 10 °C, JS 4.2 rotor, Beckman Coulter, U.S.A.).

Membrane protein solubilisation

Pelleted cells were resuspended in TSG (300 mM NaCl, 10 % v/v glycerol, 20 mM Tris-HCl, pH 8) and subsequently disrupted (cell disruptor, Constant Cell Disruption Systems, U.K.). The membrane fraction was sedimented by centrifugation (40000 RPM, 1 h, 4 °C, 45 Ti rotor, Beckman Coulter, U.S.A.) and the supernatant discarded. Membranes from 30 l cell culture were resuspended in 170 ml ice-cold TSG buffer

containing detergent. The suspension was homogenised with a glass homogeniser (ice). The homogenised suspension was stirred for 1.5 h at 4 °C and clarified by centrifugation (40000 RPM, 1 h, 4 °C, 45 Ti rotor).

Nickel-chelating chromatography

From the crude membrane extracts, YidC, YidC$_{\Delta 278}$ and YidC$_{\Delta 323}$ were purified employing specific binding of their His-tags (2.4.1) to immobilised Ni^{2+}-ions (Nickel-chelating chromatography) (Porath et al. 1975).

Solubilised membrane proteins from 30 l of cell culture were applied onto a column (Bio-Rad, U.S.A.) packed with approximately 8 ml Fast Flow Chelating Sepharose™ (Amersham Pharmacia, U.S.A.). The column was sequentially washed with 20 ml water, 20 ml NiCl$_2$ solution (0.3 M), 30 ml TSG (300 mM NaCl, 10 % v/v glycerol, 20 mM Tris-HCl, pH 8) and 15 ml TSG supplemented with detergent. Column-bound protein was washed with 250 ml TS (300 mM NaCl, 20 mM Tris-HCl, pH 8), supplemented with detergent and 30 mM imidazole. The protein was eluted with TS buffer containing detergent and 300 mM imidazole. The eluate was collected in fractions.

Size-exclusion chromatography

YidC, YidC$_{\Delta 278}$ or YidC$_{\Delta 323}$ in the protein containing fractions eluted from Nickel-chelating chromatography was further purified using size-exclusion chromatography (gel filtration) (Lathe and Ruthven 1956; Lindner et al. 1959; Porath and Flodin 1959; Porath 1960). The purification was performed at room temperature using a Sephacryl S-300 (26/60) HR gel filtration column (Amersham Pharmacia, U.S.A.) with buffer containing detergent. The YidC containing eluate was collected in fractions. For three-dimensional crystallisation, purified YidC was concentrated in a Centriprep® device (MWCO 50 kDa, Amicon Bioseparations, Millipore, U.S.A.) and subsequently dialysed (2 days, 4 °C, MWCO 14 kDa) in the gel filtration buffer in order to reduce the detergent concentration.

3 Two-dimensional crystallisation

3.1 Preparation of lipid in detergent solution

From the lipid (Avanti® Polar Lipids, U.S.A.), chloroform was removed by evaporation (nitrogen flow). The dried lipid was resolved by stirring (4 °C or room temperature) and in some cases sonication (Sonorex Super AK 102 P, Bandelin, Berlin) in water containing detergent.

3.2 SecYEG/LamB$_{SP}$

Purified SecYEG was diluted to a concentration of 3.3 µM in respect to the SecYEG monomer. Thereby, the detergent in the protein/lipid mixture was adjusted to 0.11 % w/v $C_{12}E_9$. The diluted SecYEG was mixed with PE lipid (4 mg/ml, dissolved in 1 % w/v DM; LPR 1.5 - 0.2 w/w) and 0.36 µM LamB signal sequence peptide (H-MMITLRKLPLAVAVAAGVMSAQAYAC-NH$_2$, synthesised with an additional carboxy-terminal thyrosine for radioactive labelling, Jerini Peptide Technologies, Berlin); using this set-up, the absolute ratio of LamB peptide and SecYEG was about 36 moles LamB peptide per mol of monomeric SecYEG. Two-dimensional crystallisation was performed by dialysis (120 mM NaCl, 2 mM NaN$_3$, 1 mM EDTA, 0.48 µM LamB peptide, 20 mM Tris-HCl, pH 8; buffer to sample ratio: 250:1 v/v).

In order to adsorb detergent, hydrophobic beads (Bio-Beads®, SM-2 adsorbent, Bio-Rad, U.S.A.) were washed with methanol and water, filled into dialysis bags (MWCO 12 - 14 kDa, Roth, Karlsruhe or Spectrum Laboratories, U.S.A.) and added into the dialysis buffer.

3.3 YidC

In order to achieve the two-dimensional crystallisation of YidC, detergent was removed by dialysis from mixtures containing solubilised YidC and lipids. Used dialysis devices were membrane bags (Roth, Karlsruhe or Spectrum Laboratories, U.S.A.), bent glass tubes sealed at one end with a membrane (hockey sticks) or pre-casted dialysis devices (Slide-A-Lyzer® cassettes, Pierce, U.S.A.). The MWCO of the membranes was in the range between 12 and 14 kDa; in some experiments, a MWCO of 50 kDa was used. Employing optimised conditions, dialysis buffers were

100 mM NaCl, 2 mM NaN_3, 1 mM EDTA, 20 mM ADA, pH 5.6 for reconstitution (buffer 1; dialysis buffer to sample ratio: 1:1000 v/v) and 2 mM NaN_3, 1 mM EDTA, 20 mM ADA, pH 5.6 for induction of crystal formation (buffer 2; dialysis buffer to sample ratio: 1:500 v/v). The dialysis was carried out for 7 days at 30 °C (buffer 1) and 3 days at 20 °C (buffer 2).

Dilution

Alternatively to a detergent removal by dialysis, the protein/lipid mixture was stepwise diluted below the CMC (dilution buffer: 2 mM NaN_3, 1 mM EDTA, 20 mM ADA, pH 5.6; various schedules) in order to achieve a crystallisation of YidC.

Buffer incubation of reconstituted YidC specimens

10 μl of the reconstituted YidC was transferred into an Eppendorf cup and gently mixed with 190 μl buffer (various). The diluted specimens were incubated over night (4, 20, 25 or 30 °C).

4 Three-dimensional crystallisation of YidC

Three-dimensional crystallisation experiments were conducted by vapour diffusion in a hanging drop set-up (Davies and Segal 1971). 500 μl of mother liquor were pipetted into wells of a 24 well cell culture plate (Hampton Research). Drops of 0.8 to 1 μl protein solution were pipetted onto silanised cover slides and mixed with the equal volume of mother liquor (optimised conditions see chapter 8, Tab. 2). The wells were closed with the cover slides and a ring of silicone for sealing. The plates were incubated at 18 °C and sequentially checked with a light microscope (Carl Zeiss, Jena).

5 Electron microscopy

5.1 Carbon support film and carbon-coated grids

An approximately 100 Å thick layer of carbon was evaporated onto the surface of freshly split mica using a carbon evaporator (Edwards Auto 306 Turbo, Edwards High Vacuum International, U.K.).

For the preparation of carbon-coated grids, copper grids (400 squares per grid) were washed with acetone and arranged in a water-filled carbon coating tank (produced by workshop of Max-Planck-Institute of Biophysics) below the water surface on filter paper. Carbon film on mica was moistened by incubation for about 1 h in a sealed dish containing wet filter paper for facilitating the detaching of the carbon film. The carbon was floated in the coating tank and layered onto the grids by water removal. In order to make the carbon less hydrophobic, the dried carbon-coated grids were glow discharged (25 secs, $\approx$ 10 mA, CTA 010, Balzers Union, Liechtenstein).

5.2   Staining with uranyl acetate

0.9 µl sample was applied onto a carbon-coated glow-discharged electron microscopy grid. After 30 secs, excessive sample was blotted off with filter paper. The sample was immediately washed and stained with 2 x 1.3 µl uranyl acetate solution (1 % w/v); the second portion uranyl acetate was left for approximately 20 secs on the grid in order to achieve sufficient staining.

5.3   Preparation of frozen-hydrated specimens

5.3.1   Cryo-protectant embedding

In order to freeze specimens in amorphous ice, the back injection method (Wang and Kühlbrandt 1991) was used: an approximately 3 x 3 mm large piece of carbon was floated on the surface of 0.5 ml cryo-protectant solution (embedding medium) and picked up with an electron microscopy grid. The grid was brought in contact to the surface of the embedding medium in order to remove excessive carbon. The grid was inverted and about 2 µl of sample was applied on the not carbon covered side (back side). The sample was mixed on the grid with embedding medium containing various cryo-protectants. The grid was inverted again and blotted with the sample side onto filter paper. Afterwards, the sample was frozen in liquid nitrogen.

5.3.2   Vitrification in liquid ethane

Vitrobot™

Freezing in liquid ethane was done with a vitrification robot (Vitrobot™, FEI Company, U.S.A.). Using the Vitrobot™, the blotting and the plunging conditions could be accurately controlled with respect to temperature and humidity. Furthermore, the Vitrobot™ was equipped with a pneumatic guillotine. The guillotine served to plunge the samples with a high velocity into the liquid ethane in order to obtain high freezing rates.

The freezing pot was pre-cooled with liquid nitrogen and the outer chamber was filled with liquid nitrogen. Ethane gas was condensed on the cold metal surface of the inner chamber to form liquid ethane. A carbon-coated glow-discharged electron microscopy grid (5.1) was clamped into a pair of Vitrobot™ tweezers. 0.9 µl sample was pipetted onto the side of the carbon support film facing away from the electron microscopy grid (front side). The sample was left for about 30 secs in order to allow the settling of the specimens onto the carbon. The pair of tweezers holding the grid was placed into the Vitrobot™. After blotting, the sample was plunged into liquid ethane. Excessive ethane was stripped off from the grid with a liquid ethane-drenched filter paper and the grid immediately frozen in liquid nitrogen.

Manual blotting and plunging

A glow-discharged carbon-coated electron microscopy grid was clamped into a pair of tweezers. 0.9 µl of sample were pipetted onto the side of the carbon support film facing away from the electron microscopy grid (front side). The grid was blotted with the front side onto dry filter paper. After blotting, the samples were briefly dried (about 20 secs at 20 % humidity) and plunged into liquid ethane. The plunging was thereby done either by hand or by using the Vitrobot™. Excessive ethane was stripped off with a liquid ethane-drenched filter paper and the grid immediately frozen in liquid nitrogen.

Alternatively, the filter paper used for blotting was moistened with buffer (20 mM ADA, pH 5.6) in before blotting. Otherwise, the vitrification was carried out as described for dry filter paper.

As a further option, the grid was laid with the opposite side (back side) onto dry filter paper. Then, the excessive sample became sucked off from the grid as soon

as the liquid came at the edge of the grid into contact with the filter paper. This served to avoid a direct contact between the specimens and the filter paper and in order to retain more specimens on the carbon film. Otherwise, the vitrification was carried out as described for blotting of the front side.

Vitrification between two layers of carbon film

The sample was prepared according to (Koning et al. 2003; Gyobu et al. 2004). Two pieces of carbon ($\approx$ 3 x 3 mm) were floated on drops ($\approx$ 0.5 ml) of buffer (20 mM ADA, pH 5.6). One piece of carbon was picked up with an electron microscopy grid. The grid was brought into contact with the buffer surface in order to remove excessive carbon. Afterwards, excessive buffer was blotted off from the grid using a filter paper. Subsequently, 1 µl of sample was pipetted onto the not carbon covered side of the grid. By using a platinum loop ($\approx$ 5 mm diameter), the second piece of carbon was transferred in a buffer lens onto the grid, such that the sample was enclosed between the two layers of carbon. Excessive liquid between the two carbon layers was removed by blotting the side of the grid onto filter paper. After blotting, the samples were plunged manually into liquid ethane. Excessive ethane was stripped off with a liquid ethane-drenched filter paper and the grid immediately frozen in liquid nitrogen.

5.4   Recording of crystal images by electron microscopy

Images from negatively stained specimens were recorded using a CM12, CM120 or a Tecnai Spirit electron microscope (all 120 kV acceleration voltage, all FEI Company, U.S.A.). Images of frozen-hydrated specimens were recorded with a Tecnai Spirit, Tecnai F20 (acceleration voltage 200 kV, FEG, FEI Company, U.S.A.) or JEOL 3000 SFF (acceleration voltage 300 kV, FEG, JEOL, Japan) electron microscope; the latter type of electron microscope was equipped with a spotscan camera working in the set-up developed by Ivo Tews (Tews 1991): the electron beam was deflected by computer-controlled changes of the condenser lens current. 24 x 30 single spots recorded on film formed one image. Each spot was exposed for 40 to 42 msecs.

The JEOL 3000 SFF electron microscope was operated at liquid helium temperature. All other microscopes were run at liquid nitrogen temperature. Grids with frozen-hydrated specimens were transferred into the pre-cooled electron

microscopes using cryo-specimen holders (for CM12, CM120, Tecnai Spirit and Tecnai F20 purchased from Gatan, U.S.A.).

Images (negative stained and frozen-hydrated specimens) were recorded employing low-dose conditions (Williams and Fisher 1970). Thereby, films (SO-163, Eastman Kodak Company, U.S.A.) were exposed to only half saturation. The low-dose conditions were employed for not exceeding a total electron dose of 10 (liquid nitrogen temperature) or 25 (liquid helium temperature) electrons per Å^2. Image magnifications were 45,000x to 70,000x (frozen-hydrated specimens) and 3,200x to 45,000x (negative stain), respectively. Alternatively to film, images of negatively stained specimens were recorded using CCD cameras (1,000 x 1,000 or 2,000 x 2,000 pixels, Gatan, U.S.A.).

Films exposed to half saturation were developed for 12 min using full-strength developer (D-19, Eastman Kodak Company, U.S.A.), washed for 1 min in distilled water, fixed (fixer: Eastman Kodak Company, U.S.A.) for 8 min and washed for 30 min in water. Afterwards, the films were rinsed for 1 min in photo-flow and dried.

5.5 Freeze-fracture analysis

In order to visualise membrane-embedded proteins, lipid bilayers can be split by applying freeze-fracturing. Thereby artificial surfaces are generated between the two lipidic half membrane layers (Fig. 5). Membrane proteins retained in both half membranes can then be visualised in an electron microscope by shadowing with heavy metals.
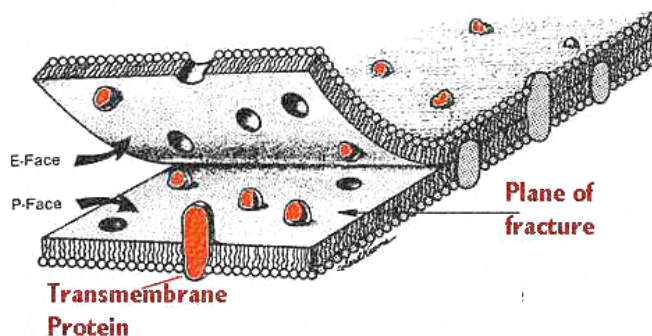
Fig. 5   Scheme of membrane splitting by freeze-fracturing. P-Face: Protoplasmic fracture face. E-Face: Exoplasmic fracture face. Modified from www.cytochemistry.net, original in (Bloom and Fawcett 1994).

Proteoliposomes (1 to 2 μl) were frozen in liquid ethane between two small copper plates serving as sample holders. The freeze-fracturing was carried out with a BAF 400T machine (Balzers Union, Liechtenstein) at a temperature of -140 °C and a

pressure of 2 x 10^{-7} mbar. After the fracture, the sample was shadowed with platinum/carbon at an angle of 45 in respect to the specimen stage (film thickness approximately 2.5 nm). Immediately, the so generated replica was stabilised by a carbon layer with a thickness of about 25 nm, evaporated in an angle of 90 . Afterwards, the sample was thawed and the replica floated on water. The replica was incubated over night in chromo-sulfuric acid (40 % v/v) in order to digest organic material adhering to the replica. After washing with water, the replica was transferred onto a Formvar® (Plano, Wetzlar) coated copper grid. The sample was analysed in an electron microscope (EM208S, FEI Company, U.S.A.). Images were recorded with a 1,000 x 1,000 pixel CCD camera (TVIPS, Tietz, Munich).

5.6 Immunogold-labelling of YidC in membrane sheets

Proteins can be detected in lipid membranes by a labelling with antibodies against specific domains. In order to visualise the bound antibody for electron microscopy, a secondary, gold particle coupled antibody can be used, which is directed against the first antibody (immunogold-labelling). Due to their high density, the gold particles generate a high contrast in the electron microscope. Therefore, they appear as black dots close to the antibody-detected proteins in the electron micrographs. Labelling of YidC membranes was performed according to (Kleymann et al. 1995).

On-grid labelling

A copper grid for electron microscopy was coated with a Formvar® film (Plano, Wetzlar). The Formvar® film was coated with 0.01 % w/v poly-L-lysine. The two-dimensional YidC crystals were adsorbed onto the so prepared film. For this, the coated grid was floated on a drop of the crystal suspension. In order to reduce the loss of specimens in the following incubation steps, the crystals were fixed on the poly-L-lysine film with paraformaldehyde (4 % v/v in PBS, pH 7.5). The sample was subsequently treated with solutions of the following order, pipetted in small droplets onto parafilm: PBS, 2 % w/v glycine in PBS, PBS and 0.1 % w/v BSA in PBS, all pH 7.5. Afterwards, the specimens were incubated with the primary antibody (monoclonal mouse anti-myc antibody, 9E10, Abcam, U.K.). Unbound antibody was washed off with 0.1 % w/v BSA in PBS, pH 7.5. The specimens were incubated with the secondary antibody (gold-coupled, polyclonal goat anti-mouse antibody, Jackson

ImmunoResearch Laboratories, distributed by Dianova, Hamburg, diluted 1:50 in PBS, pH 7.5). After removing unbound antibodies by repeated washings with PBS, pH 7.5, the sample was shortly fixed with 0.5 % v/v glutaraldehyde in PBS, pH 7.5, briefly washed in distilled water and stained with uranyl acetate. The sample was analysed in an electron microscope (EM208S, FEI Company, U.S.A.). Images were recorded with a 1,000 x 1,000 pixel CCD camera (TVIPS, Tietz, Munich).

Labelling of cross-sectioned samples

From the YidC crystal sample, membranes and two-dimensional crystals were adsorbed onto a 0.01 % w/v poly-L-lysine coated coverslip (Thermanox by Ted Pella, Inc., distributed by Plano, Wetzlar). After 20 min, non-adsorbed membranes were rinsed off with PBS (pH 7.5). After sequentially blocking with 2 % glycine, 1 % BSA and 0.1 % BSA (all in PBS, pH 7.5), specimens were incubated with the primary antibody (monoclonal mouse anti-myc antibody, 9E10, Abcam, U.K.). Excess antibody was washed off, and specimens were incubated with the secondary antibody (gold-coupled polyclonal goat anti-mouse antibody, Jackson ImmunoResearch Laboratories, distributed by Dianova, Hamburg, diluted 1:50 in PBS, pH 7.5). After washing, the sample was fixed by incubation with 1 % v/v glutaraldehyde in PBS, pH 7.5 and 1 % w/v osmium-tetroxide in 0.1 M Na-cacodylate buffer, pH 7.2. The sample was contrasted further by incubation in 2 % uranyl acetate over night and subsequently washed in water. Dehydration was achieved by incubation with increasing concentrations of alcohol, a prerequisite for infiltration with liquid synthetic resin (Spurr 1969). After polymerisation of the resin (70 °C), a plastic block was polymerised onto the membranes. The Thermanox cover slip was removed, and the thin sections prepared from the immunogold-labelled membranes were additionally contrasted by exposing to osmic vapour. Then, sections were double contrasted with uranyl acetate and lead citrate. The sample was analysed in an electron microscope (EM208S, FEI Company, U.S.A.). Images were recorded with a 1,000 x 1,000 pixel CCD camera (TVIPS, Tietz, Munich).

6   Computational analysis of crystallographic data

The image analysis was done using the UNIX operation system and a DEC Alpha 4100 computer. Furthermore, the MRC software package was used (Crowther et al.

1996), which consists of an assembly of FORTRAN routines (routines named in upper case), which can be combined and connected to variables and data sets via scripts.

6.1   Calculation of projection structures

Assessment and scanning of crystal lattices on film

In order to localise and assess crystalline areas on film, a polarised red laser mounted on an optical bench (Klug and Berger 1964) was used. The beam was spread with two lenses and the beam width adjusted with an aperture in respect to the lattice size. The negatives were placed into the beam. After passage through the negative, the laser light was detected with a CCD camera. The recorded signal was displayed on a monitor. Crystal lattices resulted in diffraction patterns showing reflections. Best crystal areas were marked on the film and later scanned (4,000 x 4,000 or 6,000 x 6,000 pixels) by using a CCD line scanner (Zeiss SCAI, Oberkochen) into the digital TIFF format. The pixel size of the scanner was 7 μm, which corresponded to a distance of 1.0 Å at a primary image magnification of 70,000x (maximal reachable resolution 3 Å).

Assignment of h, k, 0 reflections from the crystal image

The digitised data was converted into the MRC file format (TIF2MRC). For the initial analysis, the image was reduced by averaging each 2 x 2 pixels (LABEL) and the image edges were tapered to an average density (TAPEREDGE) in order to avoid spikes in the later calculated FFT. Subsequently, a Fourier transform was calculated from the image (FFTRANS). The Fourier transform was displayed by the program Ximdisp (Smith 1999). The Miller indices for some reflections were manually assigned on the display, which served to calculate then by Ximdisp the corresponding lattice vectors in reciprocal space. By application of the calculated lattice vectors a list of reflections was created from the Fourier transformed image (MMBOX). The list contained the Miller indices h, k, z (note: since the data was in projection, z was always set to '0') as well as the amplitude and phase of each reflection. The list contained in addition the signal over noise ratio (SON) of each reflection, quoted by

the IQ value (IQ = 7 x strength of background/ strength of signal). The IQ value can adopt all integer values between 1 and 9 (1: SON > 7, 2: SON = 3.5 ... 8: SON < 1).

Filtering and unbending

Electron micrographs contain 'noise', caused in electron crystallography for example by non-crystalline areas, contaminations and electron scattering effects. In order to delete noise (filtering), a mask was created, which assigned a circular area around the position of each spot in the reciprocal lattice (MASKTRAN). The information between the circular areas was considered as noise and therefore deleted (Fig. 6).

Principle of Digital Filtering

entire FT   enlarged area of FT   circular maskholes applied
(FT has now non-zero values only
within maskholes
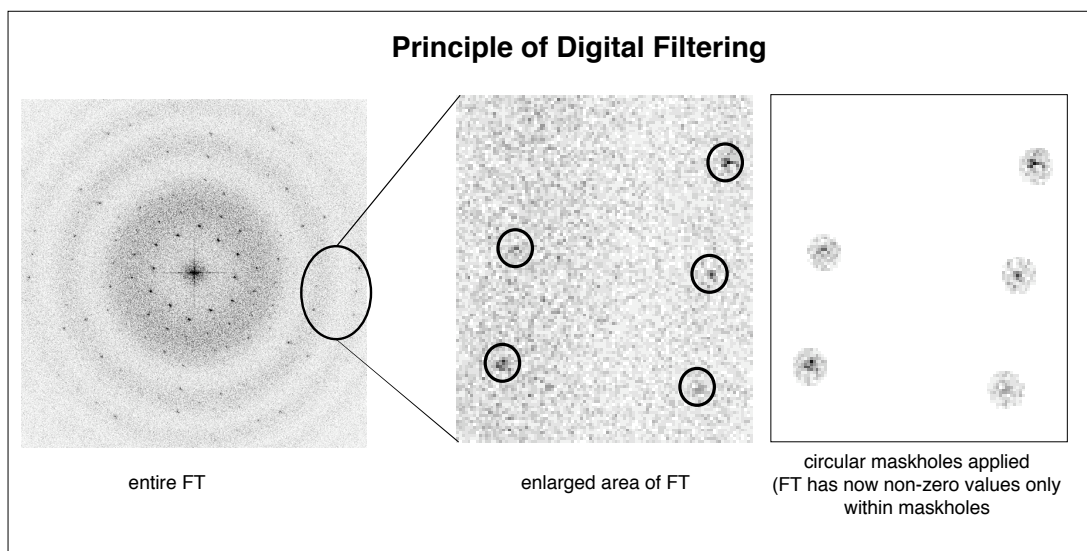
Fig. 6   Image filtering. The black circles (middle panel) represent the mask created by MASKTRAN. Modified from (Unger 2002).

A reference area (about 1/10 of the reduced image size) was cut out of the filtered image (BOXIMAGE). The Fourier transform of the reference area was multiplied with the Fourier transform of the filtered image (TWOFILE), which yielded a cross-correlation of the two images (Kunji et al. 2000). The correlation maxima of the reference area with the entire filtered image were determined (QUADSEARCH). The defective lattice areas were localised by a plot of the relative translation vectors in respect to the reference area (Fig. 7). The defective areas were set to an average grey value (BOXIMAGE), which also served to reduce noise. Two-dimensional crystal lattices are often bent, which means unit cells and lattice areas, respectively, are shifted out of their ideal position in the lattice. In order to extract the structural information in spite of the bending, the corresponding areas were shifted

back into the previously determined lattice (CCUNBEND). This procedure (unbending) yielded an image, which was widely freed from crystal distortions. For the second round of unbending, the Miller indices, amplitudes and phases obtained from the Fourier transform of the now unbent image were calculated (MMBOX) and the reflections including their IQ values plotted in resolution shells (RESPLOT). The unbent image was used as reference for further rounds of unbending. The unbending was repeated until no more lattice improvement visible by the RESPLOT output was obtained.
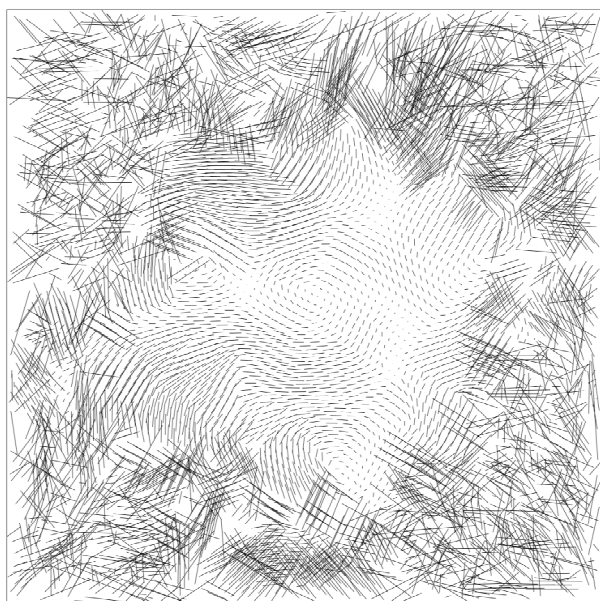
Fig. 7   Relative translation vectors. The visible represents the image area. The longer the vectors (lines), the more distorted is the lattice. Points show a high agreement with the reference area. The 'scrawl' represents regions of low agreement.

CTF correction of amplitudes and phases

The primary electron microscopic data is affected by the contrast transfer function (CTF), which is determined by the primary magnification, the defocus, the lens aberration and the acceleration voltage in the electron microscope. The CTF is visible in the Fourier transformed data as a repeating concentric contrast inversion. In the nodes of the CTF the contrast is zero and no information is present. In order to compensate for the influence of the CTF, the approximate defocus (in h- and k-direction) as well as the angle of astigmatism was calculated for the Fourier transformed data of the original image (CTFFIND2). The calculated defocus and the astigmatism angle were used as input for the routine CTFAPPLY. CTFAPPLY corrected under implication of the electron microscopic parameters the algebraic signs of the phases and the amplitudes in accordance to the CTF. If necessary, the defocus values were refined manually by a comparison of the nodes of the Fourier

transformed original and CTF corrected image. As input for the later calculation of the projection structure, CTFAPPLY created a list of reflections including the Miller indices and the corresponding CTF corrected amplitudes, phases and IQ values (APH file).

Calculation of individual projection structures

All programs used for the calculation of the projection structures accessed the CCP4 suite (Collaborative 1994). In order to make it accessible for the CCP4 suite, the APH file (see 'CTF correction of amplitudes and phases') was transformed into the MTZ-format (EXTEND_P1, F2MTZ). A Fourier transformation was carried out to calculate densities from the reflections (FFT). Thereby, only reflections with IQ-values ≤ 4 were used. The calculated densities were plotted as a projection structure by using the program NPO.

6.2   Averaging of projection structures

Correction of phase origins

Before averaging, the phase origins of all CTF corrected APH files (see 6.1, 'CTF correction of amplitudes and phases') had to be aligned. For this, the CTF corrected APH file of each individual image was analysed using the program ALLSPACE, which quotes the probabilities for all theoretically possible in-plane symmetries (Valpuesta et al. 1994). In addition, ALLSPACE proposes in respect to the symmetry for each individual image phase origins suitable for the subsequent data averaging. One APH file was chosen as reference, the phase origin set to the proposed values (p1 symmetry: random) and the phase origins of all other images iteratively corrected by using the program ORIGTILTK. Thereby, the phase residuals calculated by ORIGTILTK were used as a measurement for the image matching. After the correction of the phase origins, a new APH file was created which combined the content of all phase origin corrected APH files (combined APH file).

Averaging of the phase origin corrected data

In the combined APH file (see 'Correction of phase origins'), the amplitudes and phases for each Miller index were averaged (AVRGAMPHS). The resulting output was the 'hkl file', which contained the figure of merit (FOM) values for each reflection. From the FOM values in the hkl file, the phase errors and the overall phase error, respectively, were calculated (FOMSTATS). The phase errors served as indicators for the quality of the data set. FOMSTATS was employed furthermore to set the phases either to 0 or 180 ° for data with twofold symmetry, read out into a new hkl file (fom_hkl). From the respective hkl file, the 'combined phase error' for each unique reflection was plotted in resolution shells (PLOTALL), which was meant for a further assessment of the data quality. In the last step, the averaged projection structure was calculated and plotted from the hkl file according to the calculation of the individual projection maps (see 6.1, 'Calculation of individual projection structures'). A negative B-factor was used for the calculation of the densities from the reflections (FFT) and symmetries were taken into account (F2MTZ).

6.3 Projection structures showing single layers of SecYEG

Densities showing one layer of crystalline SecYEG (Breyton et al. 2002) were Fourier transformed into MTZ format. The Fourier transform was truncated to 10 Å resolution, using the CCP4 program suite (FFT, SFALL). Subsequently, h, k, 0 reflections were used to generate a projection structure. In order to apply non-crystallographic twofold symmetry to the projection of single-layered SecYEG, the MTZ file generated from the deconvoluted crystal layer was first transformed into hkl format (CCP4 program suite, MTZ2VARIOUS) and then re-formatted into an APH file (h, k, 0 reflections). ALLSPACE was used to determine the positions of the twofold axes, and a projection structure was created in p2 symmetry.

6.4 Difference structure and overlay with SecYEG

Densities of the SecYEG projection structure (Collinson et al. 2001) were scaled according to the projection structure of SecYEG/LamB$_{SP}$. Subsequently, the densities obtained from SecYEG were subtracted from the densities in the projection structure of SecYEG/LamB$_{SP}$. Densities of single-layered SecYEG (6.3) and helices of

SecYEG (Bostina et al. 2005), respectively, were fitted manually into the difference structure.

7   Biochemical methods

7.1   Protein quantification

The protein concentration was measured with the colourimetric assay described by Bradford (Bradford 1976) (Bradford reagent: Sigma-Aldrich; standard for assay calibration: BSA). Alternatively, the OD_{280} of the protein sample (blank: protein buffer) was used as a measurement for the protein concentration.

7.2   SDS-PAGE analysis

SDS-polyacrylamide gel electrophoresis (SDS-PAGE) analysis (Laemmli 1970) was used in order to determine the molecular weight of proteins and to examine protein preparations in respect to their protein content. The protein samples were mixed with 5x sample buffer (125 mM Tris, 50 % v/v glycerol, 10 % w/v SDS, 0.01 % w/v bromphenol blue, 10 mM β-mercaptoethanol, pH 6.8). Subsequently, the proteins were separated by PAGE (gels: Bio-Rad, U.S.A.; running buffer: 25 mM Tris, 200 mM glycine, 35 mM SDS). Afterwards, the proteins were visualised by incubation for approximately 30 min in staining buffer (0.4 % w/v Coomassie Brilliant Blue R250, 0.4 % w/v Coomassie Brilliant Blue G250, 50 % v/v methanol, 10 % v/v acetic acid) and subsequent removal of background staining (buffer: 10 % v/v methanol, 10 % v/v acetic acid / repeated washing in water).

SDS-PAGE analysis of two-dimensional crystals

80 μl of crystal suspension were dried in a nitrogen flow to a residual volume of approximately 15 μl. 1 μl SDS stock solution (10 % w/v) was added in order to resolve the membrane-embedded proteins. The sample was subsequently analysed by SDS-PAGE as described above.

7.3   Analytical size-exclusion chromatography

A Superdex 200 (10/30) column (Amersham Pharmacia, U.S.A.) was equilibrated with gel filtration buffer (200 mM NaCl, 20 mM ADA, 0.2 % w/v DM, pH 5.6). The runs were performed at room temperature and a flow rate of 0.4 ml/min. Analysed were 500 µl of sample (YidC or YidC/lipid mixtures, the latter at an LPR of 0.2 w/w). Monitored was UV_{280} absorption versus retention volume.

7.4   BN-PAGE analysis

The BN-PAGE analysis (Schägger and von Jagow 1991; Schägger et al. 1994; Heuberger et al. 2002) is described in (Raunser 2004). In brief, samples were mixed with sample buffer (5 % w/v Coomassie Brilliant Blue G250, 500 mM ε-amino capronic acid, 100 mM Bis-Tris, pH 7) and loaded into gel (4.5 - 10 % w/v polyacrylamide gradient, 180 x 160 x 1 mm) pockets, Additionally, molecular weight standards (standard for size-exclusion chromatography, Amersham Pharmacia, U.S.A.) were applied. Runs (temperature of 4 °C; anode buffer: 50 mM Bis-Tris, pH 7, cathode buffer: 0.02 % w/v Coomassie Brilliant Blue G250, 50 mM Tricine, 15 mM Bis-Tris, pH 7) were started with a current of 100 V. The current was increased to 200 V when the proteins reached the separating gel. After the run, background staining was removed (10 % v/v ethanol, 10 % v/v acetic acid) in order to make protein bands visible.

7.5   Size-exclusion chromatography and laser scattering

The size-exclusion chromatography and laser light scattering is described in (Raunser 2004). In brief, proteins (200 µg, concentration ≈1 mg/ml) were separated by gel filtration (TSK G3000SWXL gelfiltration column, TosoHaas, U.S.A.). Running buffer was 150 mM NaCl, 0.1 % DDM, 20 mM Tris-HCl, pH 7.5. Analysis of the separated proteins was carried out on-line using an UV-detector (Waters 486, Milford, U.S.A.), a light scattering photometer (Wyatt MiniDawn + QELS detector for Rh) and a refractometer (Waters 2410, Milford, U.S.A.). Molecular weights were calculated using the software ASTRA (Wyatt Technology, U.S.A.).

8   Tables: conditions for the crystallisation of YidC

Tab. 1 <u>Two-dimensional crystallisation of YidC (optimised conditions).</u>

Purification	
Membrane protein solubilisation	Buffer: TSG (300 mM NaCl, 10 % v/v glycerol, 20 mM Tris-HCl, pH 8) including 1 % w/v Cymal 6 1.5 h stirring at 4 °C
Nickel-chelating chromatography	Equilibration: TS (300 mM NaCl, 20 mM Tris-HCl, pH 8) including 0.2 % w/v DM Wash: TS, 0.2 % w/v DM, 30 mM imidazole Elution: TS, 0.2 % w/v DM, 300 mM imidazole
Size-exclusion chromatography	Column: Sephacryl S-300 (26/60) Buffer: 200 mM NaCl, 20 mM ADA, 0.2 % w/v DM, pH 5.6
Protein storage	4 °C, supplemented with 2 mM NaN_3 or 80 °C (flash-frozen in liquid Nitrogen)
Two-dimensional crystallisation	
Protein / lipid mixture	Protein concentration: ≈ 0.5 mg/ml Lipid: DPPG (synthetic, 1 mg/ml in distilled water and 1 % w/v DM) LPR: 0.092 - 0.123 w/w
Reconstitution	5 d dialysis (12 - 14 kDa MWCO) at 30 °C Buffer: 100 mM NaCl, 2 mM NaN_3, 1 mM EDTA, 20 mM ADA, pH 5.6 (buffer to sample ratio: 1000:1 v/v)
NaCl depletion	3 d dialysis (12 - 14 kDa MWCO) at 20 °C Buffer: 2 mM NaN_3, 1 mM EDTA, 20 mM ADA, pH 5.6 (buffer to sample ratio: 500:1 v/v)

Tab. 2 <u>Three-dimensional crystallisation of YidC (optimised conditions).</u>

Purification	
Membrane protein solubilisation	Buffer: TSG (Tab. 1), 1 % w/v Cymal 6 1.5 h stirring at 4 °C
Nickel-chelating chromatography	Equilibration: TSG, 0.1 % w/v Cymal 6 Wash: TSG, 0.1 % w/v Cymal 6, 30 mM imidazole Elution: TSG, 0.1 % w/v Cymal 6, 300 mM imidazole
Size-exclusion chromatography	Sephacryl S-300 (26/60) Buffer: 200 mM NaCl, 10 % v/v glycerol, 0.06 % w/v Cymal 6, 20 mM Tris-HCl, pH 7
Increase of protein concentration	50 kDa MWCO Centriprep®, Amicon Bioseparations, Millipore
Reduction of detergent after concentration step	2 d dialysis (MWCO 12 - 14 kDa) at 4 °C Buffer: same as size-exclusion chromatography (see above, buffer to sample ratio: 200:1 v/v)
Protein storage	80 °C (flash-frozen in liquid Nitrogen)
Three-dimensional crystallisation	
Precipitation method	Vapour diffusion, hanging drop Protein concentration: ≈ 8 mg/ml protein
Mother liquor	100 mM citrate buffer, pH 5 - 6 Salt: 150 mM KCl Precipitant: 30 - 35 % w/v PEG 600
Crystallisation drop	0.8 μl protein mixed with 0.8 μl mother liquor

Results

Analysis of SecYEG/LamB$_{SP}$ crystals

1   Modified two-dimensional crystallisation of SecYEG

With the objective to obtain structural information of the intramolecular rearrangements potentially occurring upon signal sequence binding, growing of two-dimensional crystal lattices formed of SecYEG with bound LamB signal peptide was pursued. Two-dimensional crystals of SecYEG take several weeks to grow (Collinson et al. 2001). The crystallisation protocol was therefore altered in order to yield two-dimensional SecYEG crystals in a shorter time. SecYEG protein was over-expressed in *Escherichia coli* and purified as described (Collinson et al. 2001). It was possible to decrease the required dialysis time from several weeks (4 °C) to 10 days (30 °C) by dissolving the required lipid PE in the detergent DM (1 % w/v for 4 mg/ml PE) instead of $C_{12}E_9$ (Collinson et al. 2001). The dialysis following the altered protocol was carried out with the same dialysis buffer as used for the earlier crystallisation conditions (120 mM NaCl, 1 mM NaN$_3$, 1 mM EDTA, 20 mM Tris-HCl, pH 8). During dialysis, a film of precipitated material built up at the inner surface of the dialysis bags. This had been also observed using the earlier crystallisation protocol (Collinson et al. 2001). Whether two-dimensional crystals of SecYEG grow or not seemed to depend on the specific batch of protein used.

The SecYEG crystals obtained by the improved, more rapid dialysis procedure were stained with uranyl acetate and analysed by electron microscopy. Like those grown previously (Collinson et al. 2001; Breyton et al. 2002), the newly obtained SecYEG crystals were mostly tubular and consisted of two membrane layers (Fig. 8 A). Crystalline specimens were recognised by the straight edges of vesicles (Fig. 8 A). The lattice appeared rectangular (Fig. 8 B). Most of the crystalline tubes seemed to grow out of aggregated material. The aggregates accounted for a large proportion of the observed material.

Images of frozen-hydrated SecYEG crystals obtained with the new crystallisation protocol were collected (JEOL 3000 SFF electron microscope, acceleration voltage 300 kV, spotscan mode). For this, the crystals had been frozen-hydrated by the back injection method (Wang and Kühlbrandt 1991), using 4 %

trehalose as cryo-protectant. The data obtained resembled the former preparation (Collinson et al. 2001).
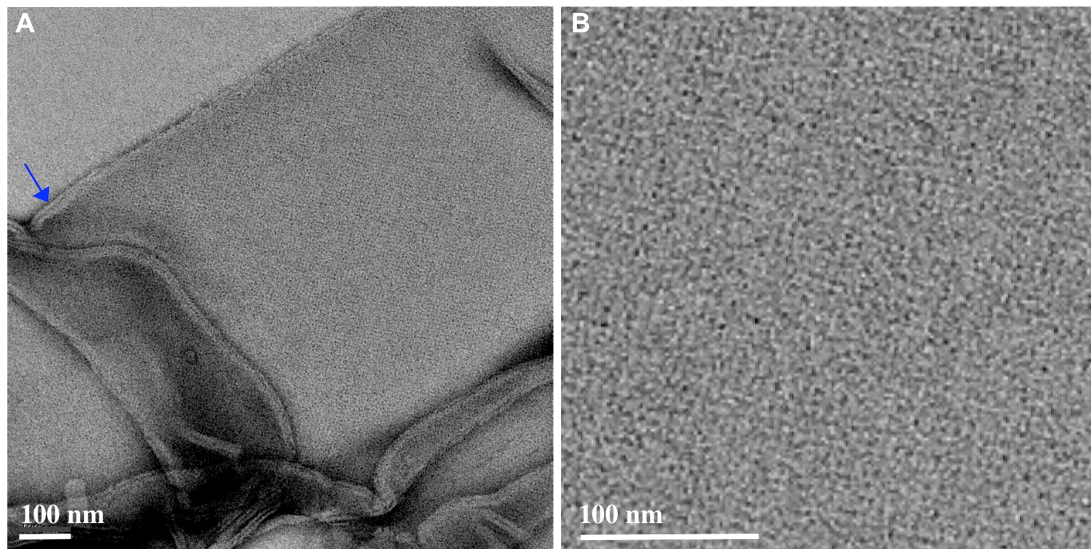

Fig. 8   Two-dimensional SecYEG crystals (uranyl acetate stain). **A**: Crystalline SecYEG vesicle. The crystals were formed by a double membrane (blue arrow). **B**: Enlarged lattice area.

2   Co-crystallisation of SecYEG and LamB peptide

In order to grow two-dimensional SecYEG crystals in presence of LamB signal peptide, the dialysis procedure for the two-dimensional crystallisation of SecYEG was modified: the LamB signal peptide was added into the dialysis buffer of the crystallisation experiment. In addition, hydrophobic Bio-Beads® were added into the dialysis buffer in order to adsorb detergent. The latter served the purpose of reducing the amount of required dialysis buffer and LamB peptide, respectively. The method yielded SecYEG crystals grown in the presence of LamB signal peptide (SecYEG/LamB$_{SP}$ crystals). Using dialysis membranes with a MWCO of 2 kDa, tested with the objective of retarding the LamB peptide ($\approx$ 2.5 kDa) within the dialysis bag, the deployed material did not form two-dimensional crystals.

3   Electron cryo-microscopic analysis

SecYEG/LamB$_{SP}$ crystals were stained with uranyl acetate and observed in the electron microscope. In negative stain, the SecYEG/LamB$_{SP}$ crystals appeared to be

similar to the two-dimensional crystals of SecYEG grown without signal peptide (Fig. 8).

SecYEG/LamB$_{SP}$ crystals were cryo-preserved by the back-injection method using 4 % w/v trehalose as cryo-protectant (Wang and Kühlbrandt 1991), and electron micrographs were recorded (JEOL 3000 SFF electron microscope, acceleration voltage 300 kV, spotscan mode). By analysis of the Fourier transformed data from SecYEG/LamB$_{SP}$ crystals with the program ALLSPACE (assessed using reflections with an IQ ≤ 7), p121_b symmetry was found. Therefore, three images were averaged with p121_b symmetry (Tab. 3; Fig. 9 A, C), meaning, all visible features were mapped onto themselves by mirroring and a translation for the length of half a unit cell along a screw axis in the image plane; the screw axis was thereby parallel to the b-axis (shorter axis) of the *real space* unit cell. The unit cell dimensions of the three individual SecYEG/LamB$_{SP}$ projection structures (Tab. 3) were essentially the same as those of the SecYEG crystals grown without substrate (Collinson et al. 2001; Breyton et al. 2002).

Resolution range [Å]	Refl.	E [°]
200 - 28.9	6	5.4
28.9 - 20.0	6	23.9
20.0 - 16.4	8	6.5
16.4 - 14.1	5	8.4
14.1 - 12.7	7	16.8
12.7 - 11.5	2	18.5
11.5 - 10.7	6	24.0
10.7 - 10.0	3	11.7
∑ Refl.	43	
Overall phase error [°]	14.0	

Dimension	∅	Dev.
a-axis	102.5 Å	2.3 Å
b-axis	57.2 Å	0.7 Å
Angle	90.0 °	4.0 °

Tab. 3 <u>Image statistics for the projection structure of SecYEG/LamB$_{SP}$.</u> 3 individual projection structures were averaged in p121_b symmetry. Refl.: Number of unique reflections in each resolution range. E: Phase error for each resolution range. ∑ Refl.: Number of reflections in total. Data significance of 'random': overall phase error of 90 °. Additionally, the average unit cell dimensions are shown. ∅: Arithmetic mean. Dev.: Lowest value subtracted from the highest.
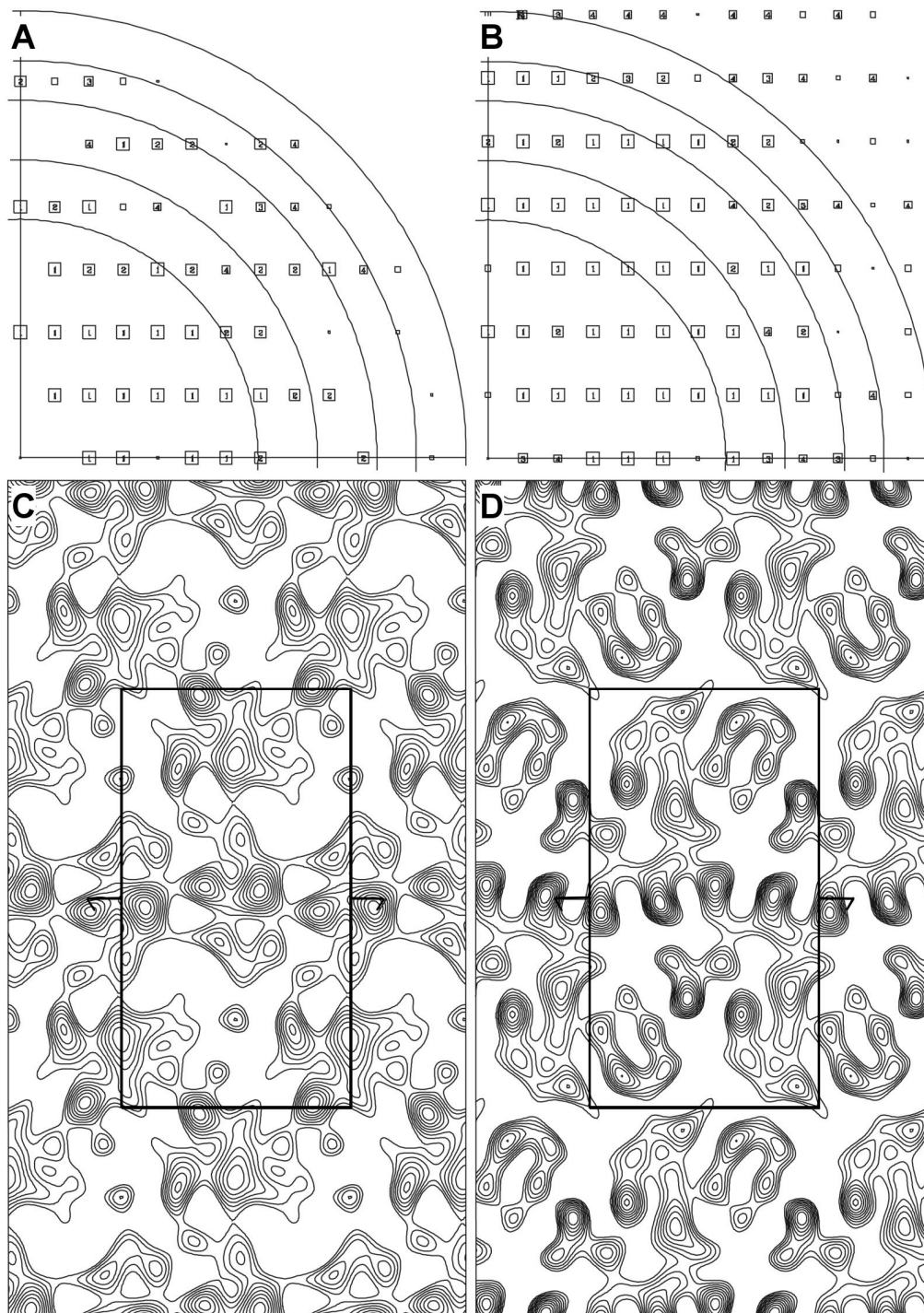
Fig. 9   Averaged projection structures of SecYEG/LamB_SP (**A**, **C**) and SecYEG (**B**, **D**; (Collinson et al. 2001)). Frozen-hydrated crystals. **A**, **B**: Reflections plotted versus resolution. Each box indicates one unique reflection. The box size for each reflection is correlated to the signal to noise ratio, depicted as IQ value (≤ 4) in each box (increasing IQ value means increasing combined phase error: $1 < 8°$, $2 < 14°$, $3 < 20°$, $4 < 30°$). Resolution shells (inner to outer ring): 15, 12, 10, 9 and 8 Å. **C**, **D**: Projection structures. Unit cells (104 x 57 Å, angle 90 °) are indicated by black parallelograms; half arrows indicate the direction of the screw axes. Resolution: 10 Å, B-factor: -600 Å^2.

Averaging of the three SecYEG/LamB$_{SP}$ images gained reflections up to about 9 Å resolution, but completeness and intensity of reflections of higher order were inferior to the reflections obtained previously with SecYEG (Fig. 9 B). Both projection structures showed similarities. This accounted particularly for densities running along the screw axes indicated in Fig. 9 C and D. However, there were significant differences apparent. These were in the unit cell regions more distant to the indicated screw axes (Fig. 9 C, D).

4   Difference structure

In order to visualise non-similar densities, a difference structure was calculated by subtraction of the densities from the SecYEG projection structure (Collinson et al. 2001) from the densities of the averaged SecYEG/LamB$_{SP}$ projection structure. Accordingly, positive peaks accounted for densities present in the projection structure of SecYEG/LamB$_{SP}$, but not in the projection structure of SecYEG and vice versa. The difference structure was plotted at three different resolutions (Fig. 10 A - C). Peaks in the difference structure in the following are also referred to as 'difference peaks'.

Visible were 3 positive and 3 negative peaks, neglecting two to three small peaks of only one contour level (the latter peaks are not numbered in Fig. 10 A); these small peaks were not visible at lower resolution. Positive peaks 1 and 2 appeared at more or less the same contour level and shape when they were plotted at various resolutions (Fig. 10 A - C). Positive peak 3, which repeats along the indicated screw axis, was less contoured and more elongated at lower resolution (Fig. 10 A - C).

In order to identify for which regions in SecYEG the difference peaks accounted, an overlay of the difference structure with a molecular model of SecYEG was created (Fig. 10 D, E). Due to the p121_b symmetry, the difference peaks always map to two alternative positions, which relate to the deconvoluted SecYEG molecules (Fig. 10 D). Referring to the SecYEG dimer, the differences observed for SecYEG with and without substrate were asymmetric: one SecYEG monomer (Fig. 10 E, upper monomer) had positive peak 2 as an additional feature central to the SecYEG molecule (Fig. 10 E, marked with an orange oval, solid line). The same SecYEG monomer overlaid with positive peak 1 and negative peak 1. Both peaks aligned to transmembrane helices 7, 8 and 9 in SecY (Fig. 10 E, outlined in cyan colour).
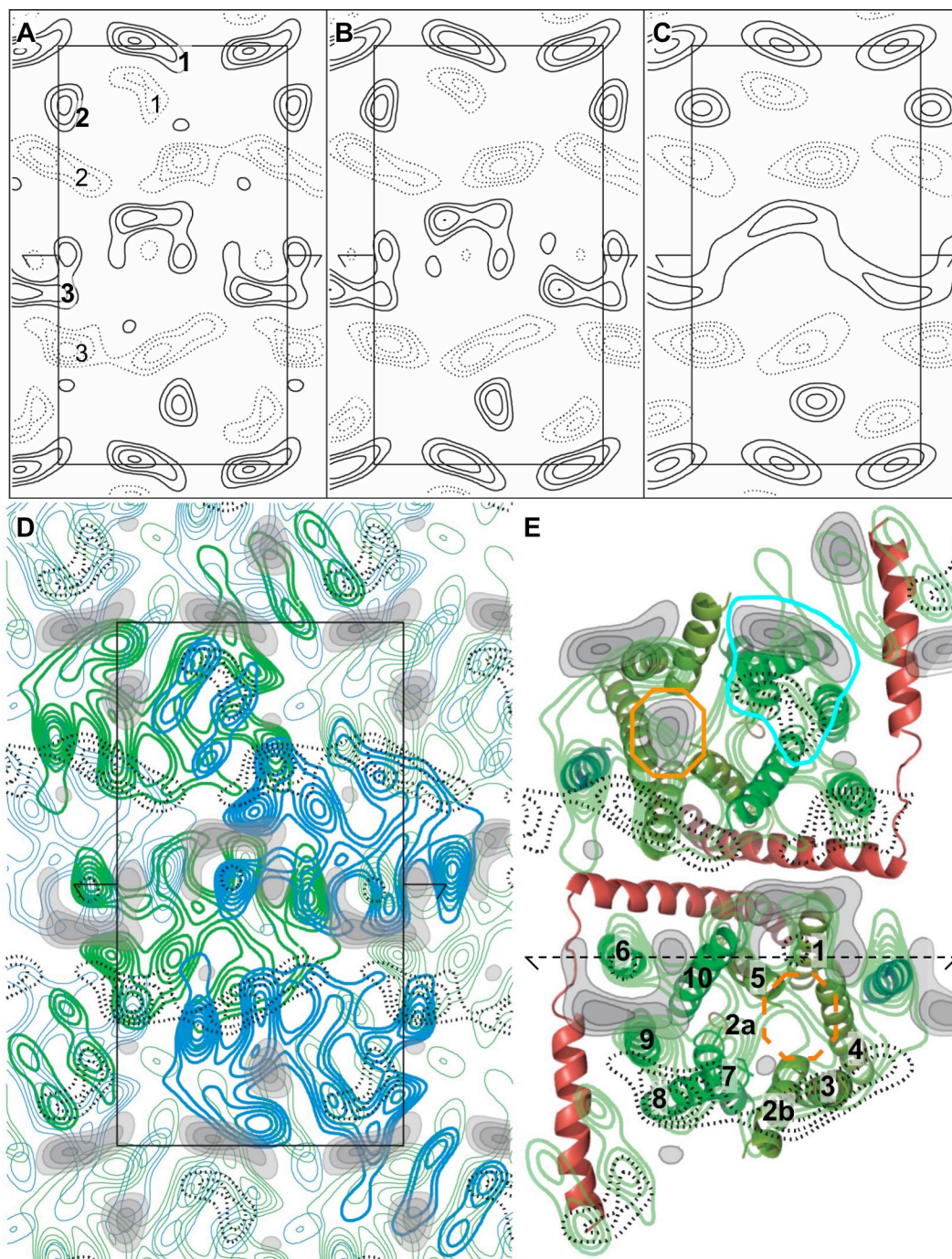
Fig. 10 Difference structure (**A**: 10, **B**: 12 and **C**: 15 Å resolution; no B-factors applied) and overlay with SecYEG (**D**, **E**). Outlined unit cells (dimensions 104 x 57 Å, angle 90 °) refer to the SecYEG double layer. Structures are contoured in steps of 0.5 x RMS; in the difference structure, contours in the range of ± 1 x RMS are omitted in order to exclude noise. **A**: Numbers assign difference peaks (positive: strokes, negative: dotted contours). **D**: Overlay of **A** (positive peaks shaded grey) with two layers of SecYEG (blue and green), the latter related by p121_b symmetry. **E**: Helices of SecY (green; numbered) (Bostina et al. 2005), SecE (red) and SecG (β subunit, blue) manually fitted into the green SecYEG dimer (**D**). Dashed horizontal arrow: Screw axis (**D**). Positions marked in orange and cyan, respectively, see text.

The second SecYEG monomer (Fig. 10 E, lower monomer) was lacking the additional density posed by positive peak 2 (Fig. 10 E, vacant position marked with orange oval, dashed line) and did not overlay with positive peak 1. Instead, in the second SecYEG molecule, peak 3 is the predominant positive peak. Furthermore, a 'rim' of density on the front side of the molecule with contributions from transmembrane helices 2b, 3, 4 and 7, 8, 9, respectively, coincided with negative peaks 2 and 3 (Fig. 10 E).

Relative to the double layer, negative peaks 2 and 3 occurred at the position where front and back of the SecYEG molecules in the two membrane layers overlap (Fig. 10 D).

Analysis of YidC

1 Two-dimensional crystallisation of YidC

1.1 Purification

Several detergents and chromatographic methods were tested for the purification of YidC (Tab. 4). Two-dimensional crystals of YidC were achieved when the YidC containing membranes were solubilised with 1 % w/v Cymal 5, 6 or 7, and by purifying YidC sequentially by Nickel-chelating and size-exclusion chromatography, using 0.2 % w/v DM as detergent (Tab. 4).

Tab. 4 <u>Conditions for the purification of YidC.</u> **MS**: Membrane solubilisation. Nickel-chelating (**NCC**), size-exclusion (**SEC**) and anion-exchange (**AEC**) chromatography. All %-values are w/v. –: No reconstitution. M: Membrane incorporation. C: Two-dimensional crystallisation. The results refer to a reconstitution by dialysis, analysed by electron microscopy.

Chromatographic methods / detergents	Result
MS - NCC	
DDM (1 % - concentration lowered from 0.1 to 0.02 %)	–
LDAO (1 % - 0.3 %)	–
MS - NCC - SEC	
DM (1 % - 0.2 % - 0.2 %)	M
2 % DDM - 0.2 % DM - 0.2 % DM	M
1 % Cymal 5, 6, 7 - 0.2 % DM - 0.2 % DM	C
DDM (1 % - 0.1% - 0.01 or 0.02 %)	–
Cymal 6 (1 % - 0.1% - 0.06 %)	–
MS - NCC - AEC	
Cymal 6 (1 % - 0.1% - 0.06 %)	–
DM (1.5 % - 0.2 % - 0.2 %)	M
MS - NCC - SEC - AEC	
OG / $C_{12}E_9$ (Purification as described for SecYEG (Collinson et al. 2001))	–

Applying this purification protocol (Material and Methods, Tab. 1), two overlaying protein peaks (retention volumes $\approx$ 135 ml and $\approx$ 145 ml, respectively) eluted from the size-exclusion column and appeared almost as one single peak (Fig. 11 A).
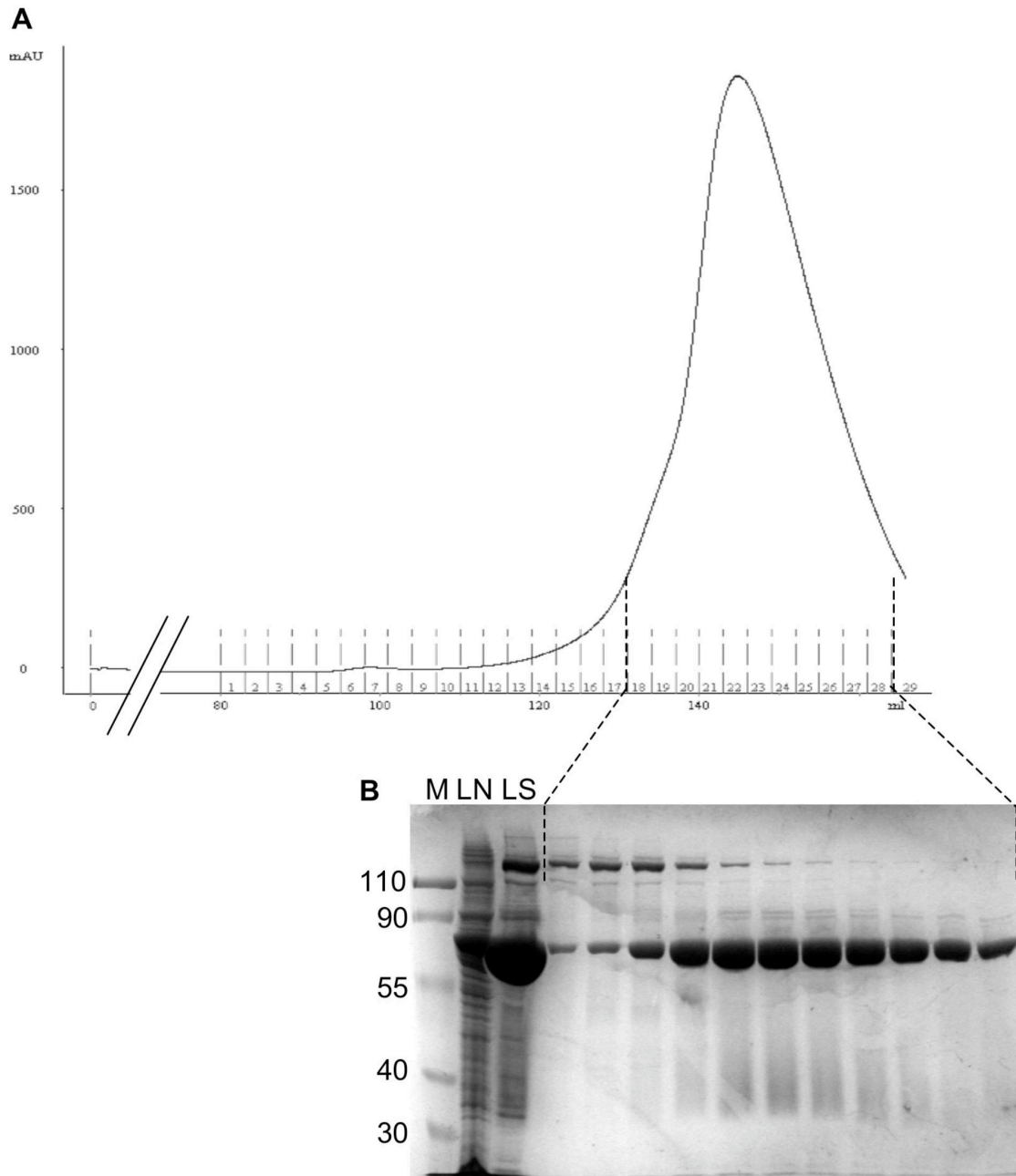
Fig. 11 Purification of YidC. The purification was performed by Nickel-chelating and size-exclusion chromatography. **A**: Chromatogram. Light absorption (UV_{280}, vertical axis) plotted versus retention volume (horizontal axis). **B**: SDS-PAGE (10 % w/v polyacrylamide, Tris-HCl). M: Marker and approximate molecular weights in kDa. LN: Load Nickel-chelating column, LS: Load size-exclusion column. Other lanes: YidC fractions 18 - 28 in **A**.

In order to obtain pure YidC, only the fractions eluting in form of the second peak were used, for example fractions 22 to 26 in Fig. 11 B. Using less than 0.75 % w/v Cymal 6 for the membrane solubilisation, less YidC was obtained, indicating that YidC was not effectively solubilised from the membranes. YidC purified following the optimised protocol (Material and Methods, Tab. 1) and supplemented with 2 mM NaN$_3$, could be stored for more than two weeks at 4 °C without detectable proteolytic degradation (Fig. 12 A) or a negative effect on the crystal quality, regarding to the analysis by electron microscopy. Alternatively, the prepared YidC could be stored at -80 °C after flash-freezing in liquid nitrogen, which did not impair the crystal quality.

Also two-dimensional YidC crystals obtained following the optimised protocol could be stored for several weeks at 4 °C without proteolytic degradation (Fig. 12 B) or visible loss in crystal order, examined by electron microscopy.
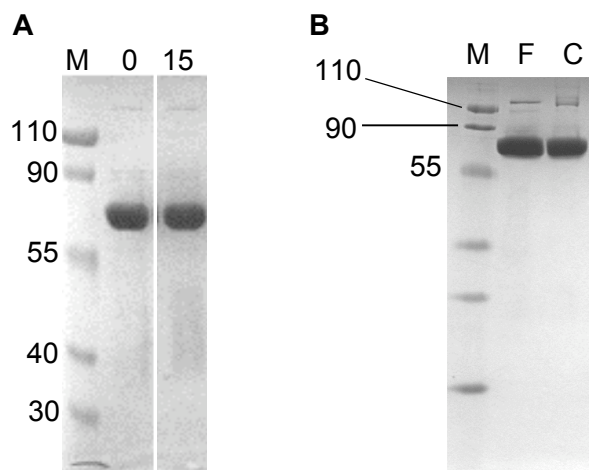
Fig. 12 Stability of YidC in respect to proteolytic degradation. SDS-PAGE (Tris-HCl; **A**: 10 % w/v, **B**:15 % w/v polyacrylamide). M: Marker and approximate molecular weights in kDa. YidC: **A**: YidC in detergent solution, stored at 4 °C (purified protein supplemented with 2 mM NaN$_3$). '0' and '15' denote days of storage. **B**: Crystalline YidC. F: YidC stored at -80 °C after purification and subsequent flash-freezing. C: YidC solubilised with SDS from two-dimensional crystals, which had been stored for more than four weeks at 4 °C. **A**, **B**: YidC (dominant band in lanes 0, 15 and F, C, respectively) had the same molecular weight in the compared samples.

1.2 Reconstitution and crystallisation

1.2.1 Protein concentration

No influence of the YidC concentration on the two-dimensional crystallisation was observed in the range tested (0.25 - 1 mg/ml).

1.2.2 Lipid

YidC could not be reconstituted without added lipids. The best incorporation of YidC into membranes was achieved with lipids dissolved in DM (also tested: $C_{12}E_9$, DDM, Cymal 6, CHAPSO). Also for a reconstitution by dilution, DM appeared to be the most suitable detergent. Using CHAPSO (Parcej and Eckhardt-Strelau 2003), crystals were obtained as well. Polar lipids or pure PE lipid (both from *Escherichia coli*) were not suitable for the reconstitution of YidC. Tubular YidC crystals were obtained with a mixture of DOPC and PG lipid, using PG lipid at a concentration between 30 and 80 % w/w (Fig. 13 C, Fig. 14 A).

If the proportion of PG lipid was increased (≥ 80 % w/w), crystalline YidC sheets formed instead of tubes (Fig. 13 D; Fig. 14 B, C). The lattices of both crystal forms were different in appearance, examined by electron microscopy: as visible on images from negative stain (Fig. 14 B), lattices in the tubes were rectangular whereas lattices in the sheets were formed by rows of protein, the latter also visualised be freeze-fracturing (Fig. 15 C).

No improvement of the crystal quality was observed after an addition of CL (1 - 40 % w/w) or PE (1 - 15 % w/w) to the reconstitution lipid. Remarkably, PE led to the aggregation of YidC, even if it was supplemented only in small amounts (≈ 5 % w/w) to the lipid mixture. Two-dimensional YidC crystals were obtained with PG lipid of various alkyl chain length and -composition (Tab. 5). The best two-dimensional crystals of YidC were obtained with pure DPPG.
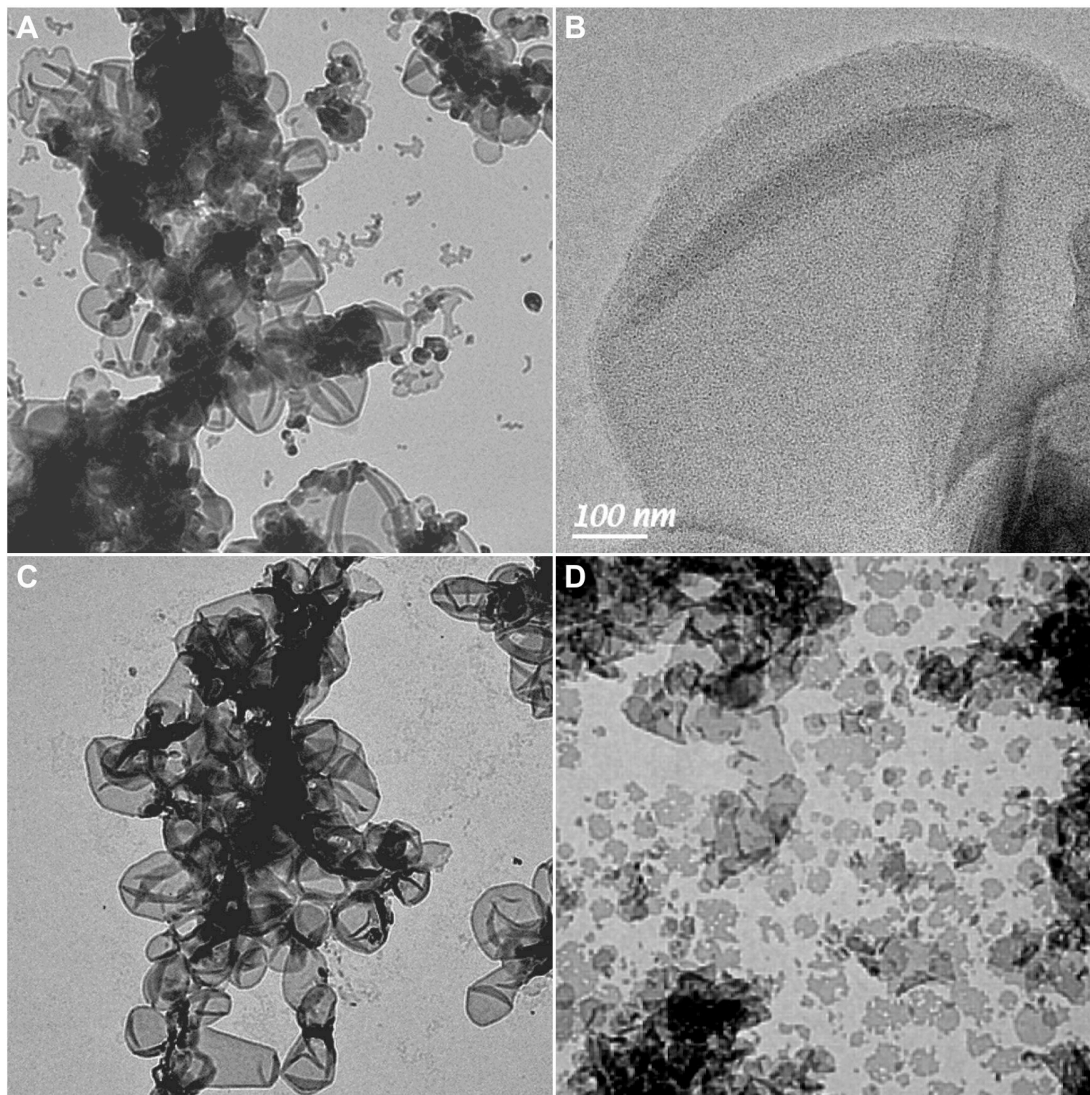
Fig. 13 Crucial steps in the two-dimensional crystallisation of YidC. The improvements are illustrated by electron micrographs (uranyl acetate stain). **A**, **C**, **D**: Specimens at low magnification (search/diffraction mode (Williams and Fisher 1970)). **B**: Non-crystalline vesicle at 35,000x magnification. **A**, **B**: Improved purification and reconstitution conditions led to vesicles of densely packed YidC. **C**: Removal of NaCl from the buffer induced the crystallisation of YidC in form of tubular crystals, easily recognisable by their straight edges. **D**: Reconstitution in pure PG lipid led to crystalline sheets.

Fig. 14 Two-dimensional YidC crystals (uranyl acetate stain). **A**: Tubular crystal, reconstituted in 50:50 w/w DOPC/DOPG. **B**, **C**: Sheet reconstituted in pure DPPG. Magnification 35,000x (**A**, **B**) and 3,200x (**C**).

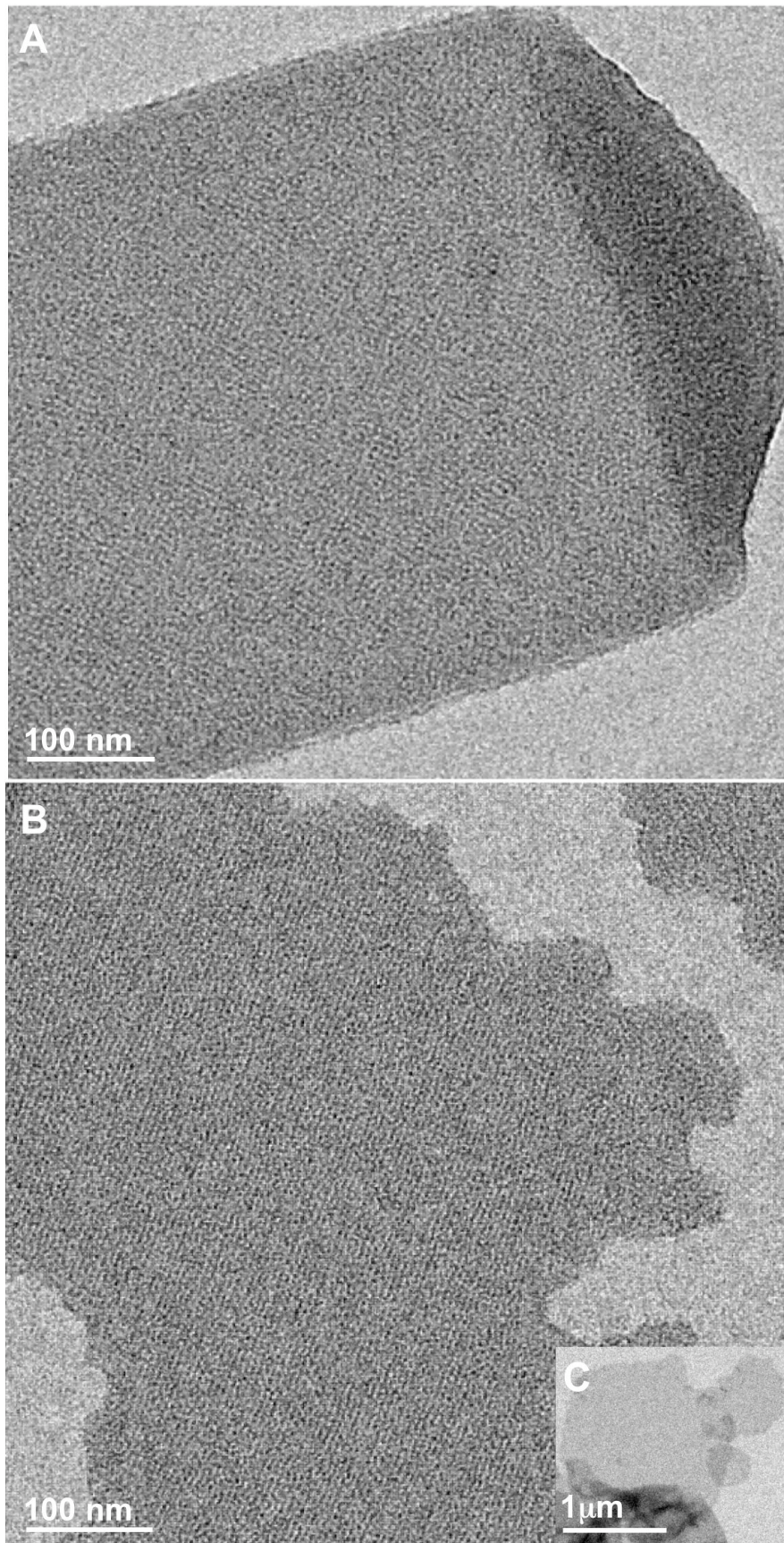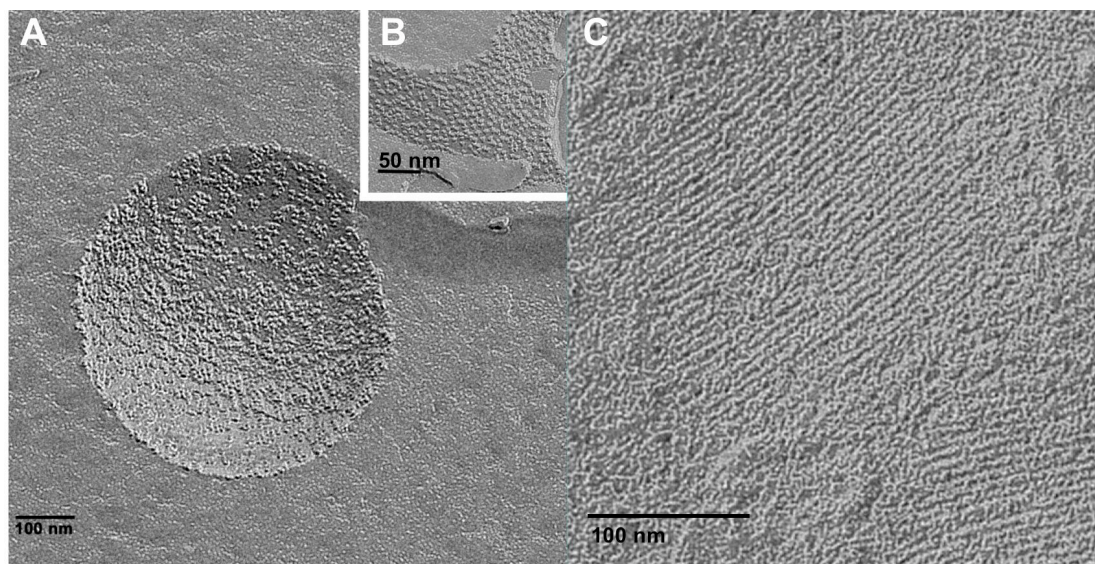Fig. 15 Freeze-fracture analysis. **A**, **B**: YidC vesicle reconstituted with DOPC/DOPG (50:50 w/w) in presence of 100 mM NaCl. Only small areas of ordered protein were visible (**B**). **C**: Sheet, obtained by reconstitution of YidC in DPPG and subsequent removal of NaCl from the buffer. Extended crystalline lattices were visible.
The freeze-fracture analysis was performed by Dr. Winfried Haase.

The LPR required for the two-dimensional crystallisation of YidC seemed to differ for the fractions of YidC eluted from the size-exclusion chromatography: a lower LPR was required to crystallise the fractions eluting at high retention volumes. The LPR required for the crystallisation of YidC with a mixture of DOPC/DOPG ($\approx$ 50:50 w/w) was higher (0.15 - 0.12 w/w) than for a crystallisation in pure PG lipid (0.123 - 0.092 w/w). An accurate adjustment of the LPR was crucial for the two-dimensional crystallisation of YidC.

Lipid	C : C=C	Crystals
DLPG	12:0	--
DMPG	14:0	+
DPPG	16:0	+
DOPG	18:1	+
DLOPG	18:2	--

Tab. 5 Different types of PG lipid tested for the crystallisation of YidC. C: Number of carbon atoms, C=C: number of double bonds in the alkyl chains.

1.2.3 Detergent removal and initial detergent concentration

Reconstitution and crystallisation of YidC was achieved by diluting the detergent in the sample (from 2 to 0.015 x CMC of DM in ≈ 24 h), but the crystals were hard to reproduce and the reconstituted samples often had a dense background of precipitated material in the electron microscope. Furthermore, the problem of recovering the reconstituted specimen out of the diluted suspension was not solved satisfyingly. Crystals were obtained by reducing the detergent in the sample by dialysis in membrane tubes (MWCO 12 - 14 kDa).

Dialysis in hockey sticks (MWCO membrane 12 - 14 kDa), membrane tubes with a higher MWCO (50 kDa) or Slide-A-lyzers® yielded crystals as well. For the purpose of reducing the detergent concentration, the dialysis was performed at 30 °C for 5 d. Dialysis for one day at 37 °C impaired the crystal quality. No improvement of crystal quality was observed, when the dialysis temperature was cycled in various schedules between 20, 30 and 37 °C.

The best crystals were obtained with 0.2 % w/v (hockey sticks: 0.1 % w/v) DM in the sample after mixing protein and lipid, referring to a reconstitution and crystallisation by dialysis. At a concentration of ≥ 0.6 % w/v, no crystals were obtained.

1.2.4 Dialysis buffer

Reconstitution and two-dimensional crystallisation of YidC was achieved between pH 5 and 6. Suitable buffer substances were ADA, citrate buffer, MES and acetic acid (all 20 mM).

Salts of monovalent cations

Although dense membrane integration of YidC was achieved, the reconstituted protein formed no or only very small crystal lattices (Fig. 15 A, B). Therefore, vesicles with reconstituted YidC (non-crystalline, Fig. 13 A, B) were exposed to various buffers. It turned out, that - after the reconstitution of YidC into proteoliposomes - a depletion of NaCl from the reconstituted material is crucial for the formation of two-dimensional YidC lattices (Fig. 13); the formation of two-dimensional YidC crystals was significantly inhibited already at 40 mM NaCl. As found later by dialysis experiments, LiCl (20 mM) and KCl (50 mM) disturb the

formation of YidC crystals as well. Lattice formation was reversible: a in this way obtained sample of two-dimensional YidC crystals was re-supplemented with 100 mM NaCl. The crystal order was destroyed.

The reconstitution of YidC appeared not particularly sensitive to NaCl: a membrane incorporation of YidC was obtained between 0 and 1 M NaCl. If YidC had been reconstituted in the presence of more than 500 mM NaCl, crystals formed only rarely after removal of NaCl. However, 100 mM NaCl in the reconstitution buffer yielded a cleaner reconstitution, compared to a buffer without NaCl.

In accordance to these findings, YidC was first reconstituted in the presence of 100 mM NaCl. The NaCl was then removed by a second dialysis step in order to induce the crystallisation of the reconstituted material. Cycling the samples through NaCl concentrations in various schedules between 0 and 100 mM or depleting the NaCl in various steps between 0 and 100 mM instead in one step, did not alter the crystal quality.

Buffer additives

Several buffer additives were tested for the two-dimensional crystallisation of YidC (Tab. 6). Only 1 mM EDTA improved the quality of the YidC crystals.

Tab. 6 Buffer additives. **–**: No visible effect. **A**: Aggregation of specimens and/or precipitation of the protein. **LA**: Less aggregation. **IC**: Impaired two-dimensional crystallisation (other than inducing aggregation). The results refer to a crystallisation by dialysis, analysed by electron microscopy.

Additives	**Effect** at concentration
$MgCl_2$ and $CaCl_2$	**A** $\geq$ 2 ($CaCl_2$) or 5 ($MgCl_2$) mM
Glycerol	**A** $\geq$ 10 % v/v
MPD (Williams et al. 1999; Ziegler et al. 2004)	**A** $\geq$ 5 % v/v
PEG (200, 400, 550 MME, 3350 and 4000)	**A** $\geq$ 10 % v/v (PEG 400); $\geq$ 3 % w/v (PEG 4000 / 3500)
Urea (temporary treatment for $\approx$ 1 d)	**–** 50, 200 and 400 mM
DTT	**–** 1 mM
EDTA (Kunji and Harding 2003)	**LA** 1 mM, **A** $\geq$ 5 mM
Glucose	**IC** $\geq$ 50 mM

2 Electron microscopy

2.1 Immunological labelling of YidC sheets

All immonogold labelling experiments were performed by Ms. Friederike Joos and Dr. Winfried Haase.

Immunogold on-grid labelling

In order to confirm that YidC was the major component of the two-dimensional crystals, the myc-epitope that had been engineered onto the carboxy-terminus of YidC, was immunologically labelled in an on-grid approach. The sheets (reconstituted in pure DPPG lipid) were extensively labelled (Fig. 16 A), indicating that the recombinant YidC formed the crystal arrays.

Immunogold-labelling of cross-sectioned sheets

Cross-sectioning and immunogold-labelling was performed on samples of crystalline sheets of YidC (reconstituted with pure DPPG) in order to find out whether the sheets consisted of one or multiple membrane layers and, secondly, if the myc-epitope genetically fused to YidC is exposed to both sides of the membrane. As already observed with the on-grid labelling, labelling occurred only after incubation with the anti-myc antibody, indicating that the labelling was specific to YidC (Fig. 16 C - F). The membranes were labelled from both sides (Fig. 16 D - F). The staining of the membranes indicated a mono-layered membrane (Fig. 16 F). The distance measured between the two lipid layers forming the membrane was approximately 50 Å (Fig. 16 F).
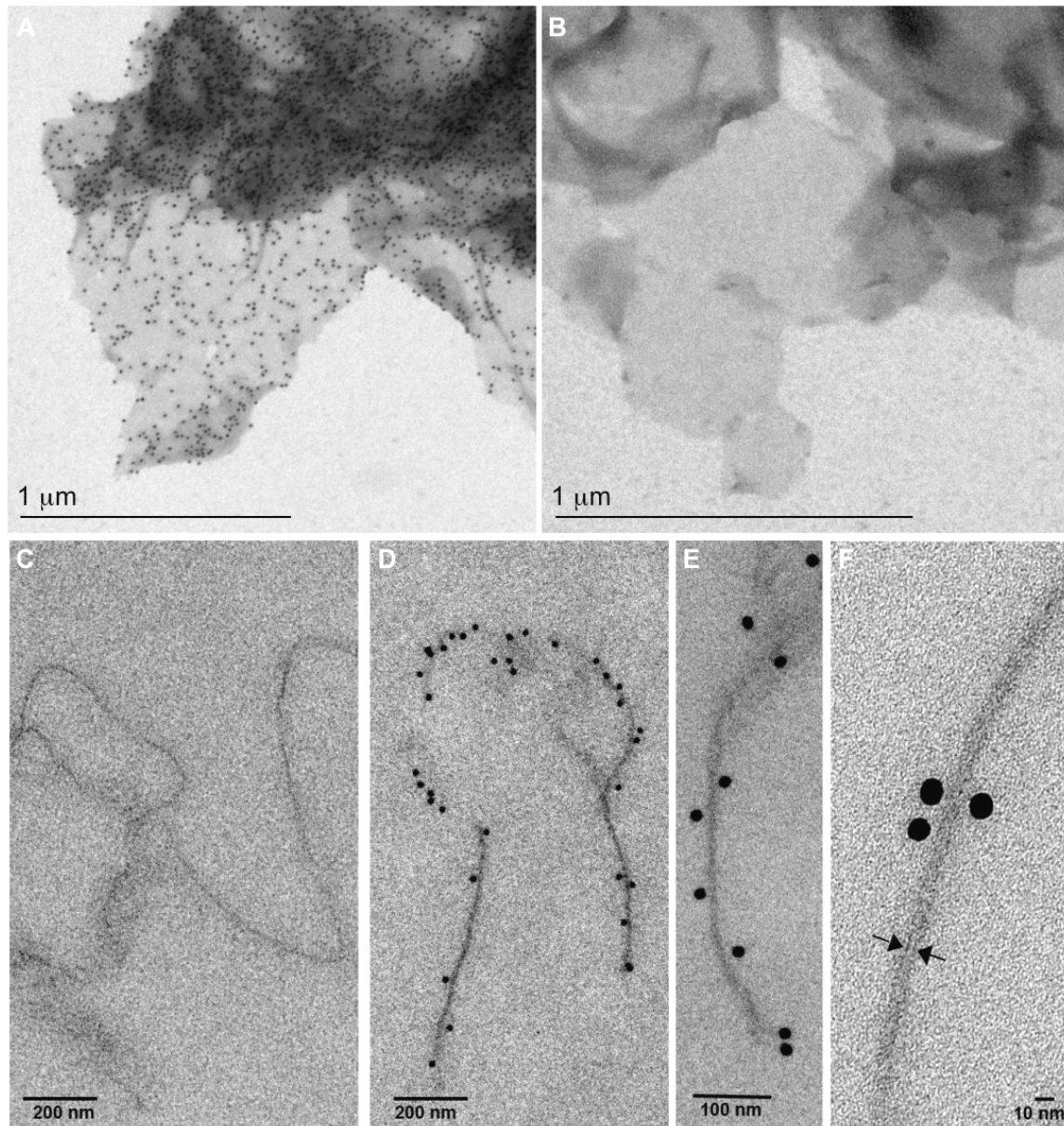
Fig. 16 <u>Immunogold-labelling of crystalline YidC sheets (uranyl acetate stain).</u>
Electron micrographs. **A**, **B**: On-grid labelling. **C** - **F**: Labelling of cross-sectioned
sheets (membrane contrast enhanced by osmic vapour). **A**; **D** - **F**: The carboxy-
terminal myc epitope of the over-expressed YidC protein was labelled with a
monoclonal anti-myc antibody (9E10). The anti-myc antibody was detected with a
secondary gold particle (18 nm diameter, Dianova) coupled antibody. The secondary
antibody bound to the crystalline sheets. **D** - **F**: Labelling occurred on both sides of
the membrane. **B**, **C**: Controls. The antibody against the myc epitope had been
omitted. No background labelling was observed. **F**: Arrows indicate where the two
lipid layers are identifiable.

2.2   Analysis of uranyl acetate stained YidC crystals

In electron microscopy, negative staining of tubular crystals and crystalline sheets of YidC yielded a very uniform distribution of the specimen on the grid, showing almost no background of stained precipitate. The negatively stained two-dimensional crystal lattices were screened according to their diffraction quality following fast Fourier transformation (Digital Micrograph software) of CCD images. The tubes yielded two orders of reflections (Fig. 17 A). The first order reflections were usually hardly visible and the second order reflections on the h- and the k-axis blurred (Fig. 17 A); probably, the reflections derived from two lattices, rotated by 90 relative to each other. The crystalline sheets yielded spots of two orders in h- and three orders in k-direction (Fig. 17 B). The reflections with the lattice co-ordinates [h = 2, k = 0] and [h = -2, k = 0] were usually very intense but often appeared blurred or split (Fig. 17 B).
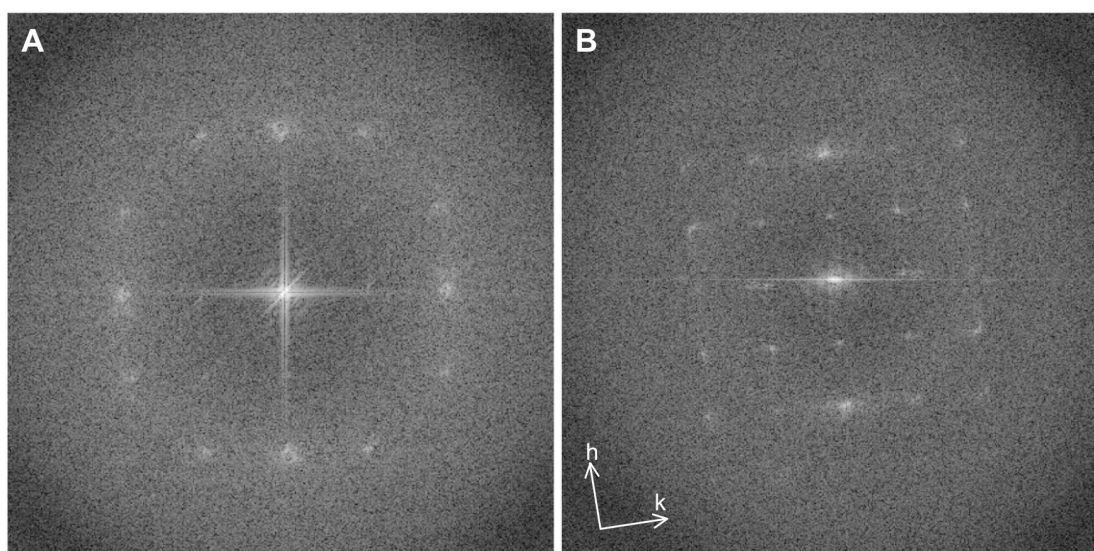
Fig. 17   Fast Fourier transforms of YidC crystals (uranyl acetate stain). **A**: Tube, reconstituted in 50:50 w/w DOPC/DOPG. The lattice orientation could not be assigned with certainty. **B**: Sheet, reconstituted in pure DPPG lipid. The lattice orientation in reciprocal space is depicted in the bottom left corner.

In order to calculate projection structures, images of uranyl acetate stained YidC crystals were recorded on film in low-dose imaging mode (magnification 45,000x). The projection structures from one crystalline sheet and one tubular crystal, respectively, were calculated in p1 symmetry (Fig. 18). The resolution of the data calculated from the tubular crystal was less than 25 Å (Fig. 18 A), whereas the sheet

provided the better information reaching to almost 20 Å resolution (Fig. 18 B). In the projection structure of the tubular crystal, two slightly different globular densities were visible per unit cell (Fig. 18 C), whereas one globular density was visible per unit cell in the projection structure of the crystalline sheet (Fig. 18 D).
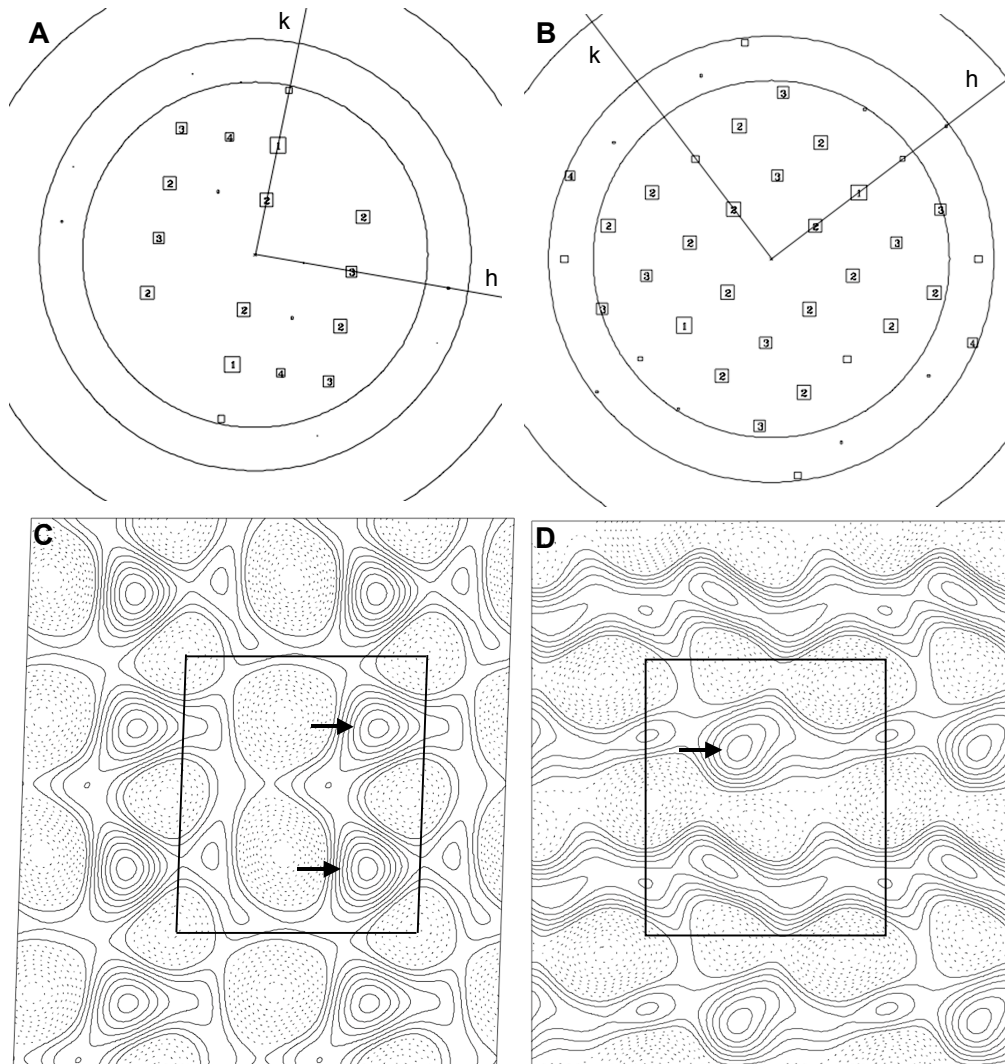
Fig. 18 Projection structures of YidC crystals (uranyl acetate stain). **A**, **C**: Tube. **B**, **D**: Sheet. **A**, **B**: Reflections plotted versus resolution. Each box indicates one unique reflection. The box size for each reflection is correlated to the signal to noise ratio, depicted as IQ value (≤ 4) in each box (increasing IQ value means also increasing combined phase error: 1 < 8 °, 2 < 14 °, 3 < 20 °, 4 < 30 °). Resolution shells (inner to outer ring): 25, 20 and 15 Å. **C**, **D**: Projection structures. Black parallelograms indicate unit cells; dimensions: 88.1 x 77.3 Å, angle 92 ° (**C**) and 81.2 x 71.1 Å, angle 90 ° (**D**). Arrows indicate globular densities.

2.3 Analysis of frozen-hydrated YidC crystals

2.3.1 Cryo-preservation

In order to collect data by electron cryo-microscopy, various methods were tested for the cryo-preservation of the two-dimensional YidC crystals. Like the negatively stained crystals, the frozen-hydrated specimens were usually uniformly distributed on the carbon support film. Since tubular crystals did not yield any cryo-data, the results reported in the following refer only to the crystalline sheets. The preparation methods were directly assessed by means of electron micrographs of frozen-hydrated crystals. The data quality was analysed by laser diffraction on an optical bench.

No reflections were observed with crystals cryo-preserved using the back-injection method (Wang and Kühlbrandt 1991) (cryo-protectants: 4 % trehalose, 2 % tannin, 10 % glucose, all values w/v). Reflections were observed with crystals vitrified in liquid ethane, using no cryo-protectants. In general, the cryo-preservation of the YidC crystals was difficult to reproduce. Most attempts to improve the cryo-preservation were directed to a freezing method that preserves the samples from drying out (blotting with buffer-drenched filter paper, working in the cold room, blotting using short blotting times, combinations of these methods); a potential drying out of the extended periplasmic domain of YidC was considered as a possible reason for the difficulties in the cryo-preservation of the crystals. Supporting this assumption, all data was collected from frozen-hydrated crystal samples that looked comparatively wet in the electron microscope.

A properly cryo-preserved sample often yielded many crystal images per grid providing reflections of high order and intensity in the Fourier transforms. Most image data averaged for generating the YidC projection structures was obtained from crystals vitrified using the Vitrobot™ (2.3.3, Tab. 7).

One attempt was undertaken to freeze the specimens sandwiched between two layers of carbon film, also referred to as the 'carbon sandwich method'. This method was originally invented with the main goal to avoid carbon wrinkling and to minimise charging effects (Koning et al. 2003; Gyobu et al. 2004), but was used in case of YidC with the aim of keeping the YidC crystals sufficiently hydrated during the cryo-preservation. A sample of YidC crystals prepared with the carbon sandwich method (no cryo-protectant) yielded data (Tecnai Spirit electron microscope, acceleration

voltage 120 kV, magnification 45,000x). The quality of the data was slightly inferior to the best data quality achieved without the second layer of carbon film.

2.3.2   Individual projection structures

Lattice areas giving rise to high order, sharp reflections by optical diffraction (2.3.1) were scanned and subsequently computationally filtered and unbent in p1 symmetry. Fig. 19 and Fig. 20 show the typical data gained from most individual images (image taken at 500 nm defocus, acceleration voltage 200 kV, magnification 50,000x):
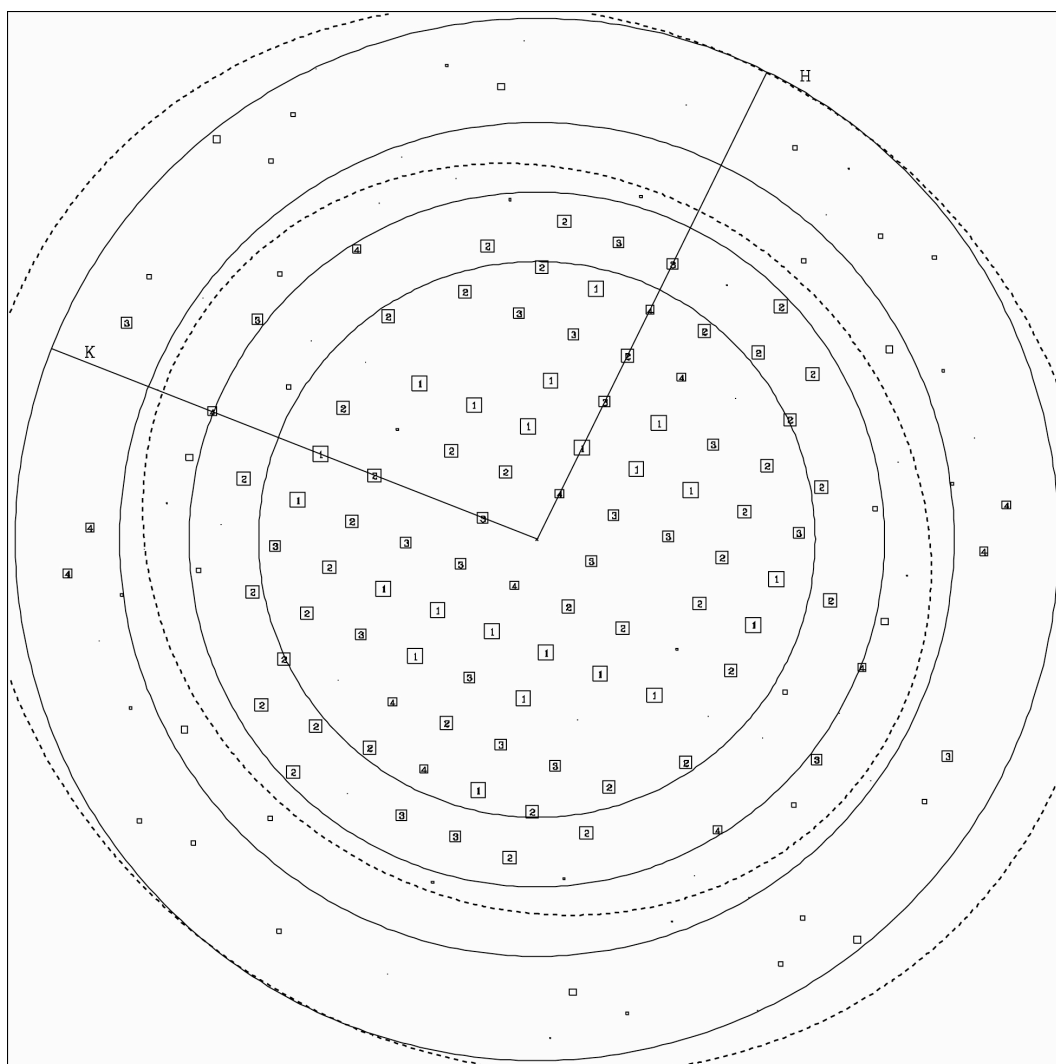

Fig. 19   <u>Fourier transform of a frozen-hydrated YidC lattice.</u> Data (IQ ≤ 4) after filtering and unbending in p1 symmetry. Reflections plotted versus resolution (plot see also Fig. 18). Resolution shells (inner to outer ring): 15, 12, 10 and 8 Å. The dashed rings indicate the nodes of the contrast transfer function.

The obtained reflections (IQ ≤ 4) were usually located before the first or the second zero of the contrast transfer function (Fig. 19). Reflections extending to about 8.5 Å resolution were obtained, but the information was less complete beyond approximately 11 Å resolution (Fig. 19). Projection structures were calculated from reflections after filtering and unbending. Proposed YidC monomers (Discussion, Analysis of YidC, 2.4) were visible, forming 'zig-zag lines' in the membranes (Fig. 20). In many projection structures, one or both of the proposed monomers had a central area of low density (Fig. 20).
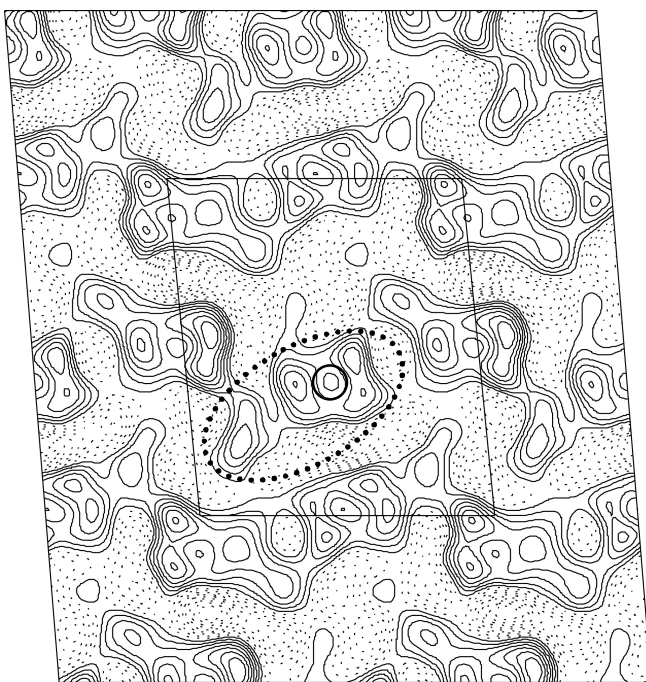
Fig. 20 Projection structure of a frozen-hydrated YidC lattice. The structure was calculated from the reflections visible in Fig. 19. The black dotted oval marks one proposed YidC monomer, the black circle the area of low density. The unit cell (81.8 x 69.4 Å, angle 85.3 °) is indicated by a black parallelogram. No B-factor was applied. Resolution: (nominal) 8 Å.

2.3.3   Averaged projection structures

The individual projection structures displayed a comparatively wide deviation in the unit cell angles, varying between 83 and 91 °. Also the lengths of the unit cell axes deviated about 4 Å in the a-direction (79.9 - 84.1 Å), and about 3 Å in the b-direction (69.9 - 72.3 Å). In order to take the varying unit cell angles into account, 10 independent projection structures from frozen-hydrated YidC crystals were grouped into two different sets before averaging. Set 1 contained individual images with included unit cell angles of about 85 °, set 2 such with unit cell angles of about 90 ° (Tab. 7). Furthermore, only images that showed matching contour lines were grouped together in order to avoid blurring of features in the averaged projection structures. In

both image sets, the unit cell axis lengths had an arithmetic mean of 82 Å (a-axis) and 71 Å (b-axis) (Tab. 7).

Tab. 7 <u>Averaged individual projection structures of YidC.</u> Images (numbered bold) were recorded from frozen-hydrated lattices at defocus values between 310 - 830 nm (set 1) and 290 - 730 nm (set 2). **C**: Cryo-preservation condition. **M**: Magnification. **D**: Unit cell dimensions. EM: Electron microscopes including acceleration voltage and camera setup, respectively. VB: Vitrobot™. hum: Humidity. CR: Cold room. ∅: Arithmetic mean. Dev.: Lowest value subtracted from the highest.

EM	Set 1			Set 2		
Tecnai F20 (200 kV)	**1** **C** VB (2 x 1 secs, 50 % hum.) **M** 50,000x **D** 83.1 x 72.3 Å, angle 83.0 ° **2** **C** VB (2 x 1.2 secs, 50 % hum.) **M** 50,000x **D** 82.9 x 71.9 Å, angle 83.6 ° **3** **C** VB (2 x 1.2 secs, 50 % hum.) **M** 50,000x **D** 81.8 x 71.9 Å, angle 85.3 °			**7** **C** VB (2 x 1 secs, 50 % hum.) **M** 50,000x **D** 81.5 x 71.8 Å, angle 89.0 ° **8** **C** VB (2 x 1 secs, 50 % hum.) **M** 50,000x **D** 82.7 x 69.9 Å, angle 90.3 ° **9** **C** VB (2 x 1 secs, 50 % hum.) **M** 50,000x **D** 82.6 x 70.4 Å, angle 89.7 °		
JEOL 3000 SFF (300 kV, spotscan)	**4** **C** VB (2 x 0.8 secs, 50 % hum.) **M** 53,000x **D** 80.5 x 70.0 Å, angle 86.8 ° **5** **C** VB (2 x 0.8 secs, 50 % hum.) **M** 53,000x **D** 81.8 x 69.4 Å, angle 85.0 ° **6** **C** Wet filter paper / CR **M** 43,000x **D** 81.1 x 71.3 Å, angle 86.8 °			**10** **C** VB (2 x 1.2 secs / CR) **M** 43,000x **D** 82.8 x 71.6 Å, angle 91.0 °		
Dimension	∅	Dev.	rms ± rms dev.	∅	Dev.	rms ± rms dev.
a-axis	81.9 Å	2.5 Å	81.8 ± 1.0 Å	82.4 Å	1.3 Å	82.7 ± 0.6 Å
b-axis	71.1 Å	2.9 Å	71.6 ± 1.2 Å	70.9 Å	1.4 Å	71.0 ± 0.9 Å
Angle	85.1 °	3.8 °	85.3 ± 1.6 °	90.0 °	2.0 °	90.0 ± 0.9 °

Symmetry

The program ALLSPACE was used to screen for in-plane symmetries in the Fourier transformed images (assessed using reflections with an IQ ≤ 7). Twofold symmetry was found for more of the images of set 1, whereas screw axis symmetry was found for both sets of images (Tab. 8). Images 2 to 4 belonged to the individual projection structures showing the most details (individual image 4 is shown in Fig. 20). In

general, comparing the features visible in the individual projection structures, the twofold symmetries were found for more images of higher quality, whereas the screw axis symmetries were found for images in a wider range of quality.

Tab. 8 <u>Symmetries proposed by ALLSPACE.</u> Acceptable (*), should be considered (!), possible ('). p121_a or p121_b: Screw axis along the a-axis (p121_a) or the b-axis (p121_b). p2 or p22121: Twofold symmetries. The p22121 symmetry furthermore implies screw axis symmetry along the a- and b-axis, respectively. The symmetries p121_a, p121_b and p22121 require by definition a unit cell angle of 90 °.

Set	Image	p121_a	p121_b	p2	p22121
1	1		'		
	2	*	*	*	*
	3	'	*	*	!
	4	'	*	*	*
	5	'			
	6		'		
2	7				
	8	!	!	'	'
	9	*			
	10		'		

Averaging in p1 symmetry

The Fourier transformed images of set 1 and set 2 were averaged in p1 symmetry. The information at higher resolution was more complete for set 1 (Fig. 21). In addition, the overall phase error for the averaged images of set 1 (Tab. 9, A) was lower than for the averaged images of set 2 (Tab. 9, B). Averaging of both sets yielded reflections of approximately 8.5 Å resolution (Fig. 21). Since the information was less complete beyond 10 Å resolution for set 1 and set 2 (Fig. 21), the averaged projection structures were truncated to 10 Å resolution.

Tab. 9 <u>Overall phase errors for the projection structures of YidC.</u> Averaged were the images of Set 1 (**A**) and Set 2 (**B**), respectively. Refl.: Number of unique reflections in each resolution range. E: Phase error for each resolution range. ∑ Refl.: Number of reflections in total. Data significance of 'random': overall phase error of 90 ° (p1 and p121_a symmetry) and 45 ° (p2 symmetry), respectively. **A**: Images 2 to 4: Images with predicted p2 symmetry. **B**: Images 8 and 9: Images with predicted p121_a symmetry.

| **A**	Set 1		Images 2 to 4			
	p1		p1		p2	
Resolution range [Å]	Refl.	E [°]	Refl.	E [°]	Refl.	E [°]
200 - 28.9	11	9.4	10	12.6	10	16.0
28.9 - 20.0	12	7.2	12	18.5	12	12.9
20.0 - 16.4	11	6.8	11	17.3	11	9.1
16.4 - 14.1	10	27.3	10	27.8	10	14.7
14.1 - 12.7	11	24.4	7	11.3	7	9.2
12.7 - 11.5	8	21.0	8	27.1	8	30.2
11.5 - 10.7	11	39.5	8	46.6	8	44.8
10.7 - 10.0	11	36.6	8	45.7	8	29.6
∑ Refl.	85		74		74	
Overall phase error [°]	21.3		25.0		19.8	
B	Set 2		Images 8 and 9			
	p1		p1		p121_a	
Resolution range [Å]	Refl.	E [°]	Refl.	E [°]	Refl.	E [°]
200 - 28.9	10	10.0	10	9.7	7	10.2
28.9 - 20.0	13	19.5	12	13.3	8	13.9
20.0 - 16.4	12	15.3	12	22.7	7	23.8
16.4 - 14.1	9	10.2	9	18.6	5	23.0
14.1 - 12.7	14	23.6	11	36.5	8	35.2
12.7 - 11.5	10	36.5	7	45.0	5	40.0
11.5 - 10.7	10	39.3	4	28.6	3	28.6
10.7 - 10.0	8	45.7	6	52.5	3	63.7
∑ Refl.	86		71		46	
Overall phase error [°]	24.2		26.0		26.6	
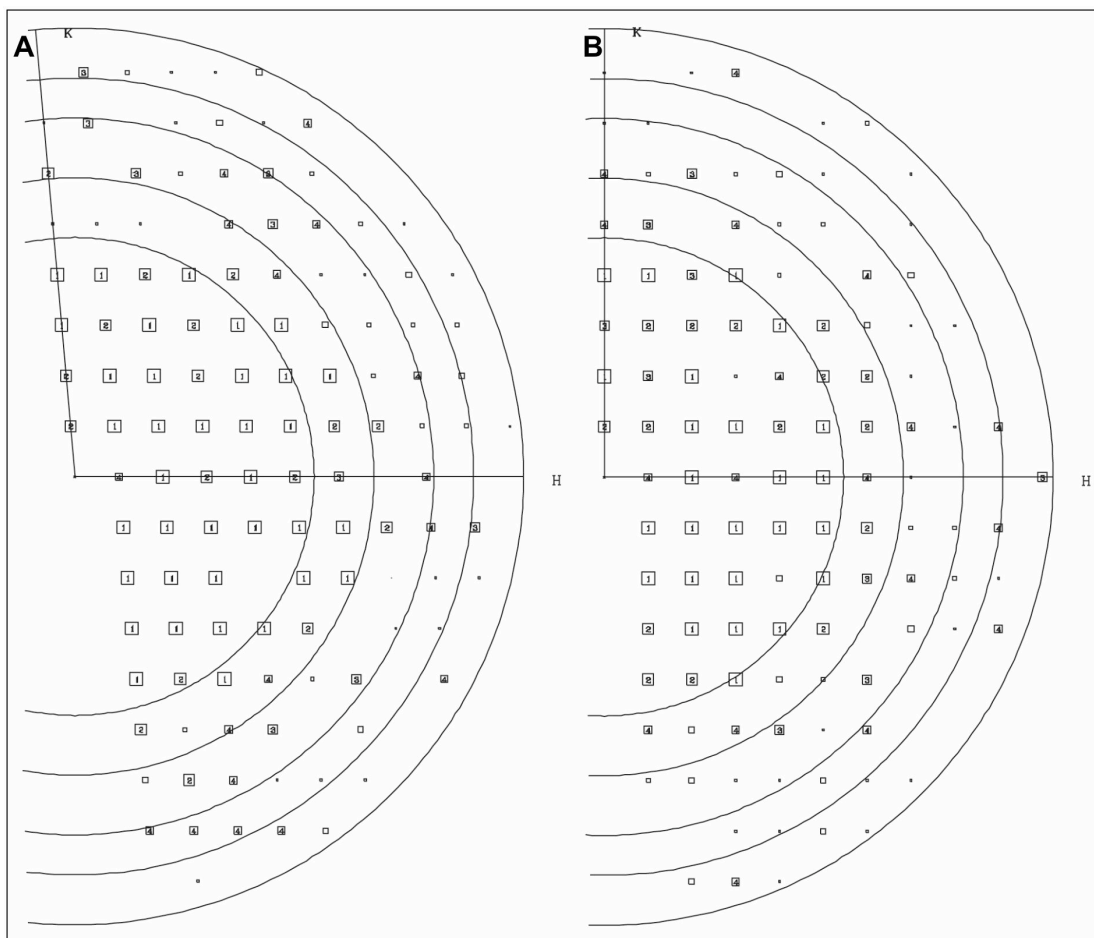
Fig. 21 Combined phase errors from averaging set 1 (**A**) and set 2 (**B**). The structures of each set were averaged in p1 symmetry. Combined phase error for each unique reflection (IQ ≤ 4) plotted versus resolution (plot see also Fig. 18). Resolution shells (inner to outer ring): 15, 12, 10, 9 and 8 Å.

After averaging, many details were no more visible in *real space*, whereas the resolution of the averaged reflections (*reciprocal space*) was not decreased compared to the individual images. Therefore, an inverse B-factor (Unger 2000) of -750 Å^2 was applied for the calculation of the projection structures, which recovered the high-resolution information and retrieved the visible details, yielding projection structures that looked widely similar to the original images (Fig. 22). In the projection structure representing the averaged projection structures of set 2, the YidC monomers were unevenly pronounced (Fig. 22 B).
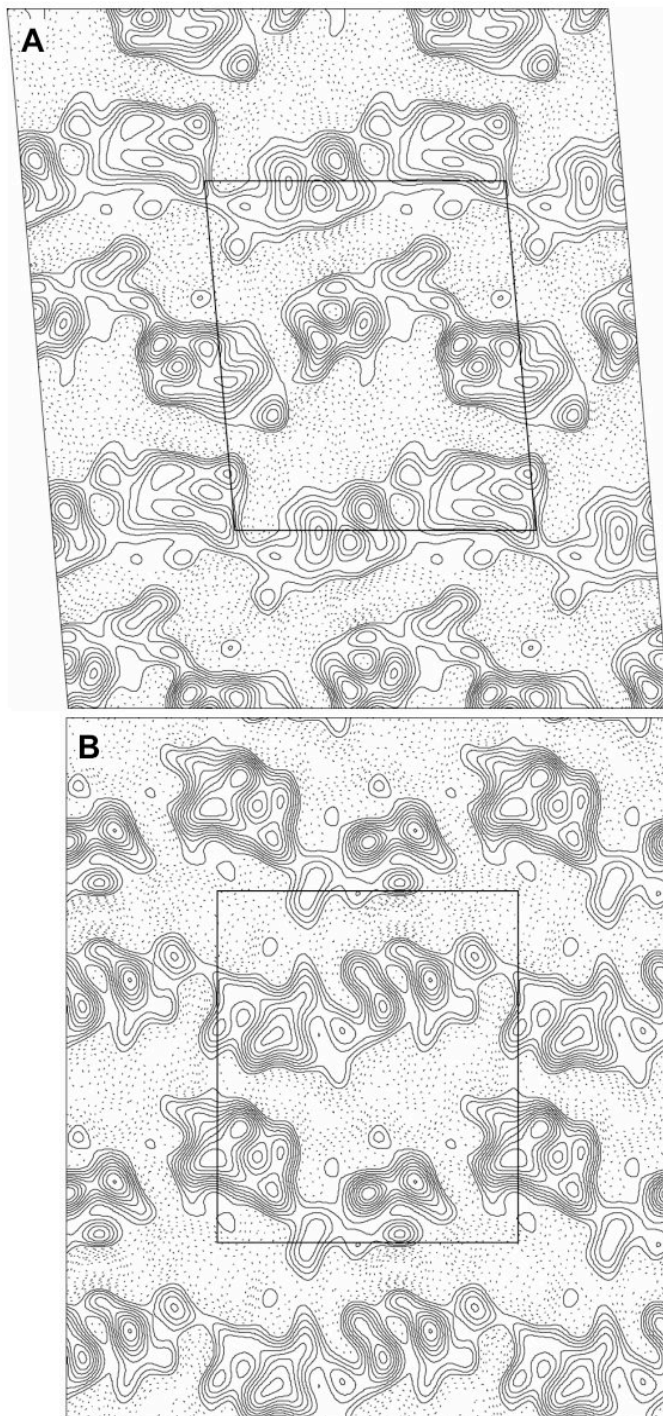
Fig. 22 <u>Averaged projection structures of set 1 (**A**) and set 2 (**B**).</u> The structures (10 Å resolution, B-factor: -750 Å^2, p1 symmetry) were calculated from the reflections visible in Fig. 21. Unit cells are indicated by black parallelograms. Unit cell dimensions: axis lengths 82 x 71 Å, angles 85 ° (**A**) and 90 ° (**B**).

Averaging in twofold symmetry

Averaging of images 2 and 4 (set 1) in p22121 symmetry with a unit cell angle 'forced' to 90 ° yielded a projection structure representing the original images poorly.

Images 2 to 4 (set 1) were averaged in p1 and p2 symmetry, both yielding reflections of approximately 9 Å resolution (Fig. 23). Implication of the p2 symmetry yielded an almost identical reciprocal lattice as obtained by averaging the three images in p1 symmetry (Fig. 23). For images 2 to 4, the overall phase error even

decreased upon implication of the p2 symmetry (Tab. 9 A). The averaged images 2 to 4 of set 1 were plotted in p1 and p2 symmetry at 10 Å resolution (Fig. 24). As observed in p1 symmetry, details of the individual images were not visible in *real space*, whereas the information in *reciprocal space* was of a quality reflecting the quality of the individual images. Therefore, inverse B-factors were used in order to restore the high-resolution information. Imposing p2 symmetry only caused slight changes in the appearance of the individual features, compared to the projection structure in p1 symmetry (Fig. 24).

Fig. 23 Combined phase errors of averaged images 2 to 4. Combined phase error for each unique reflection (IQ ≤ 4) plotted versus resolution (plot see also Fig. 18). Resolution shells (inner to outer ring): 15, 12, 10, 9 and 8 Å. **A**: p1 symmetry. **B**: p2 symmetry.

The low-density feature was also visible in the projection structures showing averaged images 2 to 4 (Fig. 24). The projection structure with p2 symmetry showed

the YidC monomers in two different representations (Fig. 24 B). A density seemed to be protruding from the 'body' of each proposed monomer (Fig. 24 B). Each YidC monomer had in-plane dimensions of roughly 40 x 25 Å, the central cavity of low density had a diameter of approximately 4.5 Å (Fig. 24 B). Obviously, YidC formed dimers in the membrane, formed by each time two YidC monomers of same representation (Fig. 24 B). The dimers were integrated in opposite orientation into the membrane and were related by a non-crystallographic symmetry (not applied) (Fig. 24 B).
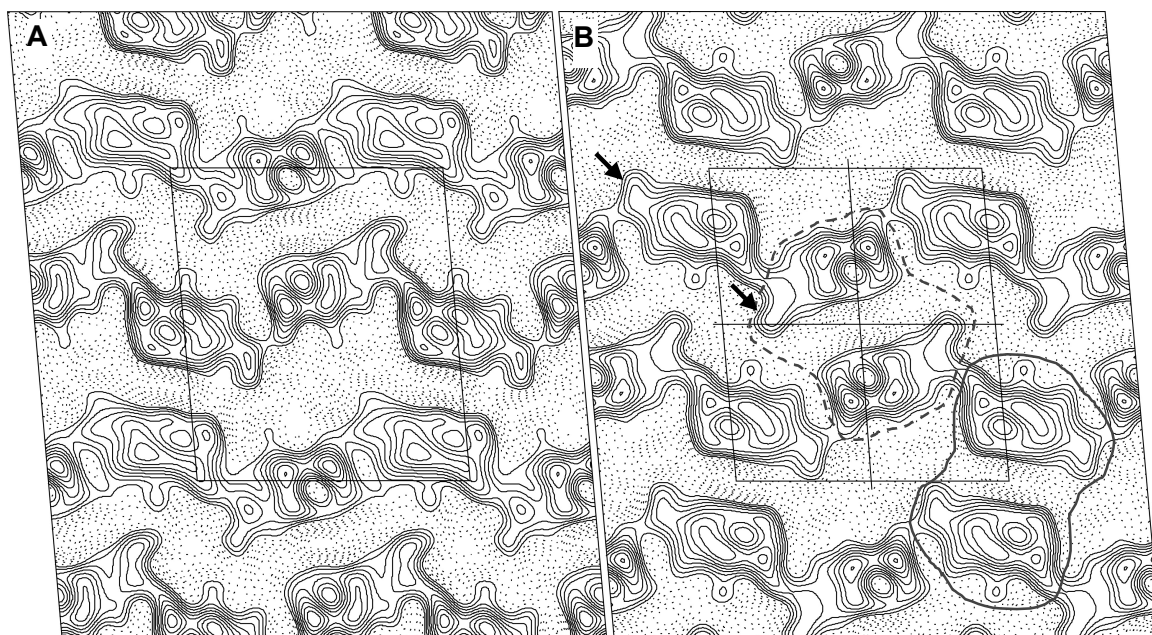
Fig. 24 <u>Projection structures of averaged images 2 to 4.</u> The structures (10 Å resolution, B-factor: -750 Å^2) were calculated in p1 (**A**) and p2 (**B**) symmetry from the reflections visible in Fig. 23. Unit cells (82 x 71 Å, angle 85 °) are indicated by black parallelograms. **B**: Locations of the twofold axes: in the centre of the black cross, in the intersection points of the cross with the unit cell axes and on the corners of the unit cell. Arrows indicate densities protruding from the body of each YidC monomer. Possible YidC dimers are marked (solid and dashed line, respectively).

Averaging in p121_a symmetry

Images 8 and 9 (set 2) were averaged in p1 and in p121_a symmetry. The data averaged in p121_a symmetry was almost complete to approximately 11 Å resolution (Fig. 25 B). Averaging of images 8 and 9 in p121_a symmetry did not lead to a significantly altered overall phase error, compared to averaging in p1 symmetry (Tab. 9 B). In both averaged projection structures, every second proposed YidC monomer

was less pronounced (Fig. 26). In general, significantly uneven pronounced YidC monomers were a feature of several individual YidC projection structures, showing less detailed features and hence were considered to be of lower quality.
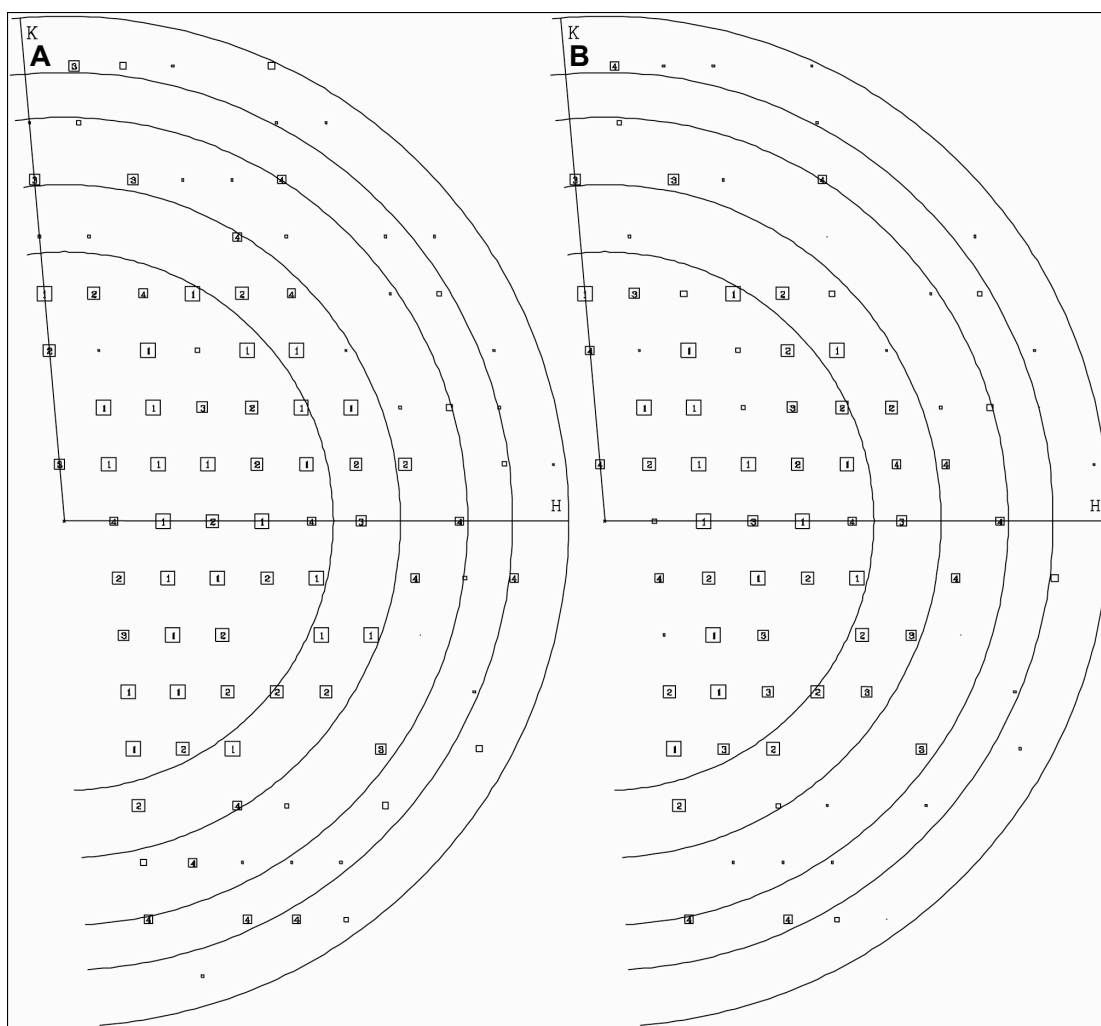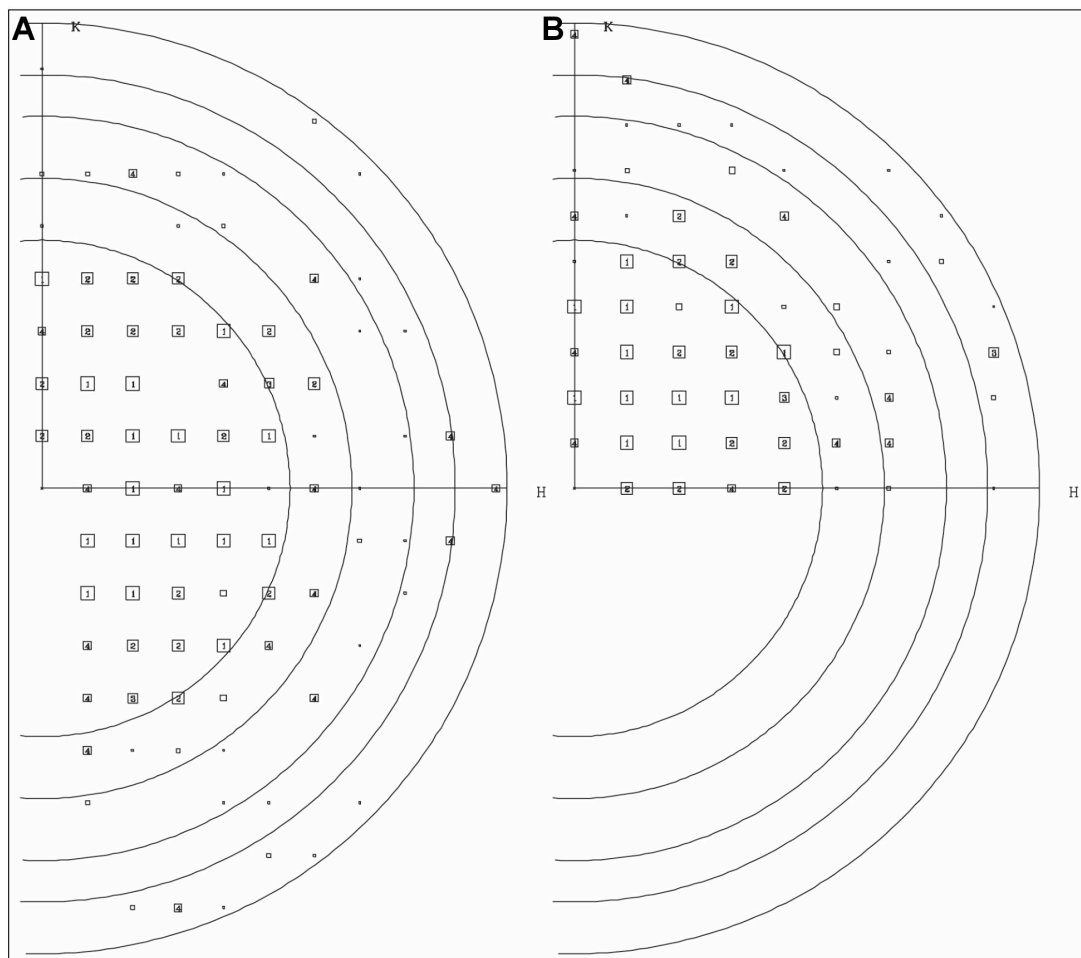

Fig. 25 Combined phase errors of averaged images 8 and 9. Combined phase error for each unique reflection (IQ ≤ 4) plotted versus resolution (plot see also Fig. 18). Resolution shells (inner to outer ring): 15, 12, 10, 9 and 8 Å. **A**: p1 symmetry. **B**: p121_a symmetry.
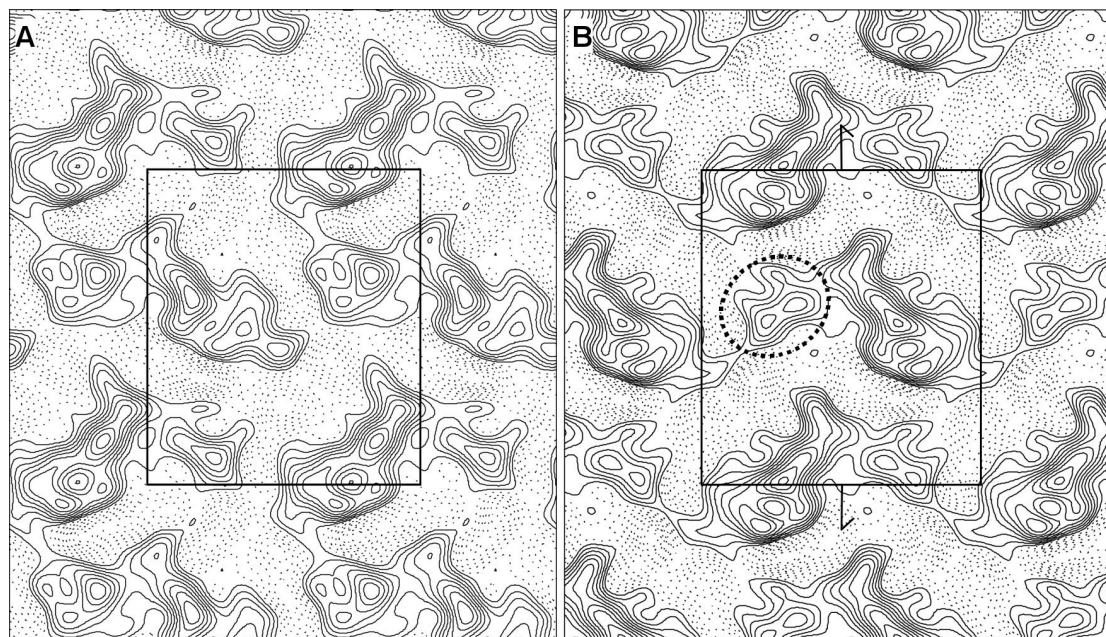
Fig. 26 <u>Projection structures of averaged images 8 and 9.</u> The structures (10 Å resolution, B-factor: -750 Å^2) were calculated in p1 (**A**) and p121_a (**B**) symmetry from the reflections visible in Fig. 25. Unit cells (82 x 71 Å, angle 90 °) are indicated by black parallelograms. **B**: The half arrows pointing away from the unit cell sides indicate the direction of the screw axes. The black dotted oval indicates a less pronounced YidC monomer.

2.4 Comparison of YidC and SecYEG

In order to compare YidC with SecYEG in projection, projection structures of dimeric SecYEG with imposed non-crystallographic twofold symmetry and the best projection structure of YidC (Fig. 24 B) were plotted at same scale, contouring and resolution. Four YidC monomers and dimeric SecYEG covered roughly the same membrane area (Fig. 27). The contours of SecYEG appeared sharper (Fig. 27). Plotted with these conditions, also monomeric SecYEG (in projection) exhibited two central regions of low density, the biggest one in proximity to the predicted lateral exit site for transmembrane helices (Fig. 27).
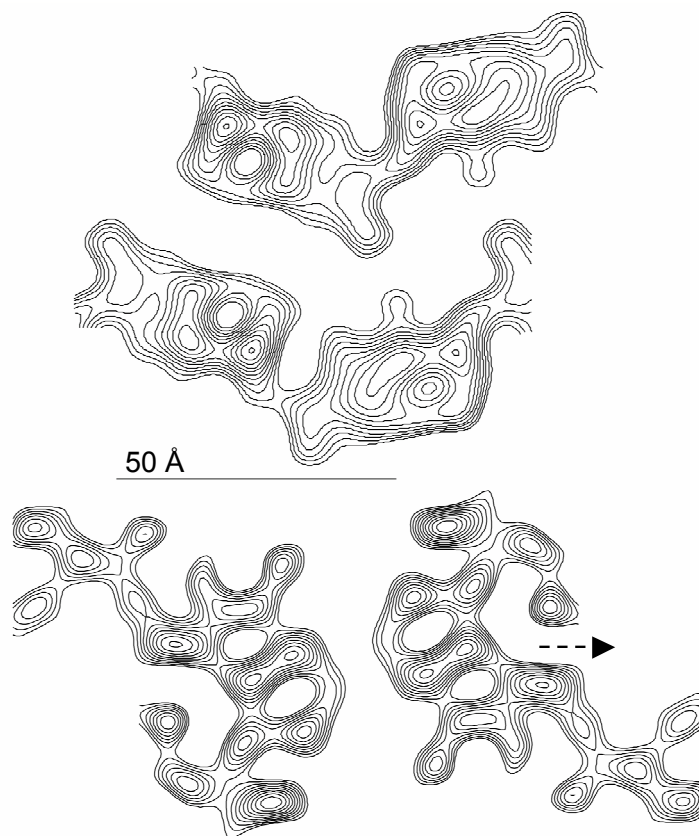
Fig. 27 <u>Comparison of YidC (above scale bar) and SecYEG (below scale bar).</u> Both structures are shown with 10 contour levels and at 10 Å resolution. YidC: densities corresponding to four proposed monomers (in total 24 predicted transmembrane helices). SecYEG: densities for one dimer (30 transmembrane helices). The dashed arrow indicates the proposed lateral exit site for transmembrane helices in the SecYEG monomer (van den Berg et al. 2004).

3 Oligomeric state of detergent-solubilised YidC

With the objective of assessing the oligomeric state of the purified YidC, a sample of YidC (protein concentration ≈ 1 mg/ml) was analysed by BN-PAGE, with and without prior incubation with 1 % w/v SDS. SDS-treated and untreated YidC formed a protein band at the same height (Fig. 28 A), suggesting that the purified YidC was monomeric. Higher oligomers or aggregates of YidC were not visible in the BN-PAGE (Fig. 28 A). The BN-PAGE was done by Dr. Stefan Raunser (Max-Planck-Institute of Biophysics, Frankfurt/Main, Germany).

The purified YidC was analysed with an analytical size-exclusion chromatography combined with laser light scattering (Fig. 28 B), which was performed by Dr. Stefan Raunser (Max-Planck-Institute of Biophysics, Frankfurt, Germany) in collaboration with Dr. Emma J. McGhie and Dr. Vassilis Koronakis (both University of Cambridge, U.K.). The experiments and the corresponding calculations are described in more detail in (Raunser 2004). The molecular weight and the oligomeric state of YidC, respectively, could not be determined unambiguously (Raunser 2004). However, the analysis showed that the purified YidC was monodisperse (Fig. 28 B).
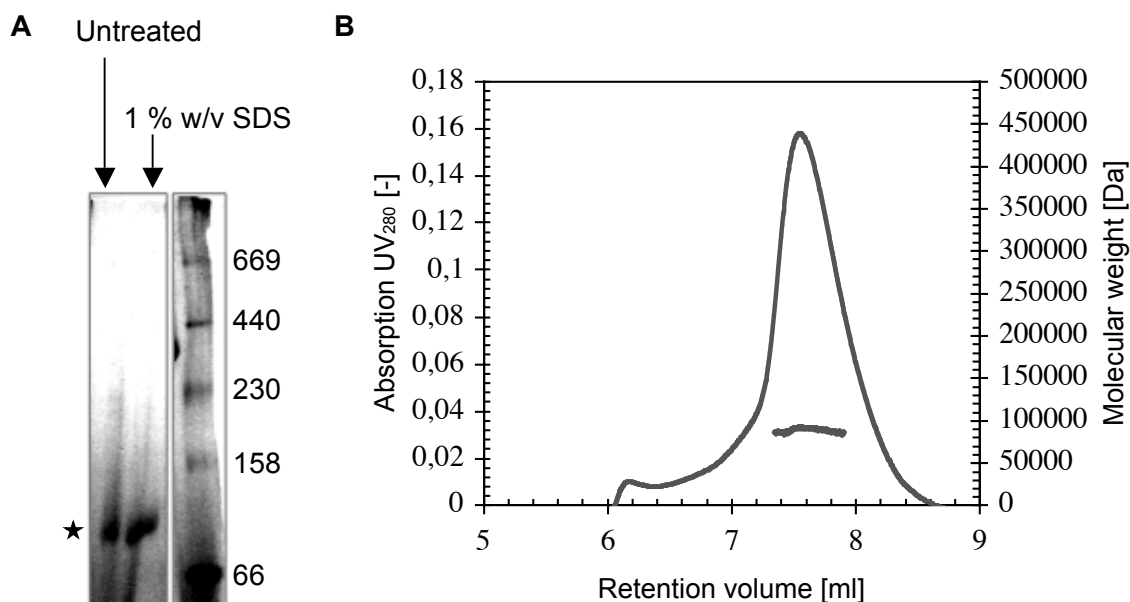
Fig. 28   Oligomeric state of detergent-solubilised YidC. **A**: BN-PAGE. YidC bands are indicated by black asterisk. Right lane: marker and indicated molecular weights in kDa. **B**: Size-exclusion chromatography and laser light scattering. The line below the curve (same line format as chromatogram) is formed of sample points at different retention volumes, determining the molecular weight of the YidC (oligomers) for each sample point. The molecular weight determined for YidC was similar for all fractions, so that the line appeared horizontal, indicating that the YidC preparation was monodisperse.

Effect of lipids on the oligomeric state of YidC

The lipid PE was found to bring about an aggregation of YidC in reconstitution experiments (1.2.2). In order to examine whether or not PE induces an oligomerisation of purified YidC, analytical size-exclusion chromatography was conducted with YidC incubated with PE and DPPG, respectively (both LPR 0.2 w/w); PG lipid had been identified as the best lipid for the reconstitution of YidC (1.2.2). The incubation with PE led to an additional peak close to the void volume of the column (Fig. 29). This additional peak was shown to be YidC by SDS-PAGE analysis. The addition of PE and DPPG also caused a slight decrease in the retention volume of the major YidC peak (Fig. 29).
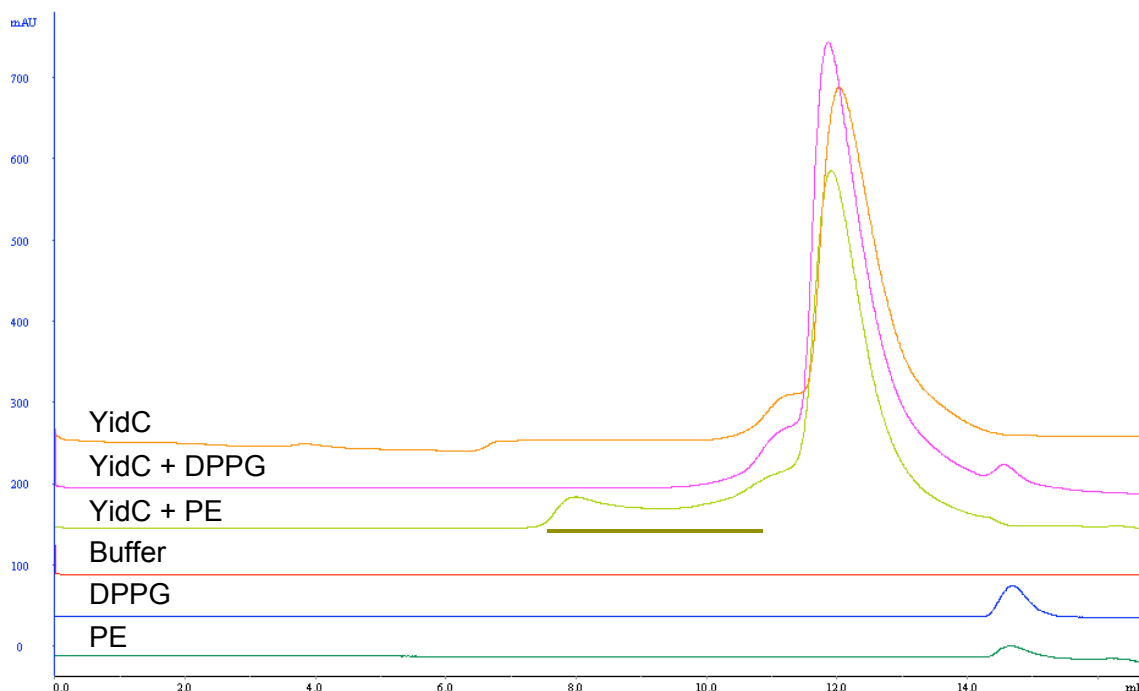
Fig. 29   <u>PE-induced aggregation of detergent-solubilised YidC.</u> Analytical size-exclusion chromatography. Light absorption (UV$_{280}$, vertical axis) plotted versus retention volumes (horizontal axis). The YidC peak occurring upon incubation of YidC with PE is underlined green. The small peaks at retention volumes around 14 ml were due to lipids.

4   Over-expression and purification of truncated YidC

With the aim to generate different or better two-dimensional crystals of YidC, two genetically truncated forms with depletions in the first amino-terminal periplasmic loop were over-expressed in *Escherichia coli* C43 cells. The mutant proteins were truncated for 298 (YidC$_{\Delta 323}$) and 253 (YidC$_{\Delta 278}$) amino acids, respectively (Jiang et al. 2003) and had been shown to be functional *in vivo* (Jiang et al. 2003). The genetic constructs were obtained from Dr. Ross Dalbey (Ohio State University, Ohio, U.S.A). The over-expression was conducted with an IPTG-inducible expression system. The purification of the over-expressed mutant proteins was performed according to the optimised procedure employed for the wild-type YidC (Materal and Methods, Tab. 1). The cells transformed with the YidC$_{\Delta 278}$ construct grew comparable to cells over-expressing wild-type YidC, but no YidC$_{\Delta 278}$ could be purified from the cells. The cells over-expressing YidC$_{\Delta 323}$ grew poorly, even before induction. However, low amounts of YidC$_{\Delta 323}$ could be purified from the membranes (Fig. 30).

A

B
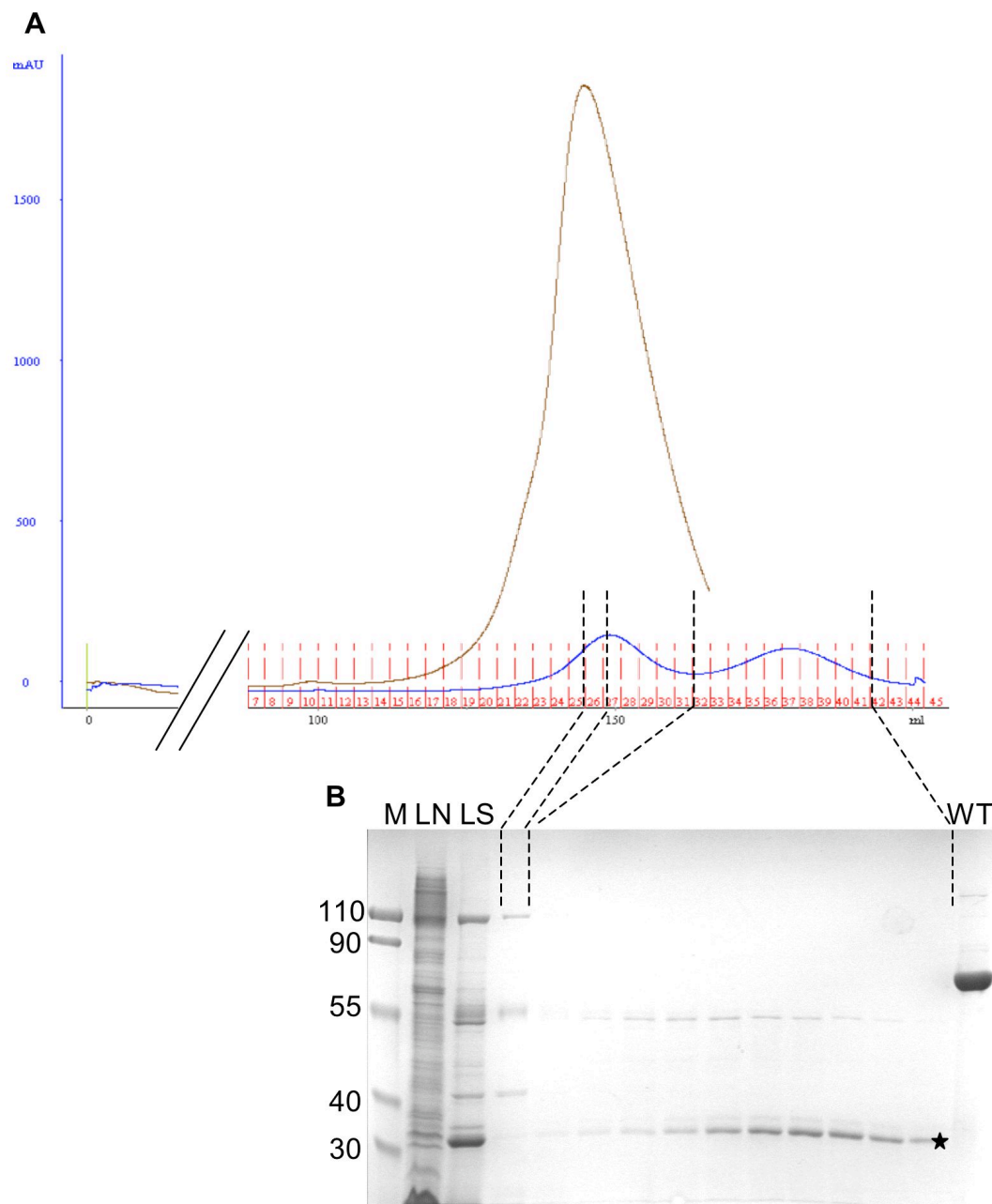
Fig. 30 Purification of YidC$_{\Delta323}$. **A**: Size-exclusion chromatography. Light absorption (UV$_{280}$, vertical axis) plotted versus retention volume (horizontal axis). Low amounts of YidC$_{\Delta323}$ (blue chromatogram) eluted at a higher retention volume (≈ 180 ml) than wild-type YidC (≈ 145 ml, brown chromatogram). Contaminating proteins separated from the YidC$_{\Delta323}$ fractions eluted in a peak at lower retention volume (≈ 150 ml). **B**: SDS-PAGE analysis (10 % w/v polyacrylamide, Tris-HCl) of the YidC$_{\Delta323}$ purification. M: Marker and approximate molecular weights in kDa. LN: Load Nickel-chelating column. LS: Load size-exclusion column. Other lanes: YidC$_{\Delta323}$ fractions 26 - 41 in (**A**). WT: Wild-type YidC. The black asterisk indicates the YidC$_{\Delta323}$ band.

The purified YidC$_{\Delta323}$ protein was analysed by SDS-PAGE. In accordance to the applied standard, the purified YidC$_{\Delta323}$ had a molecular weight of approximately 32

kDa (Fig. 30 B). The profile of proteins purified in case of YidC$_{\Delta 323}$ (Fig. 30 B) appeared similar to the proteins purified in case of wild-type YidC (Fig. 11 B), shifted to lower molecular weights. A comparatively strong band of contaminating protein with a molecular weight of approximately 53 kDa eluting in the earlier fractions from the size-exclusion column (Fig. 30 B, $\approx$ fractions 33 - 39) might resemble a YidC oligomer, not falling apart in SDS-PAGE. A few reconstitution experiments were conducted with the purified YidC$_{\Delta 323}$ protein. Thereby, no reconstitution of YidC$_{\Delta 323}$ was achieved.

5   Three-dimensional crystallisation of YidC

Purification

Three-dimensional crystals were obtained with YidC purified using Cymal 6 (1 % membrane solubilisation, 0.1 % Nickel-chelating chromatography, 0.06 % size-exclusion chromatography, all values w/v). Apart from the detergent, the purification had been performed as for the two-dimensional crystallisation of YidC. The purified YidC could be concentrated to about 10 mg/ml in centrifuge concentrators without visible aggregation.

Crystallisation conditions

Using the hanging drop method, three-dimensional crystals could be obtained at pH values between 5 and 6 using PEGs (various degree of polymerisation) as precipitating agents (Tab. 10). NH$_4$(SO)$_3$ (tested at concentrations of up to 1200 mM) precipitated the protein insufficiently, MPD led to a complete precipitation of the protein without crystallisation already at a concentration of 10 % v/v. The crystals formed, depending on the type of PEG, in about three weeks or were found after more than three months (Tab. 10). The crystal shape was dependent on the salt used: with monovalent cations, triangular crystals formed (Fig. 31 A). Using salts of divalent cations (Tab. 10), much larger crystals with different shape were obtained, containing most likely much detergent (Fig. 31 B). Interestingly, the respective crystallisation drops contained usually both, the triangular crystals obtained already with salts of monovalent cations and the much larger crystals (Fig. 31 C).

Tab. 10 <u>Conditions yielding three-dimensional crystals with purified YidC.</u>

Condition
Protein concentration   ≈ 8 mg/ml
Detergent for purification of YidC   Cymal 6
Precipitation method   Hanging drop
Temperature   18 °C
Mother liquor   ADA, citrate buffer and acetic acid (all 100 mM), pH 5 - 6   200 - 350 mM NaCl   or 50 - 350 mM KCl   or 300 - 400 mM LiCl (triangular crystals)   20 - 150 mM MgCl$_2$ or 20 mM CaCl$_2$ (larger, non-triangular crystals / triangular crystals)   25 - 30 % v/v PEG 550 MME   or 30 - 35 % w/v PEG 600   or 30 % v/v PEG 400   or 20 % w/v PEG 1000 (PEG 500 MME / 600: crystals formed in ≈ 3 weeks; PEG 1000 / 400: crystals grew after > 3 months)

Phase separation

The PEGs induced a separation of two liquid phases in the crystallisation drops (Fig. 31). This is considered to be unfavourable for the quality of the obtained three-dimensional crystals and often depends on the detergent concentration in the protein preparation. The detergent concentration was likely increased due to the concentrating of the purified YidC with Centriprep® devices, although the protein had been dialysed in order to reduce the concentration of Cymal 6 after concentrating. Attempts to save this concentration step failed. Small amphiphilic molecules can change the clouding behaviour of mixtures containing PEG and detergent (Garavito et al. 1984; Deisenhofer et al. 1985; Koepke et al. 1996; Okada et al. 2000; Palczewski et al. 2000; Rosenow et al. 2001).
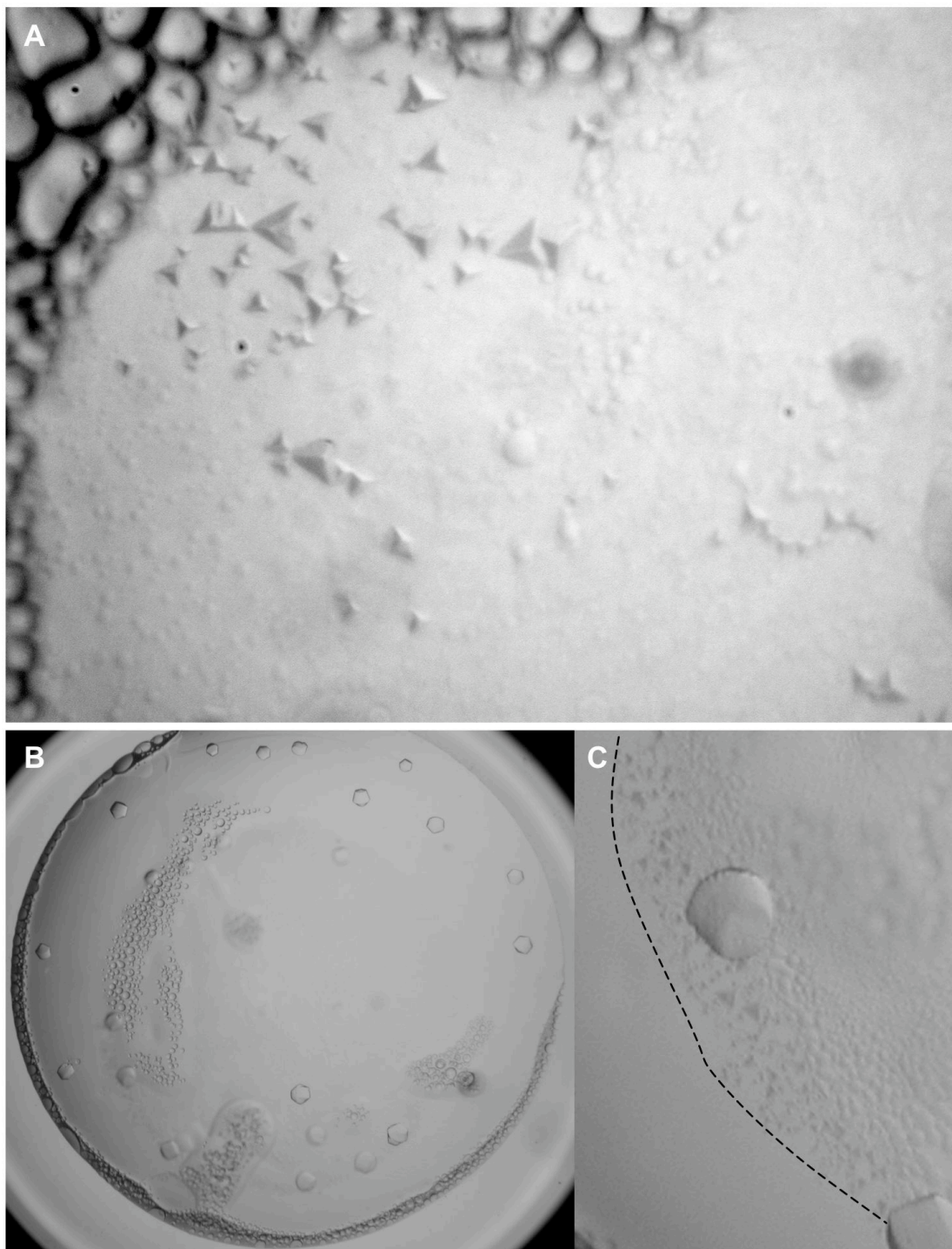
Fig. 31 <u>Three-dimensional crystals from purified YidC.</u> **A**: Crystals obtained with salts of monovalent cations (300 mM KCl). **B**: Crystals obtained with salts of divalent cations (20 mM MgCl$_2$). **C**: Crystals obtained with divalent cations (20 mM MgCl$_2$), enlarged representation. Additionally formed triangular crystals are visible along the border between the two liquid phases (along black dotted line, right hand side).

Therefore, the small amphiphilic molecules heptanetriol (up to 120 mM) and benzamidine-Cl (up to 64 mM), respectively, had been added into the YidC preparation in order to suppress the separation of a detergent-rich phase during the

crystallisation experiments. The so treated protein preparation was then used to set-up the crystallisation drops. Three-dimensional crystals were obtained in the presence of both amphiphiles, but the phase separation could not be overcome.

Discussion

Analysis of SecYEG/LamB$_{SP}$ crystals

1 Two-dimensional crystallisation of SecYEG

The existing protocol for the two-dimensional crystallisation of SecYEG (Collinson et al. 2001) was modified in order to obtain the two-dimensional SecYEG crystals faster and more reproducible. This was achieved by a change in the lipid preparation: two-dimensional SecYEG crystals were obtained in 10 days with lipid dissolved in solutions containing DM instead of $C_{12}E_9$.

The CMC of DM (0.087 % w/v) is significantly higher than that of $C_{12}E_9$ (0.0027 % w/v). Accordingly, the equilibrium concentration of monomeric DM was most likely higher than that in case of $C_{12}E_9$ (Helenius and Simons 1975; Kühlbrandt 1988). This suggests that DM could be removed much easier by dialysis out of the protein/lipid mixture explaining the shorter dialysis time required for the two-dimensional crystallisation of SecYEG. Use of two different detergents, one with low and another one with high CMC for the protein and lipid preparation in two-dimensional crystallisation, is a common determinant for two-dimensional crystal formation, reviewed by Mosser (Mosser 2001), and for example has been successfully employed for the two-dimensional crystallisation of BetP (Ziegler et al. 2004). According to the experiences made with the two-dimensional crystallisation of SecYEG and YidC and other published examples (Mosser 2001; Ziegler et al. 2004; Vinothkumar et al. 2005), DM appears to be particularly well suited for lipid solubilisation in two-dimensional crystallisation by dialysis.

Another variant with respect to crystal quality was the protein batch; attributable to variation in lipid and detergent in solution and to the protein itself. In addition, the substantial amounts of precipitate that built up on the inner surface of the dialysis bags during the two-dimensional crystallisation of SecYEG may have decreased the reproducibility of the two-dimensional crystallisation by changing the dialysis rate during the crystallisation.

2   Co-crystallisation

In order to analyse the rearrangements occurring within SecYEG upon the binding of signal peptide, co-crystallisation experiments of SecYEG and LamB signal peptide were conducted. LamB signal peptide has been shown to bind and 'open' the SecYEG complex for translocation (Simon and Blobel 1992), and SecY is required for transport of LamB through the inner membrane of *Escherichia coli* (Emr et al. 1981; Swidersky et al. 1992). Therefore, LamB signal sequence peptide was chosen as substrate for the co-crystallisation experiments. Furthermore, the high solubility of the peptide in water was advantageous for the crystallisation experiments.

In order to obtain two-dimensional crystals of SecYEG with bound LamB peptide, the LamB peptide was added to the mixture of detergent-solubilised SecYEG and lipid and added to the dialysis buffer prior to crystallisation. A potential advantage of co-crystallising SecYEG and signal peptide in a two-dimensional crystallisation approach is that the lipid bilayer resembles a native-like environment, which may favour signal peptide binding. The low amounts of LamB peptide delivered in the experiments indicate high affinity binding of LamB to SecYEG.

3   SecYEG/LamB$_{SP}$ projection structure

Compared to the projection structure of SecYEG, that of SecYEG/LamB$_{SP}$ was of slightly lower quality; the reflections corresponding to the SecYEG projection structure were more intense and included numerous reflections reaching beyond 9 Å resolution. One reason for this is that the SecYEG projection structure was averaged from 12 single images (Collinson et al. 2001), whereas the projection structure of SecYEG/LamB$_{SP}$ was the average of only 3 individual images. Therefore, the former structure has less noise.

Although the projection structures obtained with and without substrate displayed substantial differences, some regions, particularly the densities along the indicated screw axes (Fig. 9 C, D) looked similar. This indicates same packing arrangement for both types of two-dimensional crystals. Both SecYEG and SecYEG/LamB$_{SP}$ crystals were formed by two membrane layers related similarly by p121_b symmetry. This made it easier to compare the two projection structures.

4   Interpretation of the difference structure

In order to identify changes in the SecYEG molecule induced by signal peptide binding a difference structure was calculated by subtracting the densities of a former SecYEG projection structure from the densities of the one derived from SecYEG/LamB$_{SP}$ crystals. Similar approaches identified the locations of subunits in acetylcholine receptor (Kubalek et al. 1987) or demonstrated pH dependent rearrangements in two homologues of a Na$^+$/H$^+$ antiporter (Vinothkumar et al. 2005; Appel 2006).

In general, peaks in difference structures can represent two types of differences in respect to the analysed molecule. Missing or additional densities appear as single peaks in the difference structure. Thereby, the sign of the peak depends on whether the additional density was located in the reference projection structure (positive) or the subtracted one (negative). The second type of molecular differences, the relocation of domains, results in two peaks in the difference structure, a positive and a negative one, showing in combination the movement in the molecule, occurring upon substrate incubation or other (biological) issues. In this case, shape and density of the corresponding difference peaks are determined by the kind of the movement. Tilting of helices away from the bilayer normal results in a more elongated but less contoured signature, whereas pure lateral relocation changes the position but not the shape of the peaks.

The difference structure calculated from the SecYEG/LamB$_{SP}$ and the SecYEG projection structure shows three major positive and three major negative peaks. A problem in the interpretation of these peaks arose from the double membrane nature of the SecYEG crystals. Although the peaks of the difference structure map always to same regions relative to the double membrane, it is a priori not possible to say to which layer the difference peaks belong. In other words, each difference peak represents the sum of the changes in the two overlapping crystal layers and contains no crystallographic information appropriate to assign the differences to one or the other SecYEG layer and SecYEG molecules, respectively. However, assignment of difference peaks to regions in SecYEG can be tentatively made by comparing the two alternative difference peak positions in respect to the known structure of SecYEG (Breyton et al. 2002; van den Berg et al. 2004; Bostina et al. 2005). Some of the peaks can be assigned as they align well with the respective layers of the double membrane.

4.1 Conclusions on SecYEG involved in translocation

Overall, the data shows that one SecYEG dimer involved in translocation is an asymmetric molecule; it appears to be composed of two different SecYEG monomers. One of the SecYEG monomers (Fig. 10 E, upper monomer) exhibits two predominant features. The first conclusion is that it appears to have signal peptide bound. In the difference structure, this is represented by positive peak 2, which resembles an additional moiety in the centre of the molecule, close to the proposed protein channel in SecYEG (van den Berg et al. 2004; Bostina et al. 2005). This furthermore indicates that signal peptide binding occurred at a location slightly distant from the position expected according to an earlier model, which proposes binding between transmembrane helices 2b and 7 in SecY (van den Berg et al. 2004).

Secondly, this SecYEG monomer apparently has an altered conformation, compared to the other monomer: in the monomer with bound signal peptide, a domain formed of transmembrane helices 7, 8, 9 apparently moved away from the body of the SecYEG molecule, which is indicated by positive difference peak 1 and negative difference peak 1 (Fig. 10 E, outlined in cyan). The apparently relocated domain lines a lateral cleft in the SecYEG molecule, which is employed for the release of transmembrane proteins into the lipid bilayer (van den Berg et al. 2004). Release of transmembrane helices through this lateral exit region involves an opening of the cleft (van den Berg et al. 2004). Therefore, it is conceivable that the movement of transmembrane helices 7, 8, 9 indicated by the difference structure resembles this opening motion of the SecYEG molecule, occurring as result of signal peptide binding.

The second monomer (lower monomer in Fig. 10 E) overlaid with three difference peaks. These peaks are positive peak 3, negative peak 2 and negative peak 3. Positive peak 3, which runs along the indicated screw axis (Fig. 10 A), is significantly dependent on the resolution. It is more elongated and has fewer contours at lower resolution. Therefore, interpretation of positive peak 3 in terms of molecular changes is ambiguous. The latter also applies for negative peaks 2 and 3: although they align fairly accurately with the front side of the SecYEG molecule harbouring the proposed lateral exit site for transmembrane domains, positive difference peaks in positions attributable to molecular changes in the non-active SecYEG molecule are missing (Breyton et al. 2002; van den Berg et al. 2004; Bostina et al. 2005). It is reasonable to anticipate that positive peak 3, negative peak 2 and negative peak 3 are

due to the observed quality differences between the projection structure of SecYEG and the one of SecYEG/LamB$_{SP}$ (Fig. 9), not due to rearrangements in SecYEG. The difference structure therefore suggests that the second SecYEG monomer is essentially unaltered, compared to the SecYEG molecules crystallised without signal peptide (Collinson et al. 2001).

Overall, the data allows the conclusion that one SecYEG dimer involved in translocation is composed of one active and one non-active SecYEG monomer. The active monomer is the one with the bound signal peptide, which is more open towards the lipid bilayer. The non-active SecYEG monomer apparently has the lateral exit site for transmembrane helices in a more 'closed' state and has no substrate bound. The observation that dimeric SecYEG during translocation is composed of one active and one non-active monomer is in good agreement with other data (Mitra et al. 2005; Osborne and Rapoport 2007).

4.2 Alternative interpretation of difference peaks

Since the difference peaks were observed in two alternative regions relative to SecYEG, some of the positions should be discussed briefly.

First, looking at the whole SecYEG double layer, in the position of positive peak 2 densities for SecE of one SecYEG layer overlap with the putative translocation pore region of the other layer. As the contribution of one or the other SecYEG layer to the origination of positive difference peak 2 cannot be determined, in fact positive peak 2 could also represent a relocation of transmembrane domains in SecE and changes in both regions, the putative translocation pore and SecE, respectively.

In an alternative position relative to the SecYEG monomer with bound LamB peptide, positive peak 1 aligns with transmembrane helices 2b, 3 and 4 (Fig. 10 E). Anticipating that negative and positive peak 1 belong together, this position however unlikely resembles a molecular rearrangement (Fig. 10 E). Therefore, positive peak 1 in this position probably represents the described movement of transmembrane helices 7, 8 and 9, but observed for the other membrane layer (Fig. 10 D).

Positive peak 3 and negative peak 3 are located near to each other. This is particularly obvious from the difference structure not overlaid with SecYEG (Fig. 10 A). Therefore, contradicting the assumption that both peaks are due to quality differences between the two compared projection structures (4.1), both peaks together instead may resemble intramolecular rearrangements in the non-active SecYEG

monomer. Then, these difference peaks would suggest some kind of movement of transmembrane helix 8 towards a region posed by transmembrane helices 6, 9 and 10. However, this has no reasonable relation to the known structures (Breyton et al. 2002; van den Berg et al. 2004; Bostina et al. 2005) and therefore appears unlikely.

5 Outlook

Further experiments can help to interpret the data obtained from SecYEG/LamB$_{SP}$ crystals and difference structure calculation, respectively, and to verify binding of LamB to SecYEG. First, depletion of noise from the SecYEG/LamB$_{SP}$ projection structure and increase of resolution by averaging more projection structures of high resolution would serve to consolidate the interpretations done on basis of the difference structure so far and might help as well to proof whether or not LamB peptide has bound to SecYEG. The latter appears particularly important as biochemical assays confirming specific binding of LamB peptide to SecYEG in two-dimensional crystals are missing at the moment. Such an assay must also be suitable to dissect binding to SecYEG from spontaneous interactions of the LamB peptide with the lipid bilayer (McKnight et al. 1989; Jones and Gierasch 1994a; Jones and Gierasch 1994b). Although consuming regarding time and effort, building a three-dimensional reconstruction based on electron microscopic images from tilted frozen-hydrated SecYEG/LamB$_{SP}$ crystals in the end is the necessary step to deconvolute the two SecYEG/LamB$_{SP}$ crystal layers and to visualise and interpret changes in the molecular structure of SecYEG, occurring upon signal peptide binding, and for assessing LamB peptide binding unambiguously. The insights into molecular rearrangements potentially yielded by a three-dimensional structure of SecYEG/LamB$_{SP}$ could contribute substantially to the understanding of Sec-mediated protein translocation.

Analysis of YidC

1   Two-dimensional crystallisation

In order to obtain two-dimensional crystals of YidC, appropriate parameters for purification, reconstitution and crystal formation had to be found. The factors that determine the shape of a two-dimensional crystal are likely to be complex and have yet to be described comprehensively. Therefore, screening for crystallisation conditions had to be done in an essentially empirical process.

1.1   Purification

The choice of the detergent used for the purification of membrane proteins can influence the efficiency of their incorporation into lipid bilayers significantly (Mosser 2001). Therefore, the purification protocol was altered, mainly with the objective to yield a stable YidC preparation and to find detergents suitable for two-dimensional crystallisation. Accordingly, several detergents were tested for solubilising YidC out of *Escherichia coli* membranes and for the chromatographic purification of YidC, respectively. A two-dimensional crystallisation procedure was developed by dissolving membranes with one of the maltoside detergents containing a cyclic hydrophobic alkyl chain (Cymal detergents). Probably, these detergents remove the right portion of lipid from YidC when the protein is extracted from the membrane (Aveldano 1995; Banerjee et al. 1995).

PE was shown to bring about an aggregation of YidC. Probably, the Cymal detergents used for solubilising YidC out of the cellular membranes had dissociated PE from YidC, thus leading to the non-aggregated preparation of YidC. The latter preparation was shown by size-exclusion chromatography and laser light scattering to be monodisperse.

Crucial for a dense reconstitution of YidC was to exchange the detergent during the chromatographic purification to DM. YidC purified using exclusively Cymal 6 or DDM, which both have a significantly lower CMC than DM, could not be reconstituted. A sequential deployment of Cymal 6 and DM in order to purify YidC was found to be beneficial in the growth of good two-dimensional lattices of YidC. Probably, removal of DM by dialysis was easier due to its higher CMC.

1.2   Reconstitution and two-dimensional crystallisation

Lattice formation by NaCl depletion

It was absolutely necessary to eliminate NaCl from the dialysis buffer in order to induce a crystallisation of the reconstituted YidC. Accordingly, formation of the two-dimensional YidC crystals was achieved in a two-step process, with reconstitution and crystallisation separated. Experimental separation of the two steps is rather an exception referring to other crystallisation protocols, and for some proteins reconstitution and lattice formation may require to occur in one process (Kühlbrandt 1992). Ions are known to influence the formation of two-dimensional crystals in various ways (Kühlbrandt 1992; Schmidt-Krey et al. 1998; Mosser 2001), but the special high sensitivity for NaCl as observed for two-dimensional crystals of YidC is unusual, although comparable sensitivity for NaCl has recently been reported for two-dimensional lattices of the soluble protein SecA (Chen et al. 2007). Conceivably, the NaCl impaired the formation of salt bridges needed for lattice formation (Dasgupta et al. 1997; Smith and Scholtz 1998; Thomas and Elcock 2006), for example established between the extended hydrophilic parts of YidC. Maybe, the salt bridges were formed between the periplasmic domains of the YidC molecules.

Lipid

An important improvement of the YidC crystals was achieved by changing from approximately equal amounts of PC and PG to pure PG lipid. The change induced a transition from tubular crystals to sheets. The sheets had larger and more ordered crystalline areas. Changing the lipid from a mixture of PC and PG to pure PG lipid in addition caused a decrease in the LPR and an improvement in crystal order. Since crystalline membranes obtained with pure PG lipid contained less lipid, this may have resulted in tighter crystal packing, which likely is a prerequisite for highly ordered crystals. This is in line with a rational by Jap and co-workers (Jap et al. 1992) as well as with the observation that formation of well-ordered membrane protein crystals can be achieved by enzymatic reduction of the lipid content in protein containing membranes (Mannella 1984; Jap 1988; Walian and Jap 1990). Accurate LPR adjustment was very important for producing well-ordered two-dimensional YidC crystals, reflecting a high dependency of crystal formation on the amount of lipid in the sample as well.

In these conditions, the crystalline sheets contained 7 to 10 DPPG molecules per YidC molecule. Because of the large periplasmic domain of YidC, these values have to be multiplied by a factor of two in order to estimate the molar LPR referring to the membrane-embedded part of YidC. The resulting 14 to 20 lipid molecules are rather high compared with other reports (Hebert et al. 1995; Schmidt-Krey et al. 2004). Maybe, only low amounts of lipid co-purified with YidC and therefore larger amounts of lipid had to be supplemented in order to achieve the two dimensional crystals. However, because of the probably diverse interactions of lipid and protein in the crystal samples, the LPR might resemble only roughly the real ratio of protein and lipid molecules in the crystal lattices.

Cross-sectioning and immunogold-labelling indicated that the crystalline sheets reconstituted with pure DPPG had a membrane thickness of about 50 Å, which basically resembles the thickness measured for the inner membrane of *Escherichia coli* (50 ± 10 Å (Dubochet et al. 1983)).

Under natural conditions, the *Escherichia coli* inner membrane contains the lipids PE (≈78 %) and PG (≈11 %) as well as smaller fractions of various other lipids (White et al. 1972) with some variability according to the growth conditions (Arneborg et al. 1993). In this respect, the two-dimensional crystals grown with pure DPPG contained YidC in an unnatural environment, which served to reach an unnatural high enrichment of YidC in the reconstituted membranes, sufficient to establish crystal contacts between YidC molecules. However, lipids like PE occurring abundantly in the natural membrane of *Escherichia coli* could influence the function of YidC in nature. The property of PE to bring about an aggregation of YidC for example may suggest that it has some kind of functional relevance with respect to the oligomeric state of YidC in native membranes.

As no diffracting images were recorded from frozen-hydrated tubular crystals, crystal improvement and generation of the more ordered sheets by lipid adjustment was an absolutely necessary step to record electron microscopy images of the frozen-hydrated two-dimensional YidC crystals.

2   Projection structures from frozen-hydrated crystals

2.1   Preparation of frozen-hydrated samples

Well diffracting images giving rise to properly frozen-hydrated crystal lattices were collected from comparatively wet preparations (ice layer thick appearing or vitrification between two layers of carbon) of vitrified YidC crystals. Conceivably, the large soluble portion of YidC required avoiding drying out of the sample prior to vitrification and therefore had to be preserved in a certain layer of buffer. Similar requirements concerning cryo-preservation of two-dimensional crystals were observed also for other proteins with substantial hydrophilic domains (Auer et al. 1999; Schmidt-Krey et al. 2007). Maybe, the high demand in respect to the right sample humidity is also the reason why the efficiency of properly vitrified two-dimensional YidC crystals remained low, even with partially automated procedures (Vitrobot™).

2.2   Individual projection structures

The individual projection structures calculated from the frozen-hydrated YidC crystals varied with respect to their unit cell dimensions. Deviations in the unit cell angles had been also observed with the YidC projection structures calculated from negatively stained samples, showing that the angle deviations were not a particular electron cryo-microscopy problem. Probably, the crystals were lying slightly tilted relative to the grid surface when they were stained and vitrified, respectively, causing a variation of the unit cell angles in projection. Another reason for the differences in the unit cell angles might be that the crystalline sheets were sensitive to mechanical stress leading to a bending of the lattices.

Referring to the best averaged projection structure (Fig. 24 B), the area in the unit cell of the YidC crystals is 5,800 $Å^2$. Accordingly, each individual projection structure of frozen-hydrated YidC crystals represents the average of about 4,300 unit cells (the average area for each processed lattice is estimated to be 0.25 μm^2). This reflects that projection structures extracted from electron cryo-microscopic images resemble the product of an elaborate averaging process, which is required to extract the information from the originally noisy images.

2.3   Crystal symmetries and averaging

Knowledge about crystal symmetries not only provides information regarding the arrangement of the respective molecules (in the membrane). The crystal symmetries can also be applied to (projection) structures, which usually improves the structural data. In order to find symmetries in the individual projection structures of YidC, the Fourier transformed projection structures were analysed using the program ALLSPACE. ALLSPACE often found more than one possible symmetry for one and the same individual projection structure. Therefore, the symmetry proposals were ambiguous.

Found were essentially two types of in-plane symmetries. The first type were the screw axis symmetries (p121_a, p121_b). Screw axis symmetry means that all visible features can be mapped onto themselves by a two-step symmetry operation: first, the visible features are translated along the 'screw axis', which is either parallel to the a- (p121_a) or the b- (p121_b) axis of the unit cell. The amount of translation equals thereby half of the length of the a- (p121_a) and the b- (p121_b) axis, respectively. After translation, the visible features are mirrored on the screw axis. Screw axis symmetries require unit cell angles of 90 ° by definition. The latter brought about further inconsistency into the symmetry proposals, because many individual projection structures with proposed screw axis symmetries had unit cell angles deviating significantly from 90 °.

The second type of proposed symmetries were the twofold symmetries (p2, p22121). Twofold symmetries mean that all visible features can be mapped onto themselves by a rotation of 180 ° around axes perpendicular to the image plane (twofold axes). The p22121 symmetry thereby is a special case as it describes additionally screw axis symmetry along each time two axes in a- and b-direction (Fig. 32), respectively. Accordingly, p22121 symmetry requires also 90 ° unit cell angles. However, p22121 symmetry resembles a symmetry form frequently found for two-dimensional crystals.

It is hard to imagine that the crystalline sheets contained YidC in different crystal forms with different symmetries. This would contradict the observation that all individual or averaged projection structures from frozen-hydrated specimens showed YidC essentially in the same arrangement within the unit cells. Secondly, no drastic differences in the unit cell dimensions were observed, even though they differed in a certain range.

Therefore, in order to find out the right symmetry of the crystalline YidC sheets, the individual projection structures were first split into two sets regarding their unit cell angles (85 ° and 90 °, respectively) and averaged without symmetry. The prior splitting of the projection structures in respect of their unit cell angles should avoid a 'blurring-up' of the visible features due to averaging of not sufficiently congruent projection structures. Then, the symmetries were carefully applied for combinations of images and individual images, respectively. The resulting structures were assessed in respect to phase errors and in how far the structures after application of the symmetries show the features visible before, in the projection structures without applied symmetry.
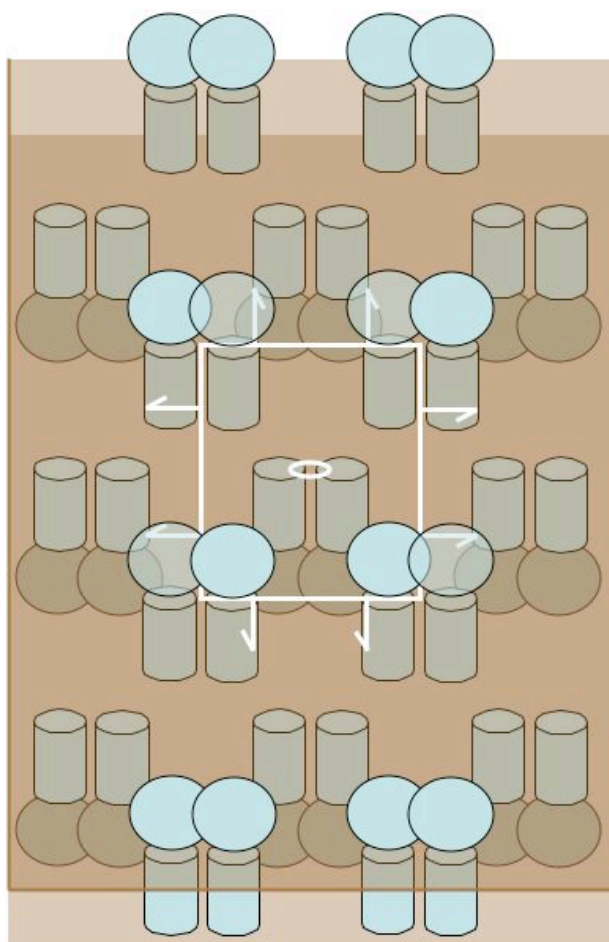

Fig. 32 Two-dimensional YidC crystal with (hypothetic) p22121 symmetry. Scheme, sidelong glance onto the membrane (brownish layers). YidC monomers are shown in blue colour (cylinders: transmembrane part, globule: soluble domain). One p22121 unit cell (white; relative dimensions: 82 x 71 Å, angle 90 °) is projected onto the membrane. The arrows indicate screw axis positions, the lens indicates the position of the central twofold axis. Other twofold axes are on the corners of the unit cell and in the middle of the unit cell axes, respectively.

The results can be summarised as follows: the best individual images had p2 symmetry, and averaging of the best individual images in p2 symmetry yielded the best projection structure of YidC (Fig. 24 B). The p121_b symmetry can be neglected. The p121_a but no p2 symmetry was usually found for projection structures of inferior quality. This is also evident from comparing the intensity and order of

reflections obtained by averaging of the images in p2 (Fig. 23 A) and p121_a (Fig. 25 A) symmetry, respectively. More precisely, the latter sort of projection structures seemed to share that they show not all YidC monomers equally well pronounced (Fig. 22 B, Fig. 26). Obviously, present p121_a and missing p2 symmetry in individual projection structures was provoked by inferior fidelity in imaging of all YidC monomers in the crystal lattice.

Therefore it can be concluded, that p2, and not p121_a symmetry, is the symmetry of the crystalline YidC sheets.

No reasonable projection structure in p22121 symmetry could be derived from the images recorded so far. However, in the best averaged projection structure (Fig. 24 B) the arrangement of possible YidC dimers in the unit cell reminds on projection structures of other proteins forming two-dimensional crystals in p22121 symmetry. These are, for example, NhaA (Williams et al. 1999), MjNhaP1 (Vinothkumar et al. 2005) and PSII (da Fonseca et al. 2002). In addition, by analysis with ALLSPACE p22121 symmetry was clearly found for the images averaged in the best projection structure (Tab. 8). Therefore, it is tempting to speculate whether images of higher quality and resolution will show that the crystalline sheets have p22121 symmetry and unit cell angles of 90 ° (Fig. 32), despite this only partially supported from the data obtained so far.

2.4   Structural details visible after averaging

B-factors

Inverse B-factors had to be applied in order to yield the details visible in the individual projection structures also after averaging. The amplitude fall-off for the intermediate and high-resolution reflections observed for the YidC images is a common problem of structural data derived from electron microscopic images, caused, for example, by specimen movements and the contrast transfer function (Henderson 1992). However, all shown projection structures of YidC were truncated conservatively to a resolution of 10 Å, which reduces the risk that noise was increased in the projection structures by application of the inverse B-factors. Furthermore, inverse B-factors restore the high-resolution in dependence of a weighting factor (FOM) and therefore mainly recover the high-resolution reflections that are well determined.

Arrangement of YidC in the membrane

Features in the crystalline sheets repeat one another in a 'zig-zag' like configuration, visible in projection structures from both, negative stained and frozen-hydrated sheets. In projection structures obtained from frozen-hydrated specimens, four obviously separated features were visible per unit cell, suggesting that each of them represents densities corresponding to one YidC monomer (Fig. 20). In order to confirm this assumption, the area covered by one predicted transmembrane helix in the projection structures was calculated. This was done by dividing the area of one unit cell (5,800 $Å^2$) first by four in order to obtain the area covered by one proposed monomer, and the result subsequently by six (number of predicted transmembrane helices). The resulting value is an area of 242 $Å^2$ per transmembrane helix of YidC.

According to other membrane protein structures each transmembrane domain requires 199 $Å^2$ (SecYEG) (Collinson et al. 2001), 186 $Å^2$ (bacteriorhodopsin) (Henderson et al. 1990; Grigorieff et al. 1996), 179 $Å^2$ (NhaA) (Williams 2000) or 184 $Å^2$ (rhodopsin) (Krebs et al. 1998). It is reasonable to assume that each of the four features in the unit cell is one YidC monomer, referring to the six predicted transmembrane domains in the YidC sequence (Sääf et al. 1998). The difference between the calculated 242 $Å^2$ per transmembrane helix of YidC and the lower values for the proteins mentioned above indicates a slightly less dense packing of YidC in the crystals.

The way the YidC monomers are arranged relative to each other (Fig. 24 B) suggests that YidC forms dimers, which are integrated in an anti-parallel fashion into the membrane. The anti-parallel orientation is evident from the opposite orientations of the dimers, referring to the visible details; looking onto the membrane plane, half of the dimers appear to be in clockwise, whereas the other appears to be integrated in anti-clockwise orientation into the membrane. Furthermore, the anti-parallel orientation of YidC was confirmed by immunogold-labelling of cross-sectioned crystals.

The hydrophilic domain of YidC

At least parts of the hydrophilic domain may be visible, in the projection structures superposed with the densities of the transmembrane part. This also depends on whether the periplasmic domain was ordered sufficiently in the crystals. Often, protein structures obtained by electron crystallography do not resolve extra membrane

domains very well as they are usually less well ordered than transmembrane parts (Rhee et al. 1998a). Separation of densities corresponding to the transmembrane part and soluble domains, respectively, would require a three-dimensional reconstruction. Already obtained three-dimensional reconstructions of other proteins with substantial soluble domains (Toyoshima et al. 1993; Auer et al. 1998; Zhang et al. 1998) demonstrate that electron-crystallography is capable of visualising such hydrophilic domains. In case of YidC a three-dimensional reconstruction might also require further crystal improvement.

The TRAP complex aiding protein translocation in mammals (Görlich et al. 1992a; Mothes et al. 1994; Fons et al. 2003) was visualised at intermediate resolution by electron cryo-microscopy in association with the eukaryotic Sec-translocon and a translating ribosome. From this reconstruction, the silhouette of TRAP including its lumenal domain is visible (Menetret et al. 2005). It is a reasonable possibility that a three-dimensional reconstruction may show YidC with an outer shape essentially similar to TRAP.

Central area of low density

In the centre of YidC appears to be an area of low density. The SecYEG projection structure, calculated from a three-dimensional reconstruction (Breyton et al. 2002) was plotted and compared to the projection structure of YidC at same scale, contour level and resolution. This yielded also for SecYEG in projection several areas of low density, of which the major one appears structurally concomitant with the proposed lateral exit for transmembrane domains in the Sec-complex (Fig. 27). Hence, it is tempting to speculate that also the area of low density in YidC has functional relevance. It may represent a constriction of the membrane where polypeptides bind as they pass through or into the membrane. It is not likely to be an open pore in its resting state, as the energy conserving nature of the inner membrane needs to be preserved.

Transmembrane helices

Superposition of the densities accounting for the large periplasmic loop and the transmembrane helices of YidC, respectively, might to some extend blur the appearance of the transmembrane helices in projection. Accordingly, the appearance of the YidC molecules is reminiscent of that of other membrane proteins with

substantial soluble domains visualised in projection structures (Jahn et al. 2001; Lebeau et al. 2001; Schmidt-Krey et al. 2007). Furthermore, the 10 Å resolution as obtained for the YidC projection structures, is on the edge of the minimal resolution required to identify transmembrane helices. However, the shape of some densities in the YidC projection structure indicates that they show the location of transmembrane domains in the molecule. For example, roundish features adjacent to the central area of low density in YidC (Fig. 24 B) might be transmembrane helices.

One elongated density is protruding from the 'body' of the YidC monomers in the projection structures (Fig. 24 B), suggesting that this domain is flexible and loosely associated with the core of YidC. It could for example represent the first amino-terminal transmembrane domain of YidC, as this domain is predicted to be an uncleaved signal sequence connected to YidC by the large periplasmic domain (Sääf et al. 1998); the periplasmic domain could then bring the flexibility into the connection with YidC. Furthermore, the first amino-terminal transmembrane domain of YidC is missing in many Oxa1 homologues and is apparently not important for the translocation activity of YidC (Sääf et al. 1998; Yen et al. 2001; Jiang et al. 2003), which suggests that this domain is peripherally associated with YidC.

Maybe, a projection structure of one the truncated forms of YidC (YidC$_{\Delta278}$ or YidC$_{\Delta323}$) would show the transmembrane helices better resolved, since possible influences of the soluble domain of YidC on the appearance of the transmembrane domains in the projection structures would be diminished. However, this would require first an improvement of the over-expression of the truncated YidC.

Crystal contacts

Crystal contacts can be guessed from the projection structure (Fig. 24 B). Horizontal zig-zag lines of adjoining YidC monomers indicate protein-protein crystal contacts between the YidC molecules forming these lines. The greater distance between the horizontal lines of YidC molecules in direction of the a-axis suggests protein-lipid-protein contacts in this direction. This would essentially resemble the crystal contacts proposed for two-dimensional crystals of another protein with large hydrophilic domain (Schmidt-Krey et al. 2007). In case of YidC was integrated in form of dimers in the lipid bilayer, one YidC dimer may have established protein-protein crystal contacts with four adjacent dimers (Fig. 24 B). Anticipating that protein-protein crystal contacts are stronger than lipid-protein-lipid crystal contacts, the crystal

contacts inducing the formation of the crystal lattices were stronger, if YidC was inserted in form of dimers into the membrane.

2.5   Comparison with the projection structure of SecYEG

Plotting of SecYEG and YidC at the same resolution and contouring (Fig. 27) revealed that the densities visible in the projection of SecYEG look sharper than the densities in the projection structure of YidC. This reflects the higher quality of data used for calculating the projection of SecYEG (Breyton et al. 2002).

How the molecules of SecYEG and YidC contact one another for fulfilling the Sec-dependent pathway of YidC-mediated translocation is still unknown. Nevertheless, a sensible option is that YidC lines the lateral exit for transmembrane domains in SecYEG in order to receive synthesised transmembrane domains when they emerge from SecYEG. This may include the aid of SecDF complexes, which associate and dissociate with YidC (Duong and Wickner 1997a; Nouwen and Driessen 2002; Chen et al. 2005; Xie et al. 2006).

In accordance with the results obtained in this work, formation of a functional 'YidC-SecYEG translocon' by monomeric or dimeric YidC and SecYEG is easy to imagine. However, other oligomeric states cannot be ruled out. In either case, YidC could come into contact with two SecYEG molecules arranged back-to-back (Breyton et al. 2002; van den Berg et al. 2004; Bostina et al. 2005) or, alternatively, to a lateral exit regions posed by the interface of two SecYEG molecules facing a front-to-front arrangement, as suggest by the three-dimensional reconstruction of SecYEG with the translating ribosome (Mitra et al. 2005).

Different functions of monomeric and dimeric YidC, respectively, are conceivable. Monomeric YidC could align to the lateral exit of SecYEG in order to support the Sec-mediated co-translational translocation. The dimeric YidC then may fulfil Sec-independent, YidC-mediated translocation. In the dimer interface, the two YidC molecules thereby may provide a similar environment for the integration of transmembrane helices as found in the interface between SecYEG and YidC in the Sec-dependent pathway.

3 Three-dimensional crystallisation

YidC appears to be an attractive target for X-ray crystallography. The large hydrophilic portion of the protein might facilitate the formation of crystal contacts, leading to the formation of well-ordered three-dimensional crystals (Michel 1983). However, the success of three-dimensional crystallisation is determined also by many other factors, for example protein stability in detergent solution and conformational rigidity of the protein. Triangular crystals, obtained with salts of monovalent cations and much larger crystals only achieved with salts of divalent cations were found within the same crystallisation drops. Likely, both crystal types were formed of YidC. This is also indicated by the fact that three-dimensional crystals grew at about pH 5 to 6, the same pH at which the two-dimensional YidC crystals were obtained. Three-dimensional crystal formation could have been particularly favoured by choice of the detergent Cymal 6, maybe due to a micelle size that is appropriate for formation of the crystal contacts (Ostermeier and Michel 1997; Marone et al. 1999), and which was already successfully employed earlier for the three-dimensional crystallisation of membrane protein (Ostermeier et al. 1997).

However, the three-dimensional crystals obtained in this work need to be further characterised and the crystallisation conditions need to be improved for reaching the long-term objective of yielding three-dimensional YidC crystals, suitable for recording of high-resolution X-ray diffraction data and structure solving. A key to crystal improvement could be to overcome the phase separation observed in the crystallisation drops. Although crystal formation close to the point where phase separation occurs is a common observation (Ostermeier and Michel 1997), phase separation is considered unfavourable for the generation of highly ordered three-dimensional membrane protein crystals (Kühlbrandt 1988). Separation of a detergent rich and detergent poor phase might have been induced by high concentrations of PEG (Garavito and Rosenbusch 1986b). As repression of the phase separation with small amphiphiles (Michel 1982a; Michel 1982b) did not work out, alterations in the protein preparation or with the crystallisation conditions appear necessary to overcome this problem. However, the conditions found in this work may be a good starting point for further screening of crystallisation conditions.

Appendix

1   Abbreviations

ADA	N-[2-Acetamino]-2-iminodiacetic acid
Alb3	Albino 3
APH	Amplitudes and phases
Atp9	Subunit 9 of F_0-sector (F_1F_0-ATP synthase)
BiP	Immunoglobulin heavy-chain binding protein
BN	Blue native
Brp	Bacteriocin release protein
BSA	Bovine serum albumine
CCD	Charge coupled device
CCP4	Collaborative computational project
CHAPSO	3-[(3-cholamidopropyl)-dimethylammonio]-2-hydroxy-1-propanesulfonate
CL	Cardiolipin
CMC	Critical micelle concentration
Cox	Subunit of cytochrome oxidase complex
CTF	Contrast transfer function
CV	Column volume
Cymal 5	5-cyclohexyl-1-pentyl-β-D-maltoside
Cymal 6	6-cyclohexyl-1-hexyl-β-D-maltoside
Cymal 7	7-cyclohexyl-1-heptyl-β-D-maltoside
DM	Decyl-β-D-maltopyranoside
EDTA	Ethylene diamine tetra acetic acid
ER	Endoplasmic reticulum
FEG	Field emission gun
FOM	Figure of merit
His	Histidine
HPLC	High pressure liquid chromatography
HR	High resolution
IMAC	Immobilised metal chelating chromatography
IPTG	Isopropyl-beta-D-thiogalactopyranoside
kV	Kilo Volts
$LamB_{SP}$	Signal sequence peptide of LamB
LB	Luria Bertani
LDAO	Lauryldimethylamine-N-oxide
LPR	Lipid to protein ratio
MES	2-Morpholinoethanesulfonic acid
min	Minute(s)
msecs	Milliseconds
MPD	2-methyl-2,4-pentanediol
Mpp	Murein lipoprotein
MWCO	Molecular weight cut-off
NMR	Nuclear magnetic resonance
OD_{280} / OD_{560}	Optical density for light at wavelength 280 / 560 nm
Oxa1	Oxidase assembly 1
PEG	Polyethylene glycol
PG	Phosphatidylglycerol

RPM	Revolutions per minute
SDS	Sodium dodecyl sulfate
PAGE	Polyacrylamide gelelectrophoresis
sec	Second
SON	Signal over noise ratio
SR	Signal recognition particle receptor
SRP	Signal recognition particle
Su8	F_1F_0-ATP synthase subunit 8
TF	Trigger factor
TRAM	Translocating chain associating membrane protein
TRAP	Translocon associated protein
Tris	Tris-(amino)-hydroxymethane
UV_{280}	Ultra violet light at wavelength 280 nm
v/v	Volume / volume
w/v	Weight / volume

2 Index of figures and tables

Figures

Tables

3   References

Akimaru, J., S. Matsuyama, H. Tokuda and S. Mizushima (1991). Reconstitution of a protein translocation system containing purified SecY, SecE, and SecA from *Escherichia coli*. Proc Natl Acad Sci U S A **88**(15): 6545-6549.

Akita, M., S. Sasaki, S. Matsuyama and S. Mizushima (1990). SecA interacts with secretory proteins by recognizing the positive charge at the amino terminus of the signal peptide in *Escherichia coli*. J Biol Chem **265**: 8164-8169.

Akita, M., A. Shinkai, S. Matsuyama and S. Mizushima (1991). SecA, an Essential Component of the Secretory Machinery of *Escherichia coli*, Exists As Homodimer. Biochem Biophys Res Commun **174**(1): 211-216.

Akiyama, Y. and K. Ito (1987). Topology analysis of the SecY protein, an integral membrane protein involved in protein export in *Escherichia coli*. EMBO J **6**: 3465-3470.

Altamura, N., N. Capitanio, N. Bonnefoy, S. Papa and G. Dujardin (1996). The Saccharomyces cerevisiae Oxa1 gene is required for the correct assembly of cytochrome c oxidase and oligomycin-sensitive ATP synthase. FEBS Lett **382**(1-2): 111-115.

Angelini, S., S. Deitermann and H. Koch (2005). FtsY, the bacterial signal-recognition particle receptor, interacts functionally and physically with the SecYEG translocon. EMBO Rep. **6**(5): 476-481.

Appel, M. (2006). Proteinproduktion und Strukturuntersuchungen von Natrium/Protonen-Austauschern. Doktorarbeit. Max-Planck-Institut für Biophysik. Frankfurt am Main, Johann Wolfgang Goethe Universität.

Arneborg, N., A. S. Salskov-Iversen and D. E. Mathiasen (1993). The effect of growth rate and other growth conditions on the lipid composition of *Escherichia coli*. Appl Microbiol Biotechnol **39**(3): 353-357.

Auer, M., G. A. Scarborough and W. Kühlbrandt (1998). Three-dimensional map of the plasma membrane H+-ATPase in the open conformation. Nature **392**(6678): 840-843.

Auer, M., G. A. Scarborough and W. Kühlbrandt (1999). Surface crystallisation of the plasma membrane H+-ATPase on a carbon support film for electron crystallography. J Mol Biol **287**(5): 961-968.

Aveldano, M. I. (1995). Phospholipid solubilization during detergent extraction of rhodopsin from photoreceptor disk membranes. Arch Biochem Biophys **324**(2): 331-343.

Bacallao, R., E. Crooke, K. Shiba, W. Wickner and K. Ito (1986). The SecY protein can act post-translationally to promote bacterial protein export. J Biol Chem. **261**(27): 12907-12910.

Bald, W. B. (1986). On crystal size and cooling rate. J Microsc **143 (Pt 1)**: 89-102.

Banerjee, P., J. B. Joo, J. T. Buse and G. Dawson (1995). Differential solubilization of lipids along with membrane proteins by different classes of detergents. Chem Phys Lipids **77**(1): 65-78.

Barnakov, A. N., V. V. Demin, A. P. Kuzin, A. A. Zargarov, A. S. Zolotarev and N. G. Abdulaev (1990). Two-dimensional crystallization of reaction centers from *Chloroflexus aurantiacus*. <u>FEBS Lett</u> **265**(1-2): 126-128.

Bauer, M., M. Behrens, K. Esser, G. Michaelis and E. Pratje (1994). PET1402, a nuclear gene required for proteolytic processing of cytochrome oxidase subunit 2 in yeast. <u>Mol Gen Genet</u> **245**(3): 272-278.

Beck, K., G. Eisner, D. Trescher, R. E. Dalbey, J. Brunner and M. Muller (2001). YidC, an assembly site for polytopic *Escherichia coli* membrane proteins located in immediate proximity to the SecYE translocon and lipids. <u>EMBO Rep</u> **2**(8): 709-714.

Beck, K., L. Wu, J. Brunner and M. Muller (2000). Discrimination between SRP- and SecA/SecB-dependent substrates involves selective recognition of nascent chains by SRP and trigger factor. <u>EMBO J</u> **19**(1): 134-143.

Beckmann, R., D. Bubeck, R. Grassucci, P. Penczek, A. Verschoor, G. Blobel and J. Frank (1997). Alignment of conduits for the nascent polypeptide chain in the ribosome-Sec61 complex. <u>Science</u> **278**(5346): 2123-2126.

Beckmann, R., C. Spahn, N. Eswar, J. Helmers, P. Penczek, A. Sali, J. Frank and G. Blobel (2001). Architecture of the Protein-Conducting Channel Associated with the Translating 80S Ribosome. <u>Cell</u> **107**(3): 361-372.

Bellafiore, S., P. Ferris, H. Naver, V. Gohre and J. D. Rochaix (2002). Loss of Albino3 leads to the specific depletion of the light-harvesting system. <u>Plant Cell</u> **14**(9): 2303-2314.

Bernstein, H., M. Poritz, K. Strub, P. Hoben, S. Brenner and P. Walter (1989). Model for signal sequence recognition from amino-acid sequence of 54K subunit of signal recognition particle. <u>Nature</u> **340**: 482-486.

Bernstein, H. D., D. Zopf, D. M. Freymann and P. Walter (1993). Functional Substitution of the Signal Recognition Particle 54-kDa Subunit by Its *Escherichia coli* Homolog. <u>Proc Natl Acad Sci USA</u> **90**(11): 5229-5233.

Birnboim, H. C. and J. Doly (1979). A rapid alkaline extraction procedure for screening recombinant plasmid DNA. <u>Nucl. Acids Res.</u> **7**: 1513-1523.

Blobel, G. and B. Dobberstein (1975a). Transfer of proteins across membranes. I. Presence of proteolytically processed and unprocessed nascent immunoglobulin light chains on membrane-bound ribosomes of murine myeloma. <u>J Cell Biol</u> **67**(3): 835-851.

Blobel, G. and B. Dobberstein (1975b). Transfer to proteins across membranes. II. Reconstitution of functional rough microsomes from heterologous components. <u>J Cell Biol</u> **67**(3): 852-862.

Blobel, G. and D. D. Sabatini (1971). Ribosome-membrane interaction in eukaryotic cells. <u>Biomembranes</u> **2**: 193-195.

Bloom, W. and D. W. Fawcett (1994). <u>A textbook of histology.</u> New York, Chapman and Hall.

Bonnefoy, N., F. Chalvet, P. Hamel, P. Slonimski and G. Dujardin (1994a). Oxa1, a *Saccharomyces cerevisiae* nuclear gene whose sequence is conserved from prokaryotes to eukaryotes controls cytochrome oxidase biogenesis. J Mol Biol. **239**(2): 201-212.

Bonnefoy, N., M. Kermorgant, O. Groudinsky, M. Minet, P. P. Slonimski and G. Dujardin (1994b). Cloning of a human gene involved in cytochrome oxidase assembly by functional complementation of an Oxa1- mutation in *Saccharomyces cerevisiae*. Proc Natl Acad Sci U S A **91**(25): 11978-11982.

Bostina, M., B. Mohsin, W. Kühlbrandt and I. Collinson (2005). Atomic Model of the *Escherichia coli* Membrane-bound Protein Translocation Complex SecYEG. J Mol Biol **352**: 1035-1043.

Bradford, M. M. (1976). A rapid and sensitive method for the quantitation of microgram quantities of protein utilizing the principle of protein-dye binding. Anal Biochem **72**: 248-254.

Brenner, S. and R. W. Horne (1959). A negative staining method for high resolution electron microscopy of viruses. Biochim Biophys Acta **34**: 103-110.

Breukink, E., R. Kusters and B. de Kruijff (1992). In vitro Studies on the Folding Characteristics of the Escherichia-Coli Precursor Protein prePhoE - Evidence That SecB Prevents the Precursor from Aggregating by Forming a Functional Complex. Eur J Biochem **208**(2): 419-425.

Breukink, E., N. Nouwen, A. van Raalte, S. Mizushima, J. Tommassen and B. de Kruijff (1995). The C-terminus of SecA is involved in both lipid binding and SecB binding. J Biol Chem **270**(14): 7902-7907.

Breyton, C., W. Haase, T. A. Rapoport, W. Kühlbrandt and I. Collinson (2002). Three-dimensional structure of the bacterial protein-translocation complex SecYEG. Nature **418**: 662-665.

Brundage, L., C. J. Fimmel, S. Mizushima and W. Wickner (1992). SecY, SecE, and Band-1 Form the Membrane-Embedded Domain of *Escherichia coli* Preprotein Translocase. J Biol Chem **267**(6): 4166-4170.

Brundage, L., J. P. Hendrick, E. Schiebel, A. J. M. Driessen and W. Wickner (1990). The Purified *Escherichia coli* Integral Membrane Protein SecY/E Is Sufficient for Reconstitution of SecA-Dependent Precursor Protein Translocation. Cell **62**(4): 649-657.

Byrne, B. and S. Iwata (2002). Membrane protein complexes. Curr Opin Struct Biol. **12**(2): 239-243.

Cabelli, R. J., L. Chen, P. C. Tai and D. B. Oliver (1988). SecA protein is required for secretory protein translocation into *Escherichia coli* membrane vesicles. Cell **55**(4): 683-692.

Cao, G. Q. and R. E. Dalbey (1994). Translocation of N-terminal tails across the plasma membrane. EMBO J **13**(19): 4662-4669.

Chen, M., J. C. Samuelson, F. Jiang, M. Muller, A. Kuhn and R. E. Dalbey (2002b). Direct interaction of YidC with the Sec-independent Pf3 coat protein during its membrane protein insertion. J Biol Chem **277**(10): 7670-7675.

Chen, M., K. Xie, F. Jiang, L. Yi and R. E. Dalbey (2002a). YidC, a newly defined evolutionarily conserved protein, mediates membrane protein assembly in bacteria. Biol Chem **383**(10): 1565-1572.

Chen, M., K. Xie, J. Yuan, L. Yi, S. J. Facey, N. Pradel, L. F. Wu, A. Kuhn and R. E. Dalbey (2005). Involvement of SecDF and YidC in the Membrane Insertion of M13 Procoat Mutants. Biochemistry **44**(31): 10741-10749.

Chen, Y., P. C. Tai and S. F. Sui (2007). The active ring-like structure of SecA revealed by electron crystallography: Conformational change upon interaction with SecB. J Struct Biol.

Chou, Y. T. and L. M. Gierasch (2005). The conformation of a signal peptide bound by *Escherichia coli* preprotein translocase SecA. J Biol Chem **280**(38): 32753-32760.

Collaborative, C. P. n. (1994). The CCP4 suite: programs for protein crystallography. Acta Cryst. **D50**: 760-763.

Collier, D., V. Bankaitis, J. Weiss and P. Bassford (1988). The antifolding activity of SecB promotes the export of the *Escherichia coli* maltose-binding protein. Cell **53**: 273-283.

Collinson, I., C. Breyton, F. Duong, C. Tziatzios, D. Schubert, E. Or, T. Rapoport and W. Kühlbrandt (2001). Projection structure and oligomeric properties of a bacterial core protein translocase. EMBO J. **20**(10): 2462-2471.

Crowley, K., S. Liao, V. Worrell, G. Reinhart and A. Johnson (1994). Secretory proteins move through the endoplasmic reticulum membrane via an aqueous, gated pore. Cell **78**(3): 461-471.

Crowther, R., R. Henderson and J. Smith (1996). MRC image processing programs. J. Struct. Biol. **116**: 9-16.

Cunningham, K., R. Lill, E. Crooke, M. Rice, K. Moore, W. Wickner and D. Oliver (1989). SecA protein, a peripheral protein of the *Escherichia coli* plasma membrane, is essential for the functional binding and translocation of proOmpA. Embo J **8**(3): 955-959.

Cunningham, K. and W. Wickner (1989). Specific Recognition of the Leader Region of Precursor Proteins Is Required for the Activation of Translocation ATPase of Escherichia-Coli. P Nas Us **86**(22): 8630-8634.

da Fonseca, P., E. P. Morris, B. Hankamer and J. Barber (2002). Electron crystallographic study of photosystem II of the cyanobacterium *Synechococcus elongatus*. Biochemistry **41**(16): 5163-5167.

Dalbey, R. E. and W. Wickner (1985). Leader peptidase catalyzes the release of exported proteins from the outer surface of the *Escherichia coli* plasma membrane. J Biol Chem **260**(29): 15925-15931.

Dasgupta, S., G. H. Iyer, S. H. Bryant, C. E. Lawrence and J. A. Bell (1997). Extent and nature of contacts between protein molecules in crystal lattices and between subunits of protein oligomers. Proteins **28**(4): 494-514.

Davies, D. R. and D. M. Segal (1971). Protein crystallization: micro techniques involving vapor diffusion. Meth. Enzymol. **22**: 344-358.

De Carlo, S., M. Adrian, P. Kalin, J. M. Mayer and J. Dubochet (1999). Unexpected property of trehalose as observed by cryo-electron microscopy. J Microsc **196**(1): 40-45.

de Gier, J., P. Mansournia, Q. Valent, G. Phillips, J. Luirink and G. von Heijne (1996). Assembly of a cytoplasmic membrane protein in *Escherichia coli* is dependent on the signal recognition particle. FEBS Lett. **399**(3): 307-309.

Deisenhofer, J., O. Epp, K. Miki, R. Huber and H. Michel (1985). X-ray structure analysis at 3Å resolution of a membrane protein complex: folding of the protein subunits in the photosynthetic reaction center from *Rhodopseudomonas viridis*. Nature **318**: 618-624.

Deitermann, S., G. S. Sprie and H. G. Koch (2005). A dual function for SecA in the assembly of single spanning membrane proteins in *Escherichia coli*. J Biol Chem **280**(47): 39077-39085.

Dekker, C., B. de Kruijff and P. Gros (2003). Crystal structure of SecB from *Escherichia coli*. J Struct Biol **144**(3): 313-319.

Deshaies, R. J., S. L. Sanders, D. A. Feldheim and R. Schekman (1991). Assembly of Yeast SEC Proteins Involved in Translocation into the Endoplasmic Reticulum into a Membrane-Bound Multisubunit Complex. Nature **349**(6312): 806-808.

Deshaies, R. J. and R. Schekman (1987). A yeast mutant defective at an early stage in import of secretory protein precursors into the endoplasmic reticulum. J Cell Biol **105**(2): 633-645.

Do, H., D. Falcone, J. Lin, D. W. Andrews and A. E. Johnson (1996). The cotranslational integration of membrane proteins into the phospholipid bilayer is a multistep process. Cell **85**(3): 369-378.

Dolder, M., A. Engel and M. Zulauf (1996). The micelle to vesicle transition of lipids and detergents in the presence of a membrane protein: towards a rationale for 2D crystallization. FEBS Lett **382**(1-2): 203-208.

Dorset, D. L., A. Engel, M. Haner, A. Massalski and J. P. Rosenbusch (1983). Two-dimensional crystal packing of matrix porin. A channel forming protein in *Escherichia coli* outer membranes. J Mol Biol **165**(4): 701-710.

Douville, K., M. Leonard, L. Brundage, K. Nishiyama, H. Tokuda, S. Mizushima and W. Wickner (1994). Band 1 subunit of *Escherichia coli* preprotein translocase and integral membrane export factor P12 are the same protein. J Biol Chem **269**(29): 18705-18707.

Douville, K., A. Price, J. Eichler, A. Economou and W. Wickner (1995). SecYEG and SecA are the stoichiometric components of preprotein translocase. J Biol Chem **270**(34): 20106-20111.

Downing, K. H. (1991). Spot-scan imaging in transmission electron microscopy. Science **251**(4989): 53-59.

Driessen, A. (1993). SecA, the peripheral subunit of the *Escherichia coli* precursor protein translocase, is functional as a dimer. Biochemistry **32**(48): 13190-13197.

Driessen, A. and W. Wickner (1990). Solubilization and Functional Reconstitution of the Protein-Translocation Enzymes of *Escherichia coli*. P Nas Us **87**(8): 3107-3111.

Dubochet, J., M. Adrian, J. J. Chang, J. C. Homo, J. Lepault, A. W. McDowall and P. Schultz (1988). Cryo-electron microscopy of vitrified specimens. Q Rev Biophys **21**(2): 129-228.

Dubochet, J., A. W. McDowall, B. Menge, E. N. Schmid and K. G. Lickfeld (1983). Electron microscopy of frozen-hydrated bacteria. J Bacteriol **155**(1): 381-390.

Duong, F. and W. Wickner (1997a). Distinct catalytic roles of the SecYE, SecG and SecDFyajC subunits of preprotein translocase holoenzyme. EMBO J **16**(10): 2756-27568.

Dux, L., K. A. Taylor, H. P. Ting-Beall and A. Martonosi (1985). Crystallization of the Ca^{2+}-ATPase of sarcoplasmic reticulum by calcium and lanthanide ions. J Biol Chem **260**(21): 11730-11743.

Egea, P., S. Shan, J. Napetschnig, D. Savage, P. Walter and R. Stroud (2004). Substrate twinning activates the signal recognition particle and its receptor. Nature **427**(6971): 215-21.

Eisner, G., H. G. Koch, K. Beck, J. Brunner and M. Muller (2003). Ligand crowding at a nascent signal sequence. J Cell Biol **163**(1): 35-44.

Eisner, G., M. Moser, U. Schafer, K. Beck and M. Muller (2006). Alternate recruitment of signal recognition particle and trigger factor to the signal sequence of a growing nascent polypeptide. J Biol Chem **281**(11): 7172-7179.

Emr, S. D., S. Hanley-Way and T. J. Silhavy (1981). Suppressor mutations thatrestore export of a protein with a defective signal sequence. Cell **23**: 79-88.

Emr, S. D. and T. J. Silhavy (1983). Importance of secondary structure in the signal sequence for protein secretion. Proc Natl Acad Sci Usa **80**(15): 4599-4603.

Endo, T., H. Yamamoto and M. Esaki (2003). Functional co-operation and separation of translocators in protein import into mitochondria, the double-membrane bounded organelles. J Cell Sci **116**(Pt 16): 3259-3267.

Ernst, F., H. K. Hoffschulte, B. Thomekromer, U. E. Swidersky, P. K. Werner and M. Müller (1994). Precursor-Specific requirements for seca, secb, and delta mu(H+) during protein export of *Escherichia coli*. J Biol Chem **269**(17): 12840-12845.

Facey, S. J., S. A. Neugebauer, S. Krauss and A. Kuhn (2007). The mechanosensitive channel protein MscL is targeted by the SRP to the novel YidC membrane insertion pathway of *Escherichia coli*. J Mol Biol **365**(4): 995-1004.

Fekkes, P., d. D. C. van and A. Driessen (1997). The molecular chaperone SecB is released from the carboxy-terminus of SecA during initiation of precursor protein translocation. EMBO J **16**(20): 6105-6113.

Focia, P., I. Shepotinovskaya, J. Seidler and D. Freymann (2004). Heterodimeric GTPase core of the SRP targeting complex. Science **303**(5656): 373-377.

Fons, R., B. Bogert and R. Hegde (2003). Substrate-specific function of the translocon-associated protein complex during translocation across the ER membrane. J Cell Biol. **160**(4): 529-539.

Frazier, A. E., A. Chacinska, K. N. Truscott, B. Guiard, N. Pfanner and P. Rehling (2003). Mitochondria use different mechanisms for transport of multispanning membrane proteins through the intermembrane space. Mol Cell Biol **23**(21): 7818-7828.

Frederik, P. M., M. C. Stuart, P. H. Bomans, W. M. Busing, K. N. Burger and A. J. Verkleij (1991). Perspective and limitations of cryo-electron microscopy. From model systems to biological specimens. J Microsc **161 (Pt 2)**: 253-262.

Fröderberg, L., E. Houben, J. C. Samuelson, M. Chen, S. K. Park, G. J. Phillips, R. Dalbey, J. Luirink and J. W. De Gier (2003). Versatility of inner membrane protein biogenesis in *Escherichia coli*. Mol Microbiol **47**(4): 1015-1027.

Fröderberg, L., E. N. Houben, L. Baars, J. Luirink and J. W. de Gier (2004). Targeting and translocation of two lipoproteins in *Escherichia coli* via the SRP/Sec/YidC pathway. J Biol Chem **279**(30): 31026-31032.

Fujiyoshi, Y. (1989). High resolution cryo-electron microscopy for biological macromolecules. J Electron Microsc (Tokyo) **38 Suppl**: 97-101.

Fujiyoshi, Y., T. Mizusaki, K. Morikawa, H. Yamagishi, Y. Aoki, H. Kihara and Y. Harada (1991). Development of a superfluid helium stage for high-resolution electron microscopy. Ultramicroscopy **38**: 241-251.

Garavito, R. M., U. Hinz and J. M. Neuhaus (1984). The crystallization of outer membrane proteins from *Escherichia coli*. Studies on LamB and OmpA gene products. J Biol Chem **259**(7): 4254-4257.

Garavito, R. M. and J. P. Rosenbusch (1986b). Isolation and crystallization of bacterial porin. Methods Enzymol **125**: 309-328.

Glick, B. and G. Von Heijne (1996). *Saccharomyces cerevisiae* mitochondria lack a bacterial-type Sec-machinery. Protein Sci. **5**(12): 2651-2652.

Gonen, T., Y. Cheng, P. Sliz, Y. Hiroaki, Y. Fujiyoshi, S. C. Harrison and T. Walz (2005). Lipid-protein interactions in double-layered two-dimensional AQP0 crystals. Nature **438**(7068): 633-638.

Gonen, T., P. Sliz, J. Kistler, Y. Cheng and T. Walz (2004). Aquaporin-0 membrane junctions reveal the structure of a closed water pore. Nature **429**(6988): 193-197.

Görlich, D., E. Hartmann, S. Prehn and T. Rapoport (1992a). A protein of the endoplasmic reticulum involved early in polypeptide translocation. Nature **357**(6373): 47-52.

Görlich, D., S. Prehn, E. Hartmann, K. Kalies and T. Rapoport (1992b). A mammalian homolog of Sec61p and SecYp is associated with ribosomes and nascent polypeptides during translocation. Cell **71**(3): 489-503.

Görlich, D. and T. A. Rapoport (1993). Protein Translocation into Proteoliposomes Reconstituted from Purified Components of the Endoplasmic Reticulum Membrane. Cell **75**(4): 615-630.

Grigorieff, N., T. A. Ceska, K. H. Downing, J. M. Baldwin and R. Henderson (1996). Electron-crystallographic refinement of the structure of bacteriorhodopsin. J. Mol. Biol. **259**(3): 393-421.

Gu, S. Q., F. Peske, H. J. Wieden, M. V. Rodnina and W. Wintermeyer (2003). The signal recognition particle binds to protein L23 at the peptide exit of the *Escherichia coli* ribosome. Rna **9**(5): 566-573.

Gyobu, N., K. Tani, Y. Hiroaki, A. Kamegawa, K. Mitsuoka and Y. Fujiyoshi (2004). Improved specimen preparation for cryo-electron microscopy using a symmetric carbon sandwich technique. J Struct Biol **146**(3): 325-333.

Halic, M., T. Becker, M. R. Pool, C. M. Spahn, R. A. Grassucci, J. Frank and R. Beckmann (2004). Structure of the signal recognition particle interacting with the elongation-arrested ribosome. Nature **427**(6977): 808-814.

Hamman, B., L. Hendershot and A. Johnson (1998). Bip maintains the permeability barrier of the ER membrane by sealing the lumenal end of the translocon pore before and early in translocation. Cell **92**(6): 747-758.

Hanada, M., K. Nishiyama, S. Mizushima and H. Tokuda (1994). Reconstitution of an efficient protein translocation machinery comprising SecA and the three membrane proteins, SecY, SecE, and SecG (p12). J Biol Chem **269**(38): 23625-23631.

Hanein, D., K. Matlack, B. Jungnickel, K. Plath, K. Kalies, K. Miller, T. Rapoport and C. Akey (1996). Oligomeric rings of the Sec61p complex induced by ligands required for protein translocation. Cell **87**(4): 721-732.

Hansen, W., P. D. Garcia and P. Walter (1986). In vitro protein translocation across the yeast endoplasmic reticulum: ATP-dependent posttranslational translocation of the prepro-alpha-factor. Cell **45**(3): 397-406.

Hartl, F., S. Lecker, E. Schiebel, J. Hendrick and W. Wickner (1990). The binding cascade of SecB to SecA to SecY/E mediates preprotein targeting to the *Escherichia coli* plasma membrane. Cell **63**(2): 269-279.

Hartmann, E., T. Sommer, S. Prehn, D. Görlich, S. Jentsch and T. A. Rapoport (1994). Evolutionary conservation of components of the protein translocation complex. Nature **367**: 654-657.

He, S. and T. D. Fox (1997). Membrane translocation of mitochondrially coded Cox2p: distinct requirements for export of N and C termini and dependence on the conserved protein Oxa1p. Mol Biol Cell **8**(8): 1449-1460.

Hebert, H., I. Schmidt-Krey and R. Morgenstern (1995). The projection structure of microsomal glutathione transferase. Embo J **14**(16): 3864-3869.

Heinrich, S. U., W. Mothes, J. Brunner and T. A. Rapoport (2000). The Sec61p complex mediates the integration of a membrane protein by allowing lipid partitioning of the transmembrane domain. Cell **102**(2): 233-244.

Helenius, A. and K. Simons (1975). Solubilization of membranes by detergents. Biochim Biophys Acta **415**(1): 29-79.

Hell, K., J. Herrmann, E. Pratje, W. Neupert and R. Stuart (1997). Oxa1p mediates the export of the N- and C-termini of pCoxII from the mitochondrial matrix to the intermembrane space. FEBS Lett **418**(3): 367-370.

Hell, K., J. Herrmann, E. Pratje, W. Neupert and R. Stuart (1998). Oxa1p, an essential component of the N-tail protein export machinery in mitochondria. Proc Natl Acad Sci U S A. **95**(5): 2250-2255.

Hell, K., W. Neupert and R. A. Stuart (2001). Oxa1p acts as a general membrane insertion machinery for proteins encoded by mitochondrial DNA. Embo J **20**(6): 1281-1288.

Henderson, R. (1992). Image contrast in high-resolution electron microscopy of biological macromolecules: TMV in ice. Ultramicroscopy **46**(1-4): 1-18.

Henderson, R., J. Baldwin, T. Ceska, F. Zemlin, E. Beckmann and K. Downing (1990). Model for the structure of bacteriorhodopsin based on high-resolution electron cryo-microscopy. J Mol Biol **213**(4): 899-929.

Henderson, R. and P. N. T. Unwin (1975). Three-dimensional model of purple membrane obtained by electron microscopy. Nature **257**: 28-32.

Herrmann, J. M. and N. Bonnefoy (2004). Protein export across the inner membrane of mitochondria: the nature of translocated domains determines the dependence on the Oxa1 translocase. J Biol Chem **279**(4): 2507-2512.

Herrmann, J. M., H. Koll, R. A. Cook, W. Neupert and R. A. Stuart (1995). Topogenesis of cytochrome oxidase subunit II. Mechanisms of protein export from the mitochondrial matrix. J Biol Chem **270**(45): 27079-27086.

Herrmann, J. M., W. Neupert and R. A. Stuart (1997). Insertion into the mitochondrial inner membrane of a polytopic protein, the nuclear-encoded Oxa1p. Embo J **16**(9): 2217-2226.

Hessa, T., H. Kim, K. Bihlmaier, C. Lundin, J. Boekel, H. Andersson, I. Nilsson, S. White and G. von Heijne (2005). Recognition of transmembrane helices by the endoplasmic reticulum translocon. Nature **433**(7024): 377-381.

Heuberger, E. H., L. M. Veenhoff, R. H. Duurkens, R. H. Friesen and B. Poolman (2002). Oligomeric state of membrane transport proteins analyzed with blue native electrophoresis and analytical ultracentrifugation. J Mol Biol **317**(4): 591-600.

High, S., S. S. L. Andersen, D. Görlich, E. Hartmann, S. Prehn, T. A. Rapoport and B. Dobberstein (1993a). Sec61p Is Adjacent to Nascent Type-I and Type-II Signal-Anchor Proteins During Their Membrane Insertion. J Cell Biol **121**(4): 743-750.

Hoffschulte, H. K., B. Drees and M. Muller (1994). Identification of a soluble SecA/SecB complex by means of a subfractionated cell-free export system. J Biol Chem **269**(17): 12833-12839.

Holland, E. and K. Drickamer (1986). Signal recognition particle mediates the insertion of a transmembrane protein which has a cytoplasmic NH2 terminus. J Biol Chem **261**: 1286-1292.

Houben, E. N., P. A. Scotti, Q. A. Valent, J. Brunner, J. L. de Gier, B. Oudega and J. Luirink (2000). Nascent Lep inserts into the *Escherichia coli* inner membrane in the vicinity of YidC, SecY and SecA. FEBS Lett **476**(3): 229-233.

Houben, E. N., C. M. Ten Hagen-Jongman, J. Brunner, B. Oudega and J. Luirink (2004). The two membrane segments of leader peptidase partition one by one into the lipid bilayer via a Sec/YidC interface. EMBO Rep **5**(10): 970-975.

Houben, E. N., M. L. Urbanus, M. Van Der Laan, C. M. Ten Hagen-Jongman, A. J. Driessen, J. Brunner, B. Oudega and J. Luirink (2002). YidC and SecY mediate membrane insertion of a Type I transmembrane domain. J Biol Chem **277**(39): 35880-35886.

Houben, E. N., R. Zarivach, B. Oudega and J. Luirink (2005). Early encounters of a nascent membrane protein: specificity and timing of contacts inside and outside the ribosome. J Cell Biol **170**(1): 27-35.

Hunt, J. F., S. Weinkauf, L. Henry, J. J. Fak, P. McNicholas, D. B. Oliver and J. Deisenhofer (2002). Nucleotide Control of Interdomain Interactions in the Conformational Reaction Cycle of SecA. Science **297**(5589): 2018-2026.

Ii, M. and K. Mihara (2001). Insertion of mitochondrial DNA-encoded F_1F_0-ATPase subunit 8 across the mitochondrial inner membrane in vitro. J Biol Chem **276**(27): 24704-24712.

Ito, K., M. Wittekind, M. Nomura, K. Shiba, T. Yura, A. Miura and H. Nashimoto (1983). A temperature-sensitive mutant of *Escherichia coli* exhibiting slow processing of exported proteins. Cell **32**(3): 789-797.

Jahn, T., J. Dietrich, B. Andersen, B. Leidvik, C. Otter, C. Briving, W. Kühlbrandt and M. G. Palmgren (2001). Large scale expression, purification and 2D crystallization of recombinant plant plasma membrane H^+-ATPase. J Mol Biol **309**(2): 465-476.

Jap, B. K. (1988). High-resolution electron diffraction of reconstituted PhoE porin. J Mol Biol **199**(1): 229-231.

Jap, B. K., K. H. Downing and P. J. Walian (1990). Structure of PhoE porin in projection at 3.5 A resolution. J Struct Biol **103**(1): 57-63.

Jap, B. K., M. Zulauf, T. Scheybani, A. Hefti, W. Baumeister, U. Aebi and A. Engel (1992). 2D crystallization: from art to science. Ultramicroscopy **46**(1-4): 45-84.

Jia, L., M. Dienhart, M. Schramp, M. McCauley, K. Hell and R. A. Stuart (2003). Yeast Oxa1 interacts with mitochondrial ribosomes: the importance of the C-terminal region of Oxa1. Embo J **22**(24): 6438-6447.

Jia, L., M. K. Dienhart and R. A. Stuart (2007). Oxa1 Directly Interacts with Atp9 and Mediates Its Assembly into the Mitochondrial F_1F_0-ATP Synthase Complex. Mol Biol Cell **18**(5): 1897-1908.

Jiang, F., M. Chen, L. Yi, J. W. de Gier, A. Kuhn and R. E. Dalbey (2003). Defining the regions of *Escherichia coli* YidC that contribute to activity. J Biol Chem **278**(49): 48965-48972.

Jiang, F., L. Yi, M. Moore, M. Chen, T. Rohl, K. J. Van Wijk, J. W. De Gier, R. Henry and R. E. Dalbey (2002). Chloroplast YidC homolog Albino3 can functionally complement the bacterial YidC depletion strain and promote membrane insertion of both bacterial and chloroplast thylakoid proteins. J Biol Chem **277**(22): 19281-19288.

Jones, J. D. and L. M. Gierasch (1994a). Effect of charged residue substitutions on the membrane- interactive properties of signal sequences of the *Escherichia coli* LamB protein. Biophys J **67**(4): 1534-1545.

Jones, J. D. and L. M. Gierasch (1994b). Effect of charged residue substitutions on the thermodynamics of signal peptide-lipid interactions for the *Escherichia coli* LamB signal sequence. Biophys J **67**(4): 1546-1561.

Kalies, K. U., S. Allan, T. Sergeyenko, H. Kroger and K. Römisch (2005). The protein translocation channel binds proteasomes to the endoplasmic reticulum membrane. Embo J **24**(13): 2284-2293.

Karamyshev, A. L. and A. E. Johnson (2005). Selective SecA association with signal sequences in ribosome-bound nascent chains: A potential role for SecA in ribosome targeting to the bacterial membrane. J Biol Chem **280**(45): 37930-40.

Kawasaki, H., S. Matsuyama, S. Sasaki, M. Akita and S. Mizushima (1989). SecA protein is directly involved in protein secretion in *Escherichia coli*. FEBS Lett **242**: 431-434.

Kendrew, J. C., G. Bodo, H. M. Dintzis, R. G. Parrish, H. Wyckoff and D. C. Phillips (1958). A three-dimensional model of the myoglobin molecule obtained by X-ray analysis. Nature **181**(4610): 662-666.

Kermorgant, M., N. Bonnefoy and G. Dujardin (1997). Oxa1p, which is required for cytochrome c oxidase and ATP synthase complex formation, is embedded in the mitochondrial inner membrane. Curr Genet **31**(4): 302-307.

Kiefer, D. and A. Kuhn (1999). Hydrophobic forces drive spontaneous membrane insertion of the bacteriophage Pf3 coat protein without topological control. Embo J **18**(22): 6299-6306.

Kim, J., S. Rusch, J. Luirink and D. A. Kendall (2001). Is Ffh required for export of secretory proteins? FEBS Lett **505**(2): 245-248.

Klappa, P., M. Zimmermann and R. Zimmermann (1994). The Membrane Proteins TRAMp and Sec61 αp May Be Involved in Post-Translational Transport of Presecretory Proteins into Mammalian Microsomes. FEBS Lett **341**(2-3): 281-287.

Kleymann, G., C. Ostermeier, K. Heitmann, W. Haase and H. Michel (1995). Use of antibody fragments (Fv) in immunocytochemistry. J Histochem Cytochem **43**(6): 607-14.

Klostermann, E., I. Droste Gen Helling, J. P. Carde and D. Schünemann (2002). The thylakoid membrane protein Alb3 associates with the cpSecY-translocase in *Arabidopsis thaliana*. Biochem J **368**(Pt 3): 777-781.

Klug, A. and J. E. Berger (1964). An Optical Method for the Analysis of Periodicities in Electron Micrographs, and Some Observations on the Mechanism of Negative Staining. J Mol Biol **10**: 565-569.

Knapek, E. and J. Dubochet (1980). Beam damage to organic material is considerably reduced in cryo-electron microscopy. J Mol Biol **141**(2): 147-161.

Knoblauch, N., S. Rudiger, H. Schonfeld, A. Driessen, J. Schneider-Mergener and B. Bukau (1999). Substrate specificity of the SecB chaperone. J Biol Chem **274**(48): 34219-34225.

Koch, H. G., T. Hengelage, C. Neumann-Haefelin, J. MacFarlane, H. K. Hoffschulte, K. L. Schimz, B. Mechler and M. Muller (1999). In vitro studies with purified components reveal signal recognition particle (SRP) and SecA/SecB as constituents of two independent protein-targeting pathways of *Escherichia coli*. Mol Biol Cell **10**(7): 2163-2173.

Koch, H. G., M. Moser, K. L. Schimz and M. Müller (2002). The integration of YidC into the cytoplasmic membrane of *Escherichia coli* requires the signal recognition particle, SecA and SecYEG. J Biol Chem **277**(8): 5715-5718.

Koepke, J., X. Hu, C. Muenke, K. Schulten and H. Michel (1996). The crystal structure of the light-harvesting complex II (B800-850) from *Rhodospirillum molischianum*. Structure **4**(5): 581-597.

Koning, R. I., G. T. Oostergetel and A. Brisson (2003). Preparation of flat carbon support films. Ultramicroscopy **94**(3-4): 183-191.

Krebs, A., C. Villa, P. C. Edwards and G. F. Schertler (1998). Characterisation of an improved two-dimensional p22121 crystal from bovine rhodopsin. J Mol Biol **282**(5): 991-1003.

Kubalek, E., S. Ralston, J. Lindstrom and N. Unwin (1987). Location of subunits within the acetylcholine receptor by electron image analysis of tubular crystals from Torpedo marmorata. J Cell Biol **105**(1): 9-18.

Kühlbrandt, W. (1988). Three-dimensional crystallization of membrane protein. Q. Rev. Biophys. **21**: 429-477.

Kühlbrandt, W. (1992). Two-dimensional crystallization of membrane proteins. Q Rev Biophys **25**(1): 1-49.

Kühlbrandt, W., T. Thaler and E. Wehrli (1983). The structure of membrane crystals of the light-harvesting chlorophyll a/b protein complex. J. Cell Biol. **96**: 1414-1424.

Kühlbrandt, W., D. N. Wang and Y. Fujiyoshi (1994). Atomic model of plant light-harvesting complex by electron crystallography. Nature **367**: 614-621.

Kuhn, A., R. Stuart, R. Henry and R. E. Dalbey (2003). The Alb3/Oxa1/YidC protein family: membrane-localized chaperones facilitating membrane protein insertion? Trends Cell Biol **13**(10): 510-6.

Kuhn, A., H. Y. Zhu and R. E. Dalbey (1990). Efficient Translocation of Positively Charged Residues of M13 Procoat Protein Across the Membrane Excludes Electrophoresis As the Primary Force for Membrane Insertion. EMBO J **9**(8): 2385-2389.

Kumamoto, C. (1989). *Escherichia coli* SecB protein associates with exported protein precursors *in vivo*. Proc Natl Acad Sci USA **86**: 5320-5324.

Kunji, E. R. and M. Harding (2003). Projection structure of the atractyloside-inhibited mitochondrial ADP/ATP carrier of *Saccharomyces cerevisiae*. J Biol Chem **278**(39): 36985-36988.

Kunji, E. R., S. von Gronau, D. Oesterhelt and R. Henderson (2000). The three-dimensional structure of halorhodopsin to 5 A by electron crystallography: A new unbending procedure for two-dimensional crystals by using a global reference structure. Proc Natl Acad Sci U S A **97**(9): 4637-4642.

Kusters, R., T. de Vrije, E. Breukink and B. de Kruijff (1989). SecB Protein Stabilizes a Translocation-Competent State of Purified PrePhoe Protein. J Biol Chem **264**(35): 20827-20830.

Kusters, R., G. Lentzen, E. Eppens, A. van Geel, C. C. van der Weijden, W. Wintermeyer and J. Luirink (1995). The functioning of the SRP receptor FtsY in protein-targeting in *Escherichia coli* is correlated with its ability to bind and hydrolyse GTP. FEBS Lett **372**(2-3): 253-258.

Laemmli, U. (1970). Cleavage of structural proteins during the assembly of the head of bacteriophage T4. Nature **227**(259): 680-685.

Lathe, G. H. and C. R. Ruthven (1956). The separation of substances and estimation of their relative molecular sizes by the use of colums of starch in water. Biochem J **62**(4): 665-674.

Lebeau, L., F. Lach, C. Venien-Bryan, A. Renault, J. Dietrich, T. Jahn, M. G. Palmgren, W. Kühlbrandt and C. Mioskowski (2001). Two-dimensional crystallization of a membrane protein on a detergent-resistant lipid monolayer. J Mol Biol **308**(4): 639-647.

Lecker, S., R. Lill, T. Ziegelhoffer, C. Georgopoulos, P. J. Bassford, C. A. Kumamoto and W. Wickner (1989). 3 Pure Chaperone Proteins of *Escherichia coli* - SecB, Trigger Factor and GroEL - Form Soluble Complexes with Precursor Proteins Invitro. EMBO J **8**(9): 2703-2709.

Lecker, S. H., A. J. M. Driessen and W. Wickner (1990). Proompa Contains Secondary and Tertiary Structure Prior to Translocation and Is Shielded from Aggregation by Association with Secb Protein. EMBO J **9**(7): 2309-2314.

Lee, H. C. and H. D. Bernstein (2001). The targeting pathway of *Escherichia coli* presecretory and integral membrane proteins is specified by the hydrophobicity of the targeting signal. Proc Natl Acad Sci U S A **98**(6): 3471-3476.

Li, J. and C. Hollingshead (1982). Formation of crystalline arrays of chlorophyll a/b - light-harvesting protein by membrane reconstitution. Biophysical Journal **37**(1): 363-370.

Liao, S., J. Lin, H. Do and A. Johnson (1997). Both lumenal and cytosolic gating of the aqueous ER translocon pore are regulated from inside the ribosome during membrane protein integration. Cell **90**(1): 31-41.

Lill, R., K. Cunningham, L. Brundage, K. Ito, D. Oliver and W. Wickner (1989). SecA protein hydrolyzes ATP and is an essential component of the protein translocation ATPase of *Escherichia coli*. EMBO J **8**(3): 961-966.

Lindner, E. B., A. Elmqvist and J. Porath (1959). Gel filtration as a method for purification of protein-bound peptides exemplified by oxytocin and vasopressin. Nature **184**: 1565-1566.

Long, D., M. Martin, E. Sundberg, J. Swinburne, P. Puangsomlee and G. Coupland (1993). The maize transposable element system Ac/Ds as a mutagen in Arabidopsis: identification of an albino mutation induced by Ds insertion. Proc Natl Acad Sci U S A **90**(21): 10370-10374.

Luirink, J., S. High, H. Wood, A. Giner, D. Tollervey and B. Dobberstein (1992). Signal-Sequence Recognition by an *Escherichia coli* Ribonucleoprotein Complex. Nature **359**(6397): 741-743.

Luirink, J., T. Samuelsson and J. W. de Gier (2001). YidC/Oxa1p/Alb3: evolutionarily conserved mediators of membrane protein assembly. FEBS Lett **501**(1): 1-5.

Luirink, J., C. M. ten Hagen-Jongman, C. C. van der Weijden, B. Oudega, S. High, B. Dobberstein and R. Kusters (1994). An alternative targeting pathway in *Escherichia coli*: studies on the role of FtsY. EMBO J **13**: 2289-2296.

Macfarlane, J. and M. Müller (1995). The functional integration of a polytopic membrane protein of *Escherichia coli* is dependent on the bacterial signal-recognition particle. Eur J Biochem **233**(3): 766-771.

Mannella, C. A. (1984). Phospholipase-induced crystallization of channels in mitochondrial outer membranes. Science **224**(4645): 165-166.

Marone, P. A., P. Thiyagarajan, A. M. Wagner and D. M. Tiede (1999). Effect of detergent alkyl chain length on crystallization of a detergent-solubilized membrane protein: correlation of protein-detergent particle size and particle-particle interaction with crystallization of the photosynthetic reaction center from *Rhodobacter sphaeroides*. Journal of Crystal Growth **207**: 214-225.

McCormick, P., Y. Miao, Y. Shao, J. Lin and A. Johnson (2003). Cotranslational protein integration into the ER membrane is mediated by the binding of nascent chains to translocon proteins. Mol Cell. **12**(2): 329-341.

McKnight, C. J., M. S. Briggs and L. M. Gierasch (1989). Functional and Nonfunctional Lamb Signal Sequences Can Be Distinguished by Their Biophysical Properties. J Biol Chem **264**(29): 17293-17297.

Menetret, J., A. Neuhof, D. Morgan, K. Plath, M. Radermacher, T. Rapoport and C. Akey (2000). The structure of ribosome-channel complexes engaged in protein translocation. Mol Cell **6**(5): 1219-1932.

Menetret, J. F., R. S. Hegde, S. U. Heinrich, P. Chandramouli, S. J. Ludtke, T. A. Rapoport and C. W. Akey (2005). Architecture of the ribosome-channel complex derived from native membranes. J Mol Biol **348**(2): 445-457.

Meyer, T., J. Menetret, R. Breitling, K. Miller, C. Akey and T. Rapoport (1999). The bacterial SecY/E translocation complex forms channel-like structures similar to those of the eukaryotic Sec61p complex. J Mol Biol **285**(4): 1789-800.

Meyer, W., U. Bomer and E. Pratje (1997). Mitochondrial inner membrane bound Pet1402 protein is rapidly imported into mitochondria and affects the integrity of the cytochrome oxidase and ubiquinol-cytochrome c oxidoreductase complexes. Biol Chem **378**(11): 1373-1379.

Michel, H. (1982a). Three-dimensional crystals of a membrane protein complex. The photosynthetic reaction centre from *Rhodopseudomonas viridis*. J Mol Biol **158**(3): 567-572.

Michel, H. (1982b). Characterization and crystal packing of three-dimensional bacteriorhodopsin crystals. Embo J **1**(10): 1267-1271.

Michel, H. (1983). Crystallization of membrane proteins. TIBS **8**: 56-59.

Miller, J. D., H. D. Bernstein and P. Walter (1994). Interaction of *Escherichia coli* Ffh/4.5S ribonucleoprotein and FtsY mimics that of mammalian signal recognition particle and its receptor. Nature **367**: 657-659.

Miroux, B. and J. Walker (1996). Over-production of proteins in *Escherichia coli*: mutant hosts that allow synthesis of some membrane proteins and globular proteins at high levels. J Mol Biol **260**(3): 289-298.

Misra, M. and S. K. Malhotra (1985). Crystallization of Ca^{2+} ATPase in sarcoplasmic reticulum vesicles by phospholipase treatment. Biosci Rep **5**(7): 551-558.

Mitra, K., C. Schaffitzel, T. Shaikh, F. Tama, S. Jenni, C. L. Brooks, 3rd, N. Ban and J. Frank (2005). Structure of the *Escherichia coli* protein-conducting channel bound to a translating ribosome. Nature **438**(7066): 318-324.

Moore, M., R. L. Goforth, H. Mori and R. Henry (2003). Functional interaction of chloroplast SRP/FtsY with the Alb3 translocase in thylakoids: substrate not required. J Cell Biol **162**(7): 1245-1254.

Moore, M., M. S. Harrison, E. C. Peterson and R. Henry (2000). Chloroplast Oxa1p homolog Albino3 is required for post-translational integration of the light harvesting chlorophyll-binding protein into thylakoid membranes. J Biol Chem **275**(3): 1529-1532.

Mori, H. and K. Ito (2003). Biochemical characterization of a mutationally altered protein translocase: proton motive force stimulation of the initiation phase of translocation. J Bacteriol. **185**(2): 405-412.

Mosser, G. (2001). Two-dimensional crystallogenesis of transmembrane proteins. Micron **32**(5): 517-540.

Mothes, W., B. Jungnickel, J. Brunner and T. Rapoport (1998). Signal sequence recognition in cotranslational translocation by protein components of the endoplasmic reticulum membrane. J Cell Biol **142**(2): 355-364.

Mothes, W., S. Prehn and T. Rapoport (1994). Systematic probing of the environment of a translocating secretory protein during translocation through the ER membrane. EMBO J **13**(17): 3973-3982.

Muller, M., I. Ibrahimi, C. N. Chang, P. Walter and G. Blobel (1982). A bacterial secretory protein requires signal recognition particle for translocation across mammalian endoplasmic reticulum. J Biol Chem **257**(20): 11860-11863.

Müsch, A., M. Wiedmann and T. A. Rapoport (1992). Yeast Sec Proteins Interact with Polypeptides Traversing the Endoplasmic Reticulum Membrane. Cell **69**(2): 343-352.

Nagamori, S., I. N. Smirnova and H. R. Kaback (2004). Role of YidC in folding of polytopic membrane proteins. J Cell Biol **165**(1): 53-62.

Nargang, F. E., M. Preuss, W. Neupert and J. M. Herrmann (2002). The Oxa1 protein forms a homooligomeric complex and is an essential part of the mitochondrial export translocase in *Neurospora crassa*. J Biol Chem **277**(15): 12846-12853.

Neumann-Haefelin, C., U. Schafer, M. Muller and H. Koch (2000). SRP-dependent co-translational targeting and SecA-dependent translocation analyzed as individual steps in the export of a bacterial protein. EMBO J **19**(23): 6419-6426.

Ng, D. T., J. D. Brown and P. Walter (1996). Signal sequences specify the targeting route to the endoplasmic reticulum membrane. J Cell Biol **134**(2): 269-278.

Nishiyama, K., M. Hanada and H. Tokuda (1994). Disruption of the gene encoding p12 (SecG) reveals the direct involvement and important function of SecG in the protein translocation of *Escherichia coli* at low temperature. EMBO J **13**(14): 3272-3277.

Nishiyama, K., S. Mizushima and H. Tokuda (1995). Preferential interaction of SecG with SecE stabilizes an unstable SecE derivative in the *Escherichia coli* cytoplasmic membrane. Biochem Biophys Res Commun **217**(1): 217-223.

Nishiyama, K., T. Suzuki and H. Tokuda (1996). Inversion of the membrane topology of SecG coupled with SecA-dependent preprotein translocation. Cell **85**(1): 71-81.

Nouwen, N. and A. J. Driessen (2002). SecDFyajC forms a heterotetrameric complex with YidC. Mol Microbiol **44**(5): 1397-1405.

Ohno, I., Y. Washita and W. Wickner (1983). Reconstitution of rapid and asymmetric assembly of M13 procoat protein into liposomes which have bacterial leader peptidase. J Biol Chem **258**(3): 1895-1900.

Okada, T., I. Le Trong, B. A. Fox, C. A. Behnke, R. E. Stenkamp and K. Palczewski (2000). X-Ray diffraction analysis of three-dimensional crystals of bovine rhodopsin obtained from mixed micelles. J Struct Biol **130**(1): 73-80.

Oliver, D. and J. Beckwith (1981). *Escherichia coli* mutant pleiotropically defective in the export of secreted proteins. Cell **25**(3): 765-772.

Oliver, D. and J. Beckwith (1982). Identification of a new gene (SecA) and gene product involved in the secretion of envelope proteins in *Escherichia coli*. J Bacteriol **150**(2): 686-691.

Oliver, J., B. Jungnickel, D. Görlich, T. Rapoport and S. High (1995). The Sec61 complex is essential for the insertion of proteins into the membrane of the endoplasmic reticulum. FEBS Lett **362**(2): 126-130.

Osborne, A. R. and T. A. Rapoport (2007). Protein translocation is mediated by oligomers of the SecY complex with one SecY copy forming the channel. Cell **129**(1): 97-110.

Ossenbuhl, F., V. Gohre, J. Meurer, A. Krieger-Liszkay, J. D. Rochaix and L. A. Eichacker (2004). Efficient assembly of photosystem II in *Chlamydomonas reinhardtii* requires Alb3.1p, a homolog of Arabidopsis ALBINO3. Plant Cell **16**(7): 1790-1800.

Ostermeier, C., A. Harrenga, U. Ermler and H. Michel (1997). Structure at 2.7 A resolution of the Paracoccus denitrificans two-subunit cytochrome c oxidase complexed with an antibody FV fragment. Proc Natl Acad Sci U S A **94**(20): 10547-10553.

Ostermeier, C. and H. Michel (1997). Crystallization of membrane proteins. <u>Current Opinion in Structural Biology</u> **7**(5): 697-701.

Palczewski, K., T. Kumasaka, T. Hori, C. A. Behnke, H. Motoshima, B. A. Fox, I. Le Trong, D. C. Teller, T. Okada, R. E. Stenkamp, M. Yamamoto and M. Miyano (2000). Crystal structure of rhodopsin: A G protein-coupled receptor. <u>Science</u> **289**(5480): 739-745.

Panzner, S., L. Dreier, E. Hartmann, S. Kostka and T. Rapoport (1995). Posttranslational protein transport in yeast reconstituted with a purified complex of Sec proteins and Kar2p. <u>Cell</u> **81**(4): 561-570.

Parcej, D. N. and L. Eckhardt-Strelau (2003). Structural characterisation of neuronal voltage-sensitive K$^+$ channels heterologously expressed in *Pichia pastoris*. <u>J Mol Biol</u> **333**(1): 103-116.

Penczek, P., N. Ban, R. A. Grassucci, R. K. Agrawal and J. Frank (1999). Haloarcula marismortui 50S subunit-complementarity of electron microscopy and X-Ray crystallographic information. <u>J Struct Biol</u> **128**(1): 44-50.

Phillips, G. J. and T. J. Silhavy (1992). The *Escherichia coli* ffh-Gene Is Necessary for Viability and Efficient Protein Export. <u>Nature</u> **359**(6397): 744-746.

Plath, K., W. Mothes, B. Wilkinson, C. Stirling and T. Rapoport (1998). Signal sequence recognition in posttranslational protein transport across the yeast ER membrane. <u>Cell</u> **94**(6): 795-807.

Porath, J. (1960). Gel filtration of proteins, peptides and amino acids. <u>Biochim Biophys Acta</u> **39**: 193-207.

Porath, J., J. Carlsson, I. Olsson and G. Belfrage (1975). Metal chelate affinity chromatography, a new approach to protein fractionation. <u>Nature</u> **258**(5536): 598-599.

Porath, J. and P. Flodin (1959). Gel filtration: a method for desalting and group separation. <u>Nature</u> **183**(4676): 1657-1659.

Poritz, M. A., H. D. Bernstein, K. Strub, D. Zopf, H. Wilhelm and P. Walter (1990). An *Escherichia coli* Ribonucleoprotein Containing 4.5S RNA Resembles Mammalian Signal Recognition Particle. <u>Science</u> **250**(4984): 1111-1117.

Powers, T. and P. Walter (1997). Co-translational protein targeting catalyzed by the *Escherichia coli* signal recognition particle and its receptor. <u>Embo J</u> **16**(16): 4880-4886.

Pradel, N., A. Decorps, C. Ye, C. L. Santini and L. F. Wu (2005). YidC-dependent translocation of green fluorescence protein fused to the FliP cleavable signal peptide. <u>Biochimie</u> **87**(2): 191-196.

Preuss, M., K. Leonhard, K. Hell, R. A. Stuart, W. Neupert and J. M. Herrmann (2001). Mba1, a novel component of the mitochondrial protein export machinery of the yeast *Saccharomyces cerevisiae*. <u>J Cell Biol</u> **153**(5): 1085-1096.

Preuss, M., M. Ott, S. Funes, J. Luirink and J. M. Herrmann (2005). Evolution of mitochondrial oxa proteins from bacterial YidC. Inherited and acquired functions of a conserved protein insertion machinery. <u>J Biol Chem</u> **280**(13): 13004-13011.

Prinz, A., C. Behrens, T. A. Rapoport, E. Hartmann and K. U. Kalies (2000). Evolutionarily conserved binding of ribosomes to the translocation channel via the large ribosomal RNA. EMBO J **19**(8): 1900-1906.

Qi, H. Y. and H. D. Bernstein (1999). SecA is required for the insertion of inner membrane proteins targeted by the *Escherichia coli* signal recognition particle. J Biol Chem **274**(13): 8993-8997.

Raine, A., N. Ivanova, J. E. Wikberg and M. Ehrenberg (2004). Simultaneous binding of trigger factor and signal recognition particle to the *Escherichia coli* ribosome. Biochimie **86**(7): 495-500.

Rapiejko, P. J. and R. Gilmore (1994). Signal sequence recognition and targeting of ribosomes to the endoplasmic reticulum by the signal recognition particle do not require GTP. Mol Biol Cell **5**(8): 887-897.

Raunser, S. (2004). Überproduktion, Aufreinigung, Funktions- und Strukturanalyse und intramembrane Lokalisierung der Glutamat-Transporter GltP aus *Escherichia coli* und GLT-1 aus Rattenhirn. Doktorarbeit. Max-Planck-Institut für Biophysik. Frankfurt am Main, Johann Wolfgang Goethe Universität.

Reif, S., O. Randelj, G. Doman Ska, A. D. E, T. Krimmer, C. Motz and J. Rassow (2005). Conserved Mechanism of Oxa1 Insertion into the Mitochondrial Inner Membrane. J Mol Biol **354**(3): 520-528.

Rhee, K.-H., E. P. Morris, J. Barber and W. Kühlbrandt (1998a). Three-dimensional structure of the plant photosystem II reaction centre at 8 Å resolution. Nature **396**: 283-286.

Ribes, V., K. Römisch, A. Giner, B. Dobberstein and D. Tollervey (1990). *Escherichia coli* 4.5S RNA Is Part of a Ribonucleoprotein Particle That Has Properties Related to Signal Recognition Particle. Cell **63**(3): 591-600.

Rigaud, J. L., G. Mosser, J. J. Lacapere, A. Olofsson, D. Levy and J. L. Ranck (1997). Bio-Beads: an efficient strategy for two-dimensional crystallization of membrane proteins. J Struct Biol **118**(3): 226-235.

Rohrer, J. and A. Kuhn (1990). The Function of a Leader Peptide in Translocating Charged Amino Acyl Residues Across a Membrane. Science **250**(4986): 1418-1421.

Rojo, E. E., B. Guiard, W. Neupert and R. A. Stuart (1999). N-terminal tail export from the mitochondrial matrix. Adherence to the prokaryotic "positive-inside" rule of membrane protein topology. J Biol Chem **274**(28): 19617-19622.

Römisch, K., J. Webb, J. Herz, S. Prehn, R. Frank, M. Vingron and B. Dobberstein (1989). Homology of 54K protein of signal-recognition particle, docking protein and two *Escherichia coli* proteins with putative GTP-binding domains. Nature **340**(6233): 478-482.

Rosenow, M. A., J. C. Williams and J. P. Allen (2001). Amphiphiles modify the properties of detergent solutions used in crystallization of membrane proteins. Acta Crystallogr D Biol Crystallogr **57**(Pt 6): 925-927.

Rossomando, E. F. (1990). Ion-exchange chromatography. Methods Enzymol **182**: 309-317.

Rothblatt, J. A., R. J. Deshaies, S. L. Sanders, G. Daum and R. Schekman (1989). Multiple Genes Are Required for Proper Insertion of Secretory Proteins into the Endoplasmic Reticulum in Yeast. J Cell Biol **109**(6): 2641-2652.

Rothblatt, J. A. and D. I. Meyer (1986a). Secretion in yeast: reconstitution of the translocation and glycosylation of alpha-factor and invertase in a homologous cell-free system. Cell **44**(4): 619-628.

Sääf, A., M. Monne, J. de Gier and G. von Heijne (1998). Membrane topology of the 60-kDa Oxa1p homologue from Escherichia coli. J Biol Chem. **273**(46): 30415-30418.

Saint-Georges, Y., P. Hamel, C. Lemaire and G. Dujardin (2001). Role of positively charged transmembrane segments in the insertion and assembly of mitochondrial inner-membrane proteins. Proc Natl Acad Sci U S A. **98**(24): 13814-13819.

Samuelson, J. C., M. Chen, F. Jiang, I. Moller, M. Wiedmann, A. Kuhn, G. J. Phillips and R. E. Dalbey (2000). YidC mediates membrane protein insertion in bacteria. Nature **406**(6796): 637-641.

Samuelson, J. C., F. Jiang, L. Yi, M. Chen, J. W. de Gier, A. Kuhn and R. E. Dalbey (2001). Function of YidC for the insertion of M13 procoat protein in *Escherichia coli*: translocation of mutants that show differences in their membrane potential dependence and Sec requirement. J Biol Chem **276**(37): 34847-34852.

Schägger, H., W. A. Cramer and G. von Jagow (1994). Analysis of molecular masses and oligomeric states of protein complexes by blue native electrophoresis and isolation of membrane protein complexes by two-dimensional native electrophoresis. Anal Biochem **217**(2): 220-30.

Schägger, H. and G. von Jagow (1991). Blue native electrophoresis for isolation of membrane protein complexes in enzymatically active form. Anal Biochem **199**(2): 223-31.

Schatz, P. J., P. D. Riggs, A. Jacq, M. J. Fath and J. Beckwith (1989). The SecE gene encodes an integral membrane protein required for protein export in *Escherichia coli*. Genes Dev **3**: 1035-1044.

Schiebel, E., A. Driessen, F. Hartl and W. Wickner (1991). Delta mu H$^+$ and ATP function at different steps of the catalytic cycle of preprotein translocase. Cell **64**(5): 927-939.

Schlunzen, F., D. N. Wilson, P. Tian, J. M. Harms, S. J. McInnes, H. A. Hansen, R. Albrecht, J. Buerger, S. M. Wilbanks and P. Fucini (2005). The binding mode of the trigger factor on the ribosome: implications for protein folding and SRP interaction. Structure (Camb) **13**(11): 1685-1694.

Schmidt-Krey, I., W. Haase, V. Mutucumarana, D. W. Stafford and W. Kühlbrandt (2007). Two-dimensional crystallization of human vitamin K-dependent gamma-glutamyl carboxylase. J Struct Biol **157**(2): 437-442.

Schmidt-Krey, I., Y. Kanaoka, D. J. Mills, D. Irikura, W. Haase, B. K. Lam, K. F. Austen and W. Kühlbrandt (2004). Human leukotriene C(4) synthase at 4.5 A resolution in projection. Structure (Camb) **12**(11): 2009-2014.

Schmidt-Krey, I., G. Lundqvist, R. Morgenstern and H. Hebert (1998). Parameters for the two-dimensional crystallization of the membrane protein microsomal glutathione transferase. J Struct Biol **123**(2): 87-96.

Schuenemann, T. A., V. M. Delgado-Nixon and R. E. Dalbey (1999a). Direct evidence that the proton motive force inhibits membrane translocation of positively charged residues within membrane proteins. J Biol Chem **274**(11): 6855-6864.

Scotti, P. A., M. L. Urbanus, J. Brunner, J. W. de Gier, G. von Heijne, C. van der Does, A. J. Driessen, B. Oudega and J. Luirink (2000). YidC, the *Escherichia coli* homologue of mitochondrial Oxa1p, is a component of the Sec translocase. Embo J **19**(4): 542-549.

Scotti, P. A., Q. A. Valent, E. H. Manting, M. L. Urbanus, A. J. Driessen, B. Oudega and J. Luirink (1999). SecA is not required for signal recognition particle-mediated targeting and initial membrane insertion of a nascent inner membrane protein. J Biol Chem **274**(42): 29883-29888.

Screpanti, E., E. Padan, A. Rimon, H. Michel and C. Hunte (2006). Crucial Steps in the Structure Determination of the Na(+)/H(+) Antiporter NhaA in its Native Conformation. J Mol Biol **362**(2): 192-202.

Seluanov, A. and E. Bibi (1997). FtsY, the prokaryotic signal recognition particle receptor homologue, is essential for biogenesis of membrane proteins. J Biol Chem **272**(4): 2053-2055.

Serek, J., G. Bauer-Manz, G. Struhalla, L. van den Berg, D. Kiefer, R. Dalbey and A. Kuhn (2004). *Escherichia coli* YidC is a membrane insertase for Sec-independent proteins. Embo J **23**(2): 294-301.

Shaw, A. S., P. J. Rottier and J. K. Rose (1988). Evidence for the loop model of signal-sequence insertion into the endoplasmic reticulum. Proc Natl Acad Sci USA **85**(20): 7592-7596.

Shimohata, N., S. Nagamori, Y. Akiyama, H. R. Kaback and K. Ito (2007). SecY alterations that impair membrane protein folding and generate a membrane stress. J Cell Biol **176**(3): 307-317.

Shultz, J., T. J. Silhavy, M. L. Berman, N. Fiil and S. D. Emr (1982). A previously unidentified gene in the spc operon of *Escherichia coli* K12 specifies a component of the protein export machinery. Cell **31**(1): 227-235.

Simon, S. M. and G. Blobel (1991). A Protein-Conducting Channel in the Endoplasmic Reticulum. Cell **65**(3): 371-380.

Simon, S. M. and G. Blobel (1992). Signal peptides open protein-conducting channels in *Escherichia coli*. Cell **69**(4): 677-684.

Smith, J. M. (1999). Ximdisp--A visualization tool to aid structure determination from electron microscope images. J Struct Biol **125**(2-3): 223-228.

Smith, J. S. and J. M. Scholtz (1998). Energetics of polar side-chain interactions in helical peptides: salt effects on ion pairs and hydrogen bonds. Biochemistry **37**(1): 33-40.

Snapp, E., G. Reinhart, B. Bogert, J. Lippincott-Schwartz and R. Hegde (2004). The organization of engaged and quiescent translocons in the endoplasmic reticulum of mammalian cells. J Cell Biol. **164**(7): 997-1007.

Spence, E., S. Bailey, A. Nenninger, S. G. Moller and C. Robinson (2004). A homolog of Albino3/OxaI is essential for thylakoid biogenesis in the cyanobacterium Synechocystis sp. PCC6803. J Biol Chem **279**(53): 55792-55800.

Spurr, A. R. (1969). A low-viscosity epoxy resin embedding medium for electron microscopy. J Ultrastruct Res **26**(1): 31-43.

Standfuss, J., A. C. Terwisscha van Scheltinga, M. Lamborghini and W. Kühlbrandt (2005). Mechanisms of photoprotection and nonphotochemical quenching in pea light-harvesting complex at 2.5 A resolution. Embo J **24**(5): 919-928.

Stirling, C. J., J. Rothblatt, M. Hosobuchi, R. Deshaies and R. Schekman (1992). Protein Translocation Mutants Defective in the Insertion of Integral Membrane Proteins into the Endoplasmic Reticulum. Mol Biol Cell **3**(2): 129-142.

Swidersky, U. E., A. Rienhofer-Schweer, P. K. Werner, F. Ernst, S. A. Benson, H. K. Hoffschulte and M. Muller (1992). Biochemical analysis of the biogenesis and function of the *Escherichia coli* export factor SecY. Eur J Biochem **207**(2): 803-811.

Szyrach, G., M. Ott, N. Bonnefoy, W. Neupert and J. M. Herrmann (2003). Ribosome binding to the Oxa1 complex facilitates co-translational protein insertion in mitochondria. Embo J **22**(24): 6448-6457.

Tam, P. C., A. P. Maillard, K. K. Chan and F. Duong (2005). Investigating the SecY plug movement at the SecYEG translocation channel. Embo J **24**(19): 3380-3388.

Tani, K., K. Shiozuka, H. Tokuda and S. Mizushima (1989). Invitro Analysis of the Process of Translocation of Ompa Across the *Escherichia coli* Cytoplasmic Membrane - A Translocation Intermediate Accumulates Transiently in the Absence of the Proton Motive Force. J Biol Chem **264**(31): 18582-18588.

Taylor, G. (2003). The phase problem. Acta Crystallogr D Biol Crystallogr **59**(Pt 11): 1881-1890.

Tews, I. (1991). Spotscan in der hochauflösenden Elektronenmikroskopie: Entwicklung und Anwendung. Diplomarbeit. Heidelberg, Ruprecht-Karls-Universität.

Thomas, A. S. and A. H. Elcock (2006). Direct observation of salt effects on molecular interactions through explicit-solvent molecular dynamics simulations: Differential effects on electrostatic and hydrophobic interactions and comparisons to Poisson-Boltzmann theory. J Am Chem Soc **128**(24): 7796-7806.

Tokuda, H., K. Shiozuka and S. Mizushima (1990). Reconstitution of Translocation Activity for Secretory Proteins from Solubilized Components of *Escherichia coli*. Eur J Biochem **192**(3): 583-589.

Toyoshima, C., H. Sasabe and D. L. Stokes (1993). 3-Dimensional Cryo-Electron Microscopy of the Calcium Ion Pump in the Sarcoplasmic Reticulum Membrane. Nature **363**(6426): 286.

Tu, C. J., D. Schuenemann and N. E. Hoffman (1999). Chloroplast FtsY, chloroplast signal recognition particle, and GTP are required to reconstitute the soluble phase of light-harvesting chlorophyll protein transport into thylakoid membranes. J Biol Chem **274**(38): 27219-27224.

Ulbrandt, N. D., J. A. Newitt and H. D. Bernstein (1997). The *Escherichia coli* signal recognition particle is required for the insertion of a subset of inner membrane proteins. Cell **88**(2): 187-196.

Ullers, R. S., E. N. Houben, A. Raine, C. M. ten Hagen-Jongman, M. Ehrenberg, J. Brunner, B. Oudega, N. Harms and J. Luirink (2003). Interplay of signal recognition particle and trigger factor at L23 near the nascent chain exit site on the *Escherichia coli* ribosome. J Cell Biol **161**(4): 679-684.

Unger, V. (2002). Handout for MBB710 Spring 2002, Electron Crystallography.

Unger, V. M. (2000). Assessment of electron crystallographic data obtained from two-dimensional crystals of biological specimens. Acta Crystallogr D Biol Crystallogr **56**(Pt 10): 1259-1269.

Unwin, P. and R. Henderson (1975). Molecular structure determination by electron microscopy of unstained crystalline specimens. J Mol Biol. **94**(3): 425-440.

Urbanus, M. L., L. Froderberg, D. Drew, P. Bjork, J. W. de Gier, J. Brunner, B. Oudega and J. Luirink (2002). Targeting, insertion, and localization of *Escherichia coli* YidC. J Biol Chem **277**(15): 12718-12723.

Urbanus, M. L., P. A. Scotti, L. Froderberg, A. Saaf, J. W. de Gier, J. Brunner, J. C. Samuelson, R. E. Dalbey, B. Oudega and J. Luirink (2001). Sec-dependent membrane protein insertion: sequential interaction of nascent FtsQ with SecY and YidC. EMBO Rep **2**(6): 524-529.

Valent, Q. A., P. A. Scotti, S. High, J. W. de Gier, G. von Heijne, G. Lentzen, W. Wintermeyer, B. Oudega and J. Luirink (1998). The *Escherichia coli* SRP and SecB targeting pathways converge at the translocon. Embo J **17**(9): 2504-25012.

Valpuesta, J., J. Carrascosa and R. Henderson (1994). Analysis of electron microscope images and electron diffraction patterns of thin crystals of M-X29 connectors in ice. J. Mol. Biol. **240**: 281-287.

van Bloois, E., G. Jan Haan, J. W. de Gier, B. Oudega and J. Luirink (2004). F(1)F(0) ATP synthase subunit c is targeted by the SRP to YidC in the *Escherichia coli* inner membrane. FEBS Lett **576**(1-2): 97-100.

van Bloois, E., S. Nagamori, G. Koningstein, R. S. Ullers, M. Preuss, B. Oudega, N. Harms, H. R. Kaback, J. M. Herrmann and J. Luirink (2005). The Sec-independent function of *Escherichia coli* YidC is evolutionary-conserved and essential. J Biol Chem **280**(13): 12996-3003.

van Bloois, E. V., G. J. Haan, J. W. Gier, B. Oudega and J. Luirink (2006). Distinct requirements for translocation of the N-tail and C-tail of the *Escherichia coli* inner membrane protein CyoA. J Biol Chem **281**(15): 10002-9.

van den Berg, B., W. M. J. Clemons, I. Collinson, Y. Modis, E. Hartmann, S. C. Harrison and T. A. Rapoport (2004). X-ray structure of a protein-conducting channel. Nature **427**: 36-44.

van der Laan, M., E. N. Houben, N. Nouwen, J. Luirink and A. J. Driessen (2001). Reconstitution of Sec-dependent membrane protein insertion: nascent FtsQ interacts with YidC in a SecYEG-dependent manner. EMBO Rep **2**(6): 519-523.

van der Laan, M., N. Nouwen and A. Driessen (2004a). SecYEG proteoliposomes catalyze the Deltaphi-dependent membrane insertion of FtsQ. J Biol Chem. **279**(3): 1659-64.

van der Laan, M., M. L. Urbanus, C. M. Ten Hagen-Jongman, N. Nouwen, B. Oudega, N. Harms, A. J. Driessen and J. Luirink (2003). A conserved function of YidC in the biogenesis of respiratory chain complexes. Proc Natl Acad Sci U S A **100**(10): 5801-5806.

Vinothkumar, K. R., S. H. Smits and W. Kühlbrandt (2005). pH-induced structural change in a sodium/proton antiporter from *Methanococcus jannaschii*. Embo J **24**(15): 2720-2729.

von Heijne, G. (1996). Principles of membrane protein assembly and structure. Prog Biophys Mol Biol. **66**(2): 113-139.

Walian, P. J. and B. K. Jap (1990). Three-dimensional electron diffraction of PhoE porin to 2.8 A resolution. J Mol Biol **215**(3): 429-438.

Wallin, E. and G. von Heijne (1998). Genome-wide analysis of integral membrane proteins from eubacterial, archaean, and eukaryotic organisms. Protein Sci. **7**(4): 1029-1038.

Walter, P. and G. Blobel (1981a). Translocation of proteins across the endoplasmic reticulum. II. Signal recognition protein (SRP) mediates the selective binding to microsomal membranes of in-vitro-assembled polysomes synthesizing secretory protein. J Cell Biol **91**(2 Pt 1): 551-556.

Walter, P. and G. Blobel (1981b). Translocation of proteins across the endoplasmic reticulum III. Signal recognition protein (SRP) causes signal sequence-dependent and site-specific arrest of chain elongation that is released by microsomal membranes. J Cell Biol **91**(2 Pt 1): 557-561.

Walter, P. and G. Blobel (1982). Signal recognition particle contains a 7S RNA essential for protein translocation across the endoplasmic reticulum. Nature **299**: 691-698.

Walter, P., I. Ibrahimi and G. Blobel (1981). Translocation of proteins across the endoplasmic reticulum. I. Signal recognition protein (SRP) binds to in-vitro-assembled polysomes synthesizing secretory protein. J Cell Biol **91**(2 Pt 1): 545-550.

Wang, D. N. and W. Kühlbrandt (1991). High-resolution electron crystallography of light-harvesting chlorophyll a/b protein complex in three different media. J. Mol. Biol. **217**: 691-699.

Wang, L. and B. Dobberstein (1999). Oligomeric complexes involved in translocation of proteins across the membrane of the endoplasmic reticulum. FEBS Lett **457**(3): 316-322.

Wang, L., A. Miller, S. Rusch and D. Kendall (2004). Demonstration of a specific *Escherichia coli* SecY-signal peptide interaction. Biochemistry **43**(41): 13185-13192.

Watanabe, M. and G. Blobel (1989). Cytosolic factor purified from *Escherichia coli* is necessary and sufficient for the export of a preprotein and is a homotetramer of SecB. Proc Natl Acad Sci U S A **86**(8): 2728-2732.

Weiss, J., P. Ray and P. Bassford (1988). Purified SecB protein of *Escherichia coli* retards folding and promotes membrane translocation of the maltose-binding protein in vivo. Proc Natl Acad Sci USA **85**: 8978-8982.

White, D. A., W. J. Lennarz and C. A. Schnaitman (1972). Distribution of lipids in the wall and cytoplasmic membrane subfractions of the cell envelope of *Escherichia coli*. J Bacteriol **109**(2): 686-690.

Whitley, P., G. Gafvelin and G. von Heijne (1995). SecA-independent translocation of the periplasmic N-terminal tail of an *Escherichia coli* inner membrane protein. Position-specific effects on translocation of positively charged residues and construction of a protein with a C-terminal translocation signal. J Biol Chem. **270**(50): 29831-29835.

Williams, K. (2000). Three-dimensional structure of the ion-coupled transport protein NhaA. Nature **403**(6765): 112-115.

Williams, K. A., U. Geldmacher-Kaufer, E. Padan, S. Schuldiner and W. Kühlbrandt (1999). Projection structure of NhaA, a secondary transporter from *Escherichia coli*, at 4.0 A resolution. EMBO J. **18**(13): 3558-3563.

Williams, R. C. and H. W. Fisher (1970). Electron microscopy of tobacco mosaic virus under conditions of minimal beam exposure. J Mol Biol **52**(1): 121-123.

Wolfe, P. B., M. Rice and W. Wickner (1985). Effects of two Sec genes on protein assembly into the plasma membrane of *Escherichia coli*. J Biol Chem **260**(3): 1836-1341.

Woolhead, C. A., S. J. Thompson, M. Moore, C. Tissier, A. Mant, A. Rodger, R. Henry and C. Robinson (2001). Distinct Albino3-dependent and -independent pathways for thylakoid membrane protein insertion. J Biol Chem **276**(44): 40841-40846.

Xie, K., D. Kiefer, G. Nagler, R. E. Dalbey and A. Kuhn (2006). Different Regions of the Nonconserved Large Periplasmic Domain of *Escherichia coli* YidC Are Involved in the SecF Interaction and Membrane Insertase Activity. Biochemistry **45**(44): 13401-13408.

Xu, Z., J. D. Knafels and K. Yoshino (2000). Crystal structure of the bacterial protein export chaperone SecB. Nat Struct Biol **7**(12): 1172-1177.

Yen, M., K. Harley, Y. Tseng and M. J. Saier (2001). Phylogenetic and structural analyses of the Oxa1 family of protein translocases. FEMS Microbiol Lett. **204**(2): 223-231.

Yi, L., N. Celebi, M. Chen and R. E. Dalbey (2004). Sec/SRP requirements and energetics of membrane insertion of subunits a, b, and c of the *Escherichia coli* F_1F_0 ATP synthase. J Biol Chem **279**(38): 39260-39267.

Yi, L., F. Jiang, M. Chen, B. Cain, A. Bolhuis and R. E. Dalbey (2003). YidC is strictly required for membrane insertion of subunits a and c of the F(1)F(0)ATP synthase and SecE of the SecYEG translocase. Biochemistry **42**(35): 10537-10544.

Zhang, P., C. Toyoshima, K. Yonekura, N. M. Green and D. L. Stokes (1998). Structure of the calcium pump from sarcoplasmic reticulum at 8-A resolution. Nature **392**(6678): 835-839.

Ziegler, C., S. Morbach, D. Schiller, R. Kramer, C. Tziatzios, D. Schubert and W. Kühlbrandt (2004). Projection structure and oligomeric state of the osmoregulated sodium/glycine betaine symporter BetP of *Corynebacterium glutamicum*. J Mol Biol. **337**(5): 1137-1147.

Zopf, D., H. D. Bernstein and P. Walter (1993). GTPase Domain of the 54-kD Subunit of the Mammalian Signal Recognition Particle Is Required for Protein Translocation But Not for Signal Sequence Binding. J Cell Biol **120**(5): 1113-1121.

Acknowledgements

I wish to express my gratefulness to all people at the Max-Planck-Institute of Biophysics in Frankfurt/Main, who create the great and excellent scientific working environment and the wonderful atmosphere at this institute. Persons I like to mention because of their particular contributions to this work are Heidi, for frequent practical support and the nice time together in our lab, Götz, for the good time together sharing the office and for careful reading of my German summary, Remco, for explaining data processing more from his mathematician's and a programmer's point of view and for computer support, Gitte, for continuous computer support, Johan, Matthias, Vinoth, Sander, Stefan, Dilem, Franz and Thorsten, for being nice lab-neighbours and for joining me for lunch every day and for the valuable discussions at lunch regarding all topics of science and life, Franziska and Monika, for support in all kinds of organisational questions, Paolo, for all the valuable tips regarding the handling of graphic programmes and formatting of figures, Tiago, Panchali, Heike as well as Laura, for the nice time in our laboratory and Jörg, Ching-Ju, Fuensanta, Sivaram, Jonna and Sonja, who became good friends of mine during my stay.

I would like to thank the Max-Planck-Society and the SFB 628 of the German Research Foundation for logistic and financial support.

I sincerely thank all my friends, who are so precious to me and who all contributed to the success of this work. I want to mention particularly Ulrich, Thorsten, Ulli, Andi, Fred and Thomas, who accompanied me through my entire time as PhD student and my girlfriend Lula, who supported me since the moment we met.

Words are not sufficient to express my gratitude to my family for trusting in me and for giving me a strong support in all situations of life throughout the years, which in the end made all this possible. Particularly, I want to thank my Parents, to whom I dedicate this work.

Deutsche Zusammenfassung

1   Hintergrund und Ziele der Arbeit

Alle Proteine, welche nach ihrer Synthese für ein anderes Zellkompartiment bestimmt sind, müssen durch zelluläre Membranen transportiert werden. Der Transport von Proteinen über zelluläre Membranen hinweg oder der Einbau von Proteinen in zelluläre Membranen hinein wird "Proteintranslokation" genannt und ist wichtig für das Überleben aller Zellen.

Günter Blobel und Bernhard Dobberstein formulierten die "Hypothese für den Transport von Proteinen durch zelluläre Membranen" und beschrieben damit erstmals grundlegend den Prozess der Proteintranslokation (Blobel and Sabatini 1971; Blobel and Dobberstein 1975a). Die mRNS, welche für die Synthese eines Proteins kodiert, enthält neben der Information für die Aminosäuresequenz auch die Information über den Bestimmungsort des Proteins in der Zelle. Dieser mRNS-Abschnitt wird vom Ribosom in ein aminoterminales "Signalpeptid" übersetzt. Das Signalpeptid vermittelt die Anlagerung der synthetisierenden Ribosomen an einen Proteinkomplex in der Membran, welcher sowohl den Einbau von Proteinen in die Zellmembran als auch den Transfer von Proteinen über die Membran hinweg vermittelt. Nach dem Transfer durch die Membran oder dem Einbau in die Membran wird bei einer Reihe von Proteinen dann das Signalpeptid proteolytisch abgespalten (Blobel and Sabatini 1971; Blobel and Dobberstein 1975a).

Bei dem beschriebenen Proteinkomplex handelt es sich um das sogenannte "Sec-Translokon", welches offenbar bei allen bekannten Lebewesen vom Archäon bis zum Mensch zu finden ist und jeweils aus mehreren verschiedenen Membranproteinen besteht (Bernstein et al. 1989; Römisch et al. 1989; Görlich and Rapoport 1993; Miller et al. 1994). Generell wird zwischen der Translokation bereits synthetisierter Proteine (posttranslationale Translokation) und einer Translokation während der Proteinsynthese (kotranslationale Translokation) unterschieden. Das Sec-Translokon vermag in einigen Organismen, zum Beispiel Bakterien, beide Arten der Translokation zu vermitteln. Während der kotranslationalen Translokation kommt es zu einer Bindung des synthetisierenden Ribosoms an das Sec-Translokon. Das Sec-Translokon von *Escherichia coli* (SecYEG) ist ein heterotrimerer Komplex der Proteine SecY, SecE und SecG mit jeweils 10, drei und zwei Transmembranhelizes (Meyer et al. 1999).

Die Struktur von SecYEG wurde mittlerweile bis zu mittlerer Auflösung (Collinson et al. 2001; Breyton et al. 2002), die des Sec-Translokons von *Methanococcus jannashii* (SecYEβ) bis zu hoher Auflösung ermittelt (van den Berg et al. 2004). Trotzdem ist der Prozess der Proteintranslokation noch nicht im Detail verstanden. Was gesichert scheint ist dass der Sec-Komplex in der frühen Phase der Proteintranslokation intramolekulare Umlagerungen durchläuft, welche aber noch nicht genauer charakterisiert sind (van den Berg et al. 2004; Bostina et al. 2005; Mitra et al. 2005; Tam et al. 2005).

Das Membranprotein YidC, welches in der inneren Membran von *Escherichia coli* zu finden ist, ist ebenfalls für die Biogenese verschiedener Membranproteine essentiell. Abhängig vom Substratprotein, geschieht YidC-vermittelte Proteintranslokation sowohl in Zusammenwirkung mit der kotranslationalen Translokation des Sec-Translokons als auch unabhängig vom Sec-Translokon (Samuelson et al. 2000; Scotti et al. 2000).

Die YidC-vermittelte Proteintranslokation ist wie die Sec-vermittelte Proteintranslokation evolutionär konserviert, was Kuhn und Mitarbeiter in einer zusammenfassenden Darstellung beschreiben (Kuhn et al. 2003). Homologe von YidC sind zum Beispiel in der inneren Membran von Mitochondrien und in der Thylakoidmembran von Chloroplasten zu finden (Long et al. 1993; Hell et al. 1998; Moore et al. 2000). Alle YidC Homologe sind offenbar besonders wichtig für die Biogenese von Proteinkomplexen der Atmungskette (van der Laan et al. 2003).

Im Gegensatz zu vielen anderen Homologen besitzt YidC eine zusätzliche aminoterminale Transmembranhelix, welche als Signalpeptid zu fungieren scheint und nach dem Einbau von YidC nicht abgespalten wird. Dieses Signalpeptid ist Topologievorhersagen zufolge durch eine ausgedehnte wasserlösliche periplasmatische Domäne mit dem "funktionellen Kern" von YidC verbunden. Dieser besteht bei allen YidC Homologen aus fünf Transmembranhelizes und beinhaltet die "Translokase-Funktion" (Sääf et al. 1998; Yen et al. 2001; Jiang et al. 2003).

Die vorliegende Arbeit hatte zum einen das Ziel, die Sec-vermittelte Proteintranslokation durch strukturelle Daten von SecYEG mit gebundenem Substrat weiter aufzuklären. Dies sollte anhand zweidimensionaler Kristalle von SecYEG mit spezifisch gebundenem natürlichen Signalpeptid geschehen.

Mittels elektronenmikroskopischer Untersuchung der Kristalle in gefrierkonserviertem Zustand (Elektronen-Kryomikroskopie) und Vergleich mit früheren Strukturen von SecYEG, insbesondere mit der früheren Projektionsstruktur

(Collinson et al. 2001), sollten mit der Substratinkubation einhergehende strukturelle Veränderungen identifiziert werden. Strukturen von YidC oder homologer Proteine sind bisher noch nicht bekannt. Der zweite Teil der Arbeit hatte daher zum Ziel, ebenfalls mittels zweidimensionaler Kristallisation und Elektronen-Kryomikroskopie eine Projektionsstruktur von YidC und somit erste Strukturdaten für diese Familie von Membranproteinen zu erhalten.

2 Resultate und Schlussfolgerungen

Analyse von SecYEG/LamB$_{SP}$-Kristallen

Die früheren zweidimensionalen SecYEG-Kristalle (Collinson et al. 2001) liessen sich nur schwer reproduzieren und benötigten zudem mehrere Wochen um zu wachsen. Nach einer Modifikation des bestehenden Protokolls konnten in etwa 10 Tagen SecYEG-Kristalle erhalten werden, die hinsichtlich der zu erreichenden Auflösung struktureller Details, zumindest in Projektion, den vorherigen SecYEG glichen. Möglich machte dies das Lösen des zugesetzten Lipides mit dem Detergenz DM anstatt mit C$_{12}$E$_9$, was vermutlich ein effektiveres Entfernen des Detergenz aus der Probe mittels Dialyse ermöglichte. Basierend auf dem so modifizierten Protokoll wurden zweidimensionale SecYEG-Kristalle in Gegenwart von Signalpeptid erzeugt (SecYEG/LamB$_{SP}$-Kristalle). Mit der Absicht das benötigte Volumen an Dialysepuffer zu minimieren um somit nur eine möglichst geringe Mengen des teueren Signalpeptides dem Dialysepuffer zusetzen zu müssen, wurde dabei ein Teil des Detergenz im Dialysepuffer an hydrophobe Kügelchen adsorbiert.

Eine Gefrierkonservierung mit Trehalose als Frostschutzmittel ermöglichte das Sammeln von Strukturdaten von SecYEG/LamB$_{SP}$-Kristallen mittels Elektronen-Kryomikroskopie. Aus den Daten wurden Projektionskarten errechnet. Diese entsprachen hinsichtlich Ihrer Auflösung den im Rahmen dieser Arbeit und den früher erhaltenen Daten von SecYEG ohne Signalpeptid.

Die SecYEG-Kristalle und die SecYEG/LamB$_{SP}$-Kristalle hatten die gleiche Kristallform. Das Kristallgitter bestand aus zwei Membranschichten, welche durch eine "Schraubenachsen-Symmetrie" aufeinander abgebildet werden konnten. Besonders weil die Kristalle aus zwei Membranschichten bestanden, war es vorteilhaft für den angestrebten Vergleich, dass die SecYEG- und SecYEG/LamB$_{SP}$-Kristalle die gleiche Kristallform hatten.

Drei Projektionsstrukturen der gefrierkonservierten SecYEG/LamB$_{SP}$-Kristalle wurden unter Einbeziehung der Schraubenachsen-Symmetrie gemittelt. Die resultierende Projektionsstruktur lieferte verlässliche Daten bis zu einer Auflösung von 10 Å und höher. Um Rauschen zu vermeiden, wurde die Projektionskarte nur bis zu einer Auflösung von 10 Å ausgegeben. Obwohl sich die Projektionskarten von SecYEG/LamB$_{SP}$- und SecYEG-Kristallen hinsichtlich einer Vielzahl sichtbarer Dichten glichen, waren schon mit blossem Auge substanzielle Unterschiede in einigen Regionen der Projektionskarten zu erkennen.

Um diese Unterschiede zu lokalisieren, wurde eine Differenzstruktur durch Subtraktion der SecYEG-Elektronendichten von den SecYEG/LamB$_{SP}$-Elektronendichten berechnet. Die Differenzstruktur deutet darauf hin, dass dimeres SecYEG mit gebundenem Signalpeptid ein asymmetrisches Molekül ist. Es scheint aus einem "aktiven" und einem "inaktiven" SecYEG-Monomer zu bestehen. Dies ist auch im Einklang mit anderen Berichten (Mitra et al. 2005; Osborne and Rapoport 2007). Das aktive SecYEG-Monomer ist durch eine in der Differenzstruktur erkennbare zusätzliche Dichte, welche demzufolge gebundenes Signalpeptid darstellen könnte sowie durch intramolekulare Umlagerungen gekennzeichnet. Die beobachteten Umlagerungen lassen sich als eine Bewegung einer Moleküldomäne, gebildet durch Transmembranhelizes 7, 8 und 9 in SecY vom "Rumpf" des SecYEG-Moleküls weg zuzuordnen. Diese Veränderung in der Molekülstruktur könnte dazu dienen, den lateralen Austrittsortes für Transmembranhelizes zur umgebenden Membran hin zu öffnen (van den Berg et al. 2004). Eine weitere Interpretation der Daten wird vermutlich eine dreidimensionale Rekonstruktion von SecYEG/LamB$_{SP}$ erfordern, welche zusammen mit einer Verbesserung der Projektionsstruktur von SecYEG/LamB$_{SP}$ einen wichtigen nächsten Schritt in diesem Projekt darstellt.

Strukturelle Untersuchung von YidC

Für die strukturelle Untersuchung von YidC mussten zuerst zweidimensionale Kristalle erhalten werden. Dies erforderte eine Anpassung bestehender Reinigungsprotokolle. Wichtig war der Detergenzwechsel zu DM, wobei für das Lösen von YidC aus den zellulären Membranen Detergentien mit zyklischen hydrophoben Seitenketten, insbesondere "Cymal 6" optimal waren. Vermutlich liess sich DM besonders effektiv mittels Dialyse aus dem Kristallisationsansatz entfernen, wie schon bei der Kristallisation von SecYEG/LamB$_{SP}$ beobachtet.

Unabdingbar für die Bildung zweidimensionaler Kristallisation durch YidC war die weitestreichende Entfernung jeglichen Salzes monovalenter Ionen aus der Probe. Tubuläre YidC-Kristalle wurden durch eine Zugabe einer Lipidmischung bestehend aus jeweils etwa gleichen Anteilen von PC und PG Lipid erhalten. Besser geordnete kristalline Membran-Einzelschichten wurden mit reinem PG Lipid erhalten. Interessanterweise verursachte PE Lipid in den Kristallisationsexperimenten eine Oligomerisierung von YidC.

Von den einschichtigen Kristallen konnten Strukturdaten mittels Elektronen-Kryomikroskopie gesammelt werden. Desweiteren wurde nur mittels Vitrifizierung der Kristalle ohne Einsatz von Frostschutzmitteln in flüssigem Ethan Strukturdaten gewonnen. Die Einheitszellenwinkel der Einzelbilder variierten zwischen etwa 83 und 91 °. Daher wurden zwei unabhängige Sets aus Projektionsstrukturen gebildet. Die Unterteilung erfolgte dabei im Hinblick auf die Einheitszellenwinkel: Set 1 beinhaltete Bilder mit Einheitszell-Winkeln von etwa 85 °, Set 2 solche mit Einheitszell-Winkeln von etwa 90 °. Anschliessend wurden die Elektronendichten innerhalb der Sets gemittelt. In den gemittelten Projektionsstrukturen aus beiden Sets waren annähernd gleiche Dichten zu sehen.

Mitteln dreier Einzelbilder aus Set 1 in p2 Symmetrie brachte die Projektionskarte mit den am besten erkennbaren Details hervor (Einheitszell-Dimensionen: 82 x 71 Å, Winkel = 85 °). Die p2 Symmetrie wurde für diese Bilder zuvor durch Analyse mit dem Programm ALLSPACE gefunden. Das Vorhandensein der p2 Symmetrie wurde zudem durch niedrige Phasenfehler nach dem Mitteln bestätigt. Die Auflösung der Karte wurde auf 10 Å begrenzt.

Die Projektionskarte zeigte YidC-Dimere, die antiparallel in die kristalline Membran eingebaut sind, das heisst zu beiden Seiten der Membran weisen. Zu erkennen war die antiparallele Orientierung zum einen an der gegensätzlichen Orientierung der Dimere in Projektion. Zudem wurde sie durch eine immunologische Markierung des karboxyterminalen Endes von YidC in der Membran und anschliessendem Nachweis der Markierung im Elektronmikroskop gezeigt. Entsprechend dem Arrangement der Dimere in der Membran, formte ein YidC-Dimer vermutlich Kristallkontakte mit vier weiteren Dimeren.

Jedes YidC-Molekül bestand aus einem "Kern" mit einem zentralen Bereich niedriger Dichte. Eine Darstellung von SecYEG, gezeigt mit gleichen Darstellungsparametern wie YidC, demonstriert einen ähnlichen Bereich niedriger Dichte in der Region des lateralen Austrittsortes für Transmembranhelizes.

Demzufolge könnte der Bereich niedriger Dichte im YidC-Molekül ebenfalls eine Region darstellen, welche für den Einbau der Transmembranhelizes von Substratproteinen eine besondere Rolle spielt. Eine Dichte, die peripher mit dem „Molekülkern" von YidC assoziiert war, könnte die erste aminoterminale Transmembranhelix von YidC repräsentieren.

Aufgrund der Projektionskarte ist denkbar, dass die Sec-unabhängige Proteintranslokation durch dimeres YidC vermittelt wird. Monomeres YidC könnte indes mit dem Sec-Translokon assoziieren, um Sec-abhängig den kotranslationalen Einbau von Transmembrandomänen in die Membran zu unterstützen. Dafür muss monomeres YidC vermutlich mit dem lateralen Austrittsort für Transmembranhelizes in SecYEG (van den Berg et al. 2004) in räumliche Nähe kommen. Ein Zusammenwirken von YidC und SecYEG könnte dabei von SecDF-Komplexen propagiert werden, welche mit YidC assoziieren und dissoziieren (Duong and Wickner 1997a; Nouwen and Driessen 2002; Chen et al. 2005; Xie et al. 2006).

Lebenslauf

Mirko Lotz

Geboren	28.02.1975 in Schlüchtern
Staatsangehörigkeit	deutsch

Abitur	1994
Wehrdienst	1994 - 1995

Studium der Biotechnologie

1995 - 1997	Technische Universität Carolo-Wilhelmina zu Braunschweig, Grundstudium
1997 - 2001	Technische Universität Carolo-Wilhelmina zu Braunschweig, Hauptstudium
	Wahlpflichtfach: Immunbiologie
	Prüfungsfächer: Verfahrenstechnik, Technische Chemie, Genetik, Technische Mikrobiologie, Technische Biochemie
1999 - 2000	Studienarbeit *Entwicklung eines Nachweises für Antikörper gegen das humane Herpesvirus 6 auf Basis eines Westernblots und eines ELISAs* angefertigt bei der Firma Euroimmun GmbH in Lübeck, betreut durch Prof. Dr. Jürgen Wehland
2000 - 2001	Diplomarbeit *Expression einer modifizierten Aggrekanase in Insektenzellen* angefertigt bei der Firma Aventis Pharma Deutschland GmbH in Frankfurt am Main, betreut durch Prof. Dr. Sigmund Lang

Promotionsstudium

Seit 11/2001	Max-Planck-Institut für Biophysik in Frankfurt am Main, betreut von Dr. Ian Collinson und Prof. Dr. Werner Kühlbrandt

Publikationen

M. Lotz, W. Haase, W. Kühlbrandt and I. Collinson (2007). Projection structure of a conserved mediator of membrane protein assembly YidC. Eingereicht.

C. Tziatzios, D. Schubert, M. Lotz, D. Gundogan, H. Betz, H. Schägger, W. Haase, F. Duong and I. Collinson (2004). The bacterial protein-translocation complex: SecYEG dimers associate with one or two SecA molecules. J Mol Biol 340(3): 513-24.